

Influence of Energetic Disorder on Exciton Diffusion Properties

DISSERTATION

zur Erlangung des Grades

„Doktor der Naturwissenschaften“

im Promotionsfach Chemie

am Fachbereich Chemie, Pharmazie und Geowissenschaften

der Johannes Gutenberg-Universität

in Mainz

Irina Rörich

geboren in Solikamsk, Russland

Mainz, den 20. September 2018

1. Berichterstatter: [REDACTED]

2. Berichterstatter: [REDACTED]

Tag der mündlichen Prüfung: 12.12.2018

I hereby declare that I wrote this dissertation submitted without any unauthorized external assistance and used only sources acknowledged in the work. All textual passages which are appropriated verbatim or paraphrased from published and unpublished texts as well as all information obtained from oral sources are duly indicated and listed in accordance with bibliographical rules. In carrying out this research, I complied with the rules of standard scientific practice as formulated in the statutes of the Johannes Gutenberg-University Mainz to insure standard scientific practice.

Irina Rörich

жизнь преподносит только те задачи

с которыми мы можем справиться.

Das Leben schenkt dir nur die Herausforderungen,

die du bewältigen kannst.

Table of Contents

Scope and Motivation.....	1
Chapter 1. Theoretical Background.....	5
1.1. Electronic structure and energetic disorder in organic semiconductors	6
1.2. Photophysics in isolated conjugated molecules.....	10
1.3. Photophysics in organic semiconductors.....	14
1.3.1. Excitation energy and charge transfer processes	14
1.3.2. Intra- and interchain excitations.....	17
1.3.3. Exciton diffusion-limited quenching	19
1.4. Investigation of exciton diffusion properties in organic semiconductors.....	21
Chapter 2. Experimental Section and Materials	23
2.1. Materials	23
2.2. Sample preparation	24
2.3. Time-resolved photoluminescence spectroscopy	27
2.4. Analysis of TRPL experimental data.....	29
2.5. Fluorescence quenching measurements.....	32
2.6. Stern-Volmer equation.....	33
2.7. Monte Carlo Simulations	36
2.8. PLQY	40

2.9. Polymer light-emitting diodes	40
2.9.1. PLED device fabrication.....	40
2.9.2. PLED current efficiency and EL spectra	41
2.9.3. PLED device stressing.....	41
2.10. BEH-PPV Synthesis	42
Chapter 3. Influence of energetic disorder on the exciton lifetime and photoluminescence quantum yield in conjugated polymers	43
3.1 Introduction.....	44
3.2. Results and Discussion	46
3.2.1. Exciton lifetime in PPV derivatives	46
3.2.2. Exciton diffusion	50
3.2.3. Photoluminescence Quantum Yield	55
3.3 Conclusions.....	59
Chapter 4. Temperature dependence of photo- and electro-luminescence of poly(<i>p</i> -phenylene vinylene) based polymers	61
4.1 Introduction.....	62
4.2. Results.....	64
4.2.1. Temperature-dependent time-resolved photoluminescence	64
4.2.2. Exciton diffusion coefficient and diffusion length	68
4.2.3. Temperature-dependent polymer-light emitting diode efficiencies	70

4.3. Discussion.....	72
4.3.1. Temperature-dependent exciton decay characteristics	72
4.3.2. Downhill migration and thermally-activated hopping depends on energetic disorder.	78
4.3.3. Origin of temperature-dependent PLED efficiency enhancement in BEH-PPV.....	80
4.4. Conclusion	82
Chapter 5. Exciton quenching due to hole trap formation in aged polymer light-emitting diode	83
5.1. Introduction.....	84
5.2. Results and Discussion	86
5.2.1. Hole trap formation.....	86
5.2.2. Exciton lifetime	87
5.2.3. Monte Carlo simulation	89
5.3. Conclusion	92
5.4. Outlook	93
Summary	95
Zusammenfassung	97
References	101
List of publications	107
Appendix	109
Curriculum Vitae.....	113

List of Figures

1.1. Molecular structure of ethane (a), ethylene (b) and ethyne (c) with respective sp^3 , sp^2 and sp -hybridized carbon atoms.....	7
1.2. (a) Linear combination of atomic orbitals (LCAO) and (b) MO of ethylene.	8
1.3. Gaussian energy distribution of localized states in conjugated polymers.	10
1.4. Overview of photophysical processes summarized in Jablonski diagram.	11
1.5. Schematic representation of Franck-Condon principle.	12
1.6. (a) Förster and (b) Dexter energy transfer mechanism.	15
1.7. Schematic illustration of exciton migration in conjugated polymers.	16
2.1. Molecular structures of used materials.	24
2.2. Schematic representation of TRPL experimental set-up using streak camera system.	28
2.3. (a) Contour plot of neat BEH-PPV thin film determined from TRPL spectroscopy with (b) associated PL decay trace and PL spectrum.	30
2.4. (a) PL quenching measurements of BEH-PPV and (b) associated PL spectra.	33
2.5. Stern-Volmer plot of BEH-PPV:PCBM blends.	34
2.6. Measured and simulated PL decays for BEH-PPV (a) and SY-PPV (b).	39
3.1. PL decay curves for a series of PPV derivatives.	47
3.2. PL decay curve of polyspirobifluorene (PSBF) in a thin film.	53
3.3. Measured and simulated PL decay times for PSBF copolymer.	54
3.4. PL quantum yield versus exciton diffusion coefficient for whole series of conjugated polymers.	56

4.1. (a,c) Temperature dependent photoluminescence spectra and (b,d) associated normalized PL decay traces at specified wavelengths for SY-PPV and BEH-PPV.	65
4.2. Temperature-dependence of (a) exciton diffusion coefficient D and b) exciton diffusion length L_D for SY-PPV and BEH-PPV.	70
4.3. Current efficiencies vs. voltage of PLEDs comprised of (a) SY-PPV and (b) BEH-PPV measured at various temperatures.	71
4.4. Temperature-dependent electroluminescence spectra of the BEH-PPV PLED.	72
4.5. Exciton diffusion coefficient D dependent quenching efficiency Q for SY-PPV and BEH-PPV	75
5.1. Density of hole traps formed during degradation of BEH-PPV PLED as a function of aging time at current densities 35 mA/cm ²	86
5.2. PL decay curves of BEH-PPV PLEDs measured at the PL maximum (580–600 nm). The device was stressed for 211 h under constant current density.	87
5.3. Measured and simulated PL decay of BEH-PPV PLED stressed under constant current density of 35 mA/cm ²	91
A. 1. Normalized PL decays in SY-PPV for a wide temperature-range.	109
A. 2. Normalized PL decays in BEH-PPV for a wide temperature-range.	110
A. 3. Temperature-dependence of exciton diffusion coefficient D and diffusion length L_D for BEH-PPV, determined by using Stern-Volmer equation.	110
A. 4. Exciton transfer rates in (a) BEH-PPV and (b) SY-PPV.	112
A. 5. Determination of the excitonic Gaussian DOS σ in BEH-PPV and SY-PPV.	112

List of Tables

3.1. Determined exciton diffusion parameters using Monte Carlo Simulation for a series of PPV derivatives and a PSBF copolymer.	52
4.1. Temperature dependence of PL lifetime and relative quantum yield in SY-PPV.	67
4.2. Temperature dependence of PL lifetime and relative quantum yield in BEH-PPV.	67
4.3. Exciton transfer rates in SY-PPV.	76
4.4. Exciton transfer rates in BEH-PPV.	76
5.1. Concentration of hole traps P_t determined from electrical measurements and number of exciton quenchers c_0 determined via optical measurements.	91
A.1. Photoluminescence spectra peaks of SY-PPV determined by Gaussian fits.	109
A. 2. Photoluminescence spectra peaks of BEH-PPV determined by Gaussian fits.	110
A.3. Electroluminescence spectra peaks of BEH-PPV determined by Gaussian fits.	111
A.4. Temperature-dependent exciton diffusion coefficients and diffusion lengths for SY-PPV and BEH-PPV.	111

Scope and Motivation

Conjugated polymer materials for thin film optoelectronics are subject to energetic disorder arising from both molecular conformational irregularities as well as the sensitivity of these amorphous systems to film processing conditions. As a result, organic semiconductors are commonly associated with strongly dispersive charge carrier mobilities and exciton diffusion characteristics compared to their inorganic counterparts. In order to take advantage of the attractive properties of these systems, such as low-cost manufacturing and mechanical flexibility, it is essential to understand the interplay between energetic disorder and processes affecting optoelectronic performances. Therefore, this work puts forth a study of the exciton diffusion properties in conjugated polymers with respect to the following questions:

- How does the energetic disorder in conjugated polymers influences exciton diffusion characteristics such as the exciton lifetime, exciton diffusion coefficient, exciton diffusion length, and photoluminescence quantum yield in a solid thin film?
- How the exciton diffusion does depend on temperature with respect to various degree of energetic disorder?
- Is it possible to minimize exciton quenching at non-radiative quenching-sites by optimization of the polymer synthesis or film processing conditions?

The goal of this work is to understand on the one hand the interplay between the energetic disorder of the conjugated polymer and the device performance, and on the other hand the factors, which limit the exciton diffusion characteristics in a conjugated polymer film.

Chapter 1 puts forth the theoretical background and establishes relevant definitions for this thesis, leading to a sufficient basis for the rest of the work presented here. In the experimental section, **Chapter 2**, the implementation, time-resolved photoluminescence

(TRPL) set-up as well as the different analysis methods with respect to the exciton diffusion propagation are described. In addition, the materials as well as their properties are summarized in this chapter and collaboration partners are named.

Chapter 3 reveals the influence of energetic disorder on the exciton lifetime, exciton diffusion characteristics and photoluminescence quantum yield (PLQY) in four PPV derivatives with varying degree of energetic disorder and a model compound polyspirobifluorene copolymer (PSBF). We found that the exciton lifetime and PLQY directly correlates with the energetic disorder of the conjugated polymer, where increased energetic disorder slows down the diffusion of the exciton toward non-radiative quenching sites and strongly enhances both exciton lifetime and PLQY. This is consistent with diffusion-limited exciton quenching at non-radiative recombination centers in organic semiconductors.

In **Chapter 4**, we characterized the effect of conformational energetic disorder on photo and electroluminescence behavior in two PPV derivatives. TRPL spectroscopy at varying temperature show a correlation between the energetic disorder and the balance between radiative and non-radiative decay processes, the latter of which includes also non-radiative decay processes due to exciton diffusion toward excitonic traps. We found distinct temperature dependencies of the exciton diffusion properties based on the polymer disorder, which also determines the polymer light-emitting diode (PLED) performance. The PLED based on the more disordered polymer shows temperature independent current efficiencies, as it is reported in most polymer-based LED devices, while the PLED based on the better ordered polymer shows enhanced current efficiencies at lower temperatures due to reduced exciton quenching at defect centers.

In **Chapter 5**, TRPL spectroscopy is used to investigate the PL decay in degraded PLED, that were aged at a constant current density, leading to the formation of hole traps. The TRPL

demonstrates a decrease in exciton lifetime in the degraded PLED device with respect to the unaged one. The amount of non-radiative exciton quenching-sites in the aged devices is quantified by Monte Carlo simulations, which is found to match with the number of hole traps predicted from electrical charge transport measurements. Our results reveal the origin for the apparent different behavior of the electroluminescence and photoluminescence upon PLED degradation. The decrease of the electroluminescence is governed by recombination of free electrons with trapped holes, whereas the photoluminescence is reduced by non-radiative quenching processes between excitons and hole traps.

Chapter 1. Theoretical Background

Shirakawa, MacDiarmid and Heeger reported in 1977 a dramatic increase in electrical conductivity of the semiconducting polymer polyacetylene by doping it with halogen ions or with arsenic pentafluoride (AsF₅).¹ For their discovery and development of conductive polymers the scientists were honored with the Nobel Prize for Chemistry in 2000. After this breakthrough, conjugated polymers gained considerable attraction for application in optoelectronic devices due to their mechanical and optical properties and low-cost manufacturing, e.g. organic photovoltaics (OPVs),² organic light-emitting diodes (OLEDs),³ memories,⁴ organic field-effect transistors (OFETs)⁵ and sensors.⁶

However, the charge carrier mobility in conjugated polymers is orders of magnitude lower than in the conventional silicon devices. For instance, the hole mobility in poly(*p*-phenylenevinylene) (PPV)-derivatives determined from charge transport measurements is about 10^{-8} – 10^{-5} cm²/Vs,^{7,8} while the charge carrier mobility in crystalline silicon is about 1000 cm²/Vs.⁹ In addition, their low efficiency and short lifetime are essential drawbacks as compared to silicon, which limit the introduction of optoelectronic devices based on semiconducting polymers on the market. To date, only optoelectronic devices based on small molecules are commercially available. These materials are usually vacuum-deposited and have less intrinsic disorder, leading to higher charge carrier mobilities (1–10 cm²/Vs).⁹ In particular, OLED technology is used in smartphone displays, television screens and lightening with steady growth, reaching efficiencies up to 25-30%,^{10,11} and device lifetimes of over 10,000 hours with an initial luminance of 1,000 cd/m², as reported for green emitters.¹¹ Small molecule semiconductors are also utilized in some commercial solar cells.¹²

Despite their low device performances, however, conjugated polymers offer the added benefit of flexibility, low-weight, low cost of manufacturing and biocompatibility. With further understanding of the fundamental properties and limits to device performances, these polymers can open a new field for future applications, such as paper electronics, artificial skin and wearable electronics.¹³⁻¹⁵

1.1. Electronic structure and energetic disorder in organic semiconductors

Organic semiconductors are mainly based on carbon atoms with the electron configuration of $1s^2 2s^2 2p^2$, while only the four outer electrons of the 2s and 2p orbitals contribute to covalent bonding. By hybridization, these 2s and 2p orbitals can intermix with each other and generate new orbitals, whose energy levels have the same energy. For example, in the simplest carbon compound methane (CH_4) 4 sp^3 hybrid orbitals are formed that point to the corners of a tetrahedron, and lead to four equal σ -bonds with the hydrogen ($1s^1$) orbitals. Figure 1.1 shows the molecular structure of ethane (a), ethylene (b) and ethyne (c). Ethane (C_2H_6) is composed of 4 sp^3 hybrid orbitals, while 1 sp^3 hybrid orbital is used to form a σ -bond between the two carbon atoms. In the case of the small molecule ethylene (Figure 1.1, b and Figure 1.2), 3 sp^2 hybrid orbitals are used to form three σ -bonds, leaving one unhybridized orbital. This is commonly denoted as the p_z orbital, and is oriented perpendicular to the chemical bond direction. This p_z orbital can interact with the p_z orbital of the neighbor carbon atom by forming a π bond above and below the plane leading to a double bond between the two carbon atoms. Organic molecules can also exhibit a triple bond, as in the case of ethyne (acetylene) (Figure 1.1, c), which is formed by two sp hybrid orbitals and two unhybridized p orbitals.¹⁶

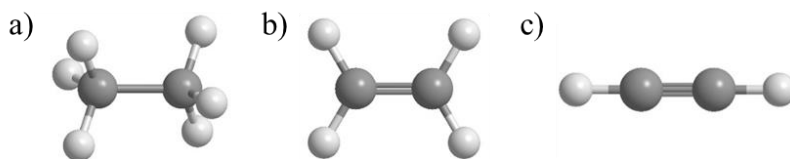


Figure 1.1. Molecular structure of ethane (a), ethylene (b) and ethyne (c) with respective sp^3 , sp^2 and sp -hybridized carbon atoms. Grey balls represent the carbon atoms, while the white ones are hydrogen atoms.

The formation of covalent bonds is described by the theory of linear combination of atomic orbitals (LCAO), wherein the combination of atom orbitals with the same wave function results in bonding molecular orbitals and the out-of-phase combination accounts for the antibonding molecular orbitals, denoted with a star (*). This is illustrated in Figure 1.2 for the molecule ethene. The associated molecular orbitals (MO) are shown schematically in Figure 1.2b.

By following the Pauli exclusion principle maximum two electrons can occupy each molecular orbital with opposite spin (see also Figure 1.2b), starting with the lowest energy level, until all electrons that are involved in the bond formation, are distributed on the orbitals. The energetically highest occupied molecular orbital (HOMO) and the lowest unoccupied molecular orbital (LUMO) play an important role for the optical and electrical properties in conjugated molecules.

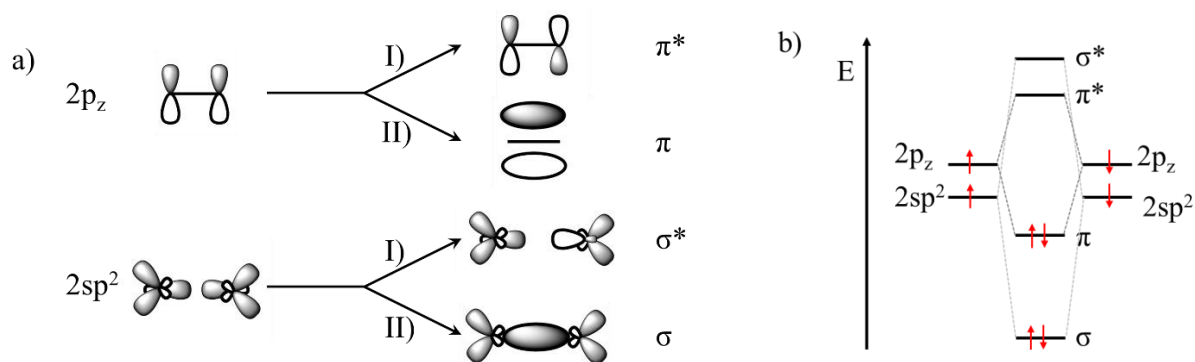


Figure 1.2. (a) Linear combination of atomic orbitals (LCAO) in ethylene. The C–H σ bonds resulting from the overlap of the two sp^2 orbitals with the hydrogen 1s orbitals are not shown in this figure. The third sp^2 orbital overlaps with the sp^2 orbital of the neighbor carbon atom and forms a bonding and antibonding MO, σ and σ^* C–C bond, respectively. The interaction between the remaining p_z orbitals leads to the formation of the π bond, while the in-phase combination (II) forms the bonding and the out-of-phase combination (I) leads to the formation of an antibonding MO (*).¹⁶ (b) MO of ethylene with relevant orbitals.

When ethyne is polymerized to polyacetylene, a π -conjugated polymer is obtained with sequences of alternating single and double bonds. There, the electrons are not limited to a specific carbon atom but are delocalized over the whole conjugated system.¹⁶ With increasing conjugation size (the more carbon atoms contribute to the π -system) the energy difference between the HOMO (π) and the LUMO (π^*) level decreases and additionally the density of states (DOS) increases.^{17,18} Typically, the energy gap between the HOMO and LUMO levels in organic semiconductors is between 1.5 and 3.5 eV, covering the wavelength range between the near infrared and the near ultraviolet (826–354 nm).^{3,19}

An ideal π -conjugated polymer requires sufficient overlap of each p_z orbital, as in a perfectly stretched macromolecule. This, however, is not the case for polymers. Instead, the polymer backbone is kinked, twisted, and has defects. Due to thermally induced displacements of the chains and various polarization effects of the disordered environment the polymer backbone exhibits intrachain torsions, which leads to conjugation breaks along the polymer backbone. As a result, conformational subunits are generated that can be regarded as chromophores of various sizes and energies.^{20,21} Consequently, the HOMO/LUMO levels in organic semiconductors are inhomogeneously distributed in energy (Figure 1.3). This energy spread is also referred to the energetic disorder σ of the organic semiconductors and is well-described by a Gaussian model:²²⁻²⁴

$$\rho(\varepsilon) = \frac{1}{\sqrt{2\pi\sigma^2}} \exp(-\varepsilon^2/2\sigma^2) \quad (1.1)$$

where $\rho(\varepsilon)$ is the density of states (DOS) related to energy ε and σ is the width of the Gaussian DOS. Therefore, each energy level in the Gaussian DOS represents conformational subunits of the polymer backbone with different sizes and energies as well as their distribution. In addition to molecular structural defects, extrinsic defects originating from chemical impurities contribute to the width of the Gaussian DOS. Therefore, conjugated polymer materials and their optoelectronic properties are subject to energetic disorder.

In this thesis, the role of energetic disorder on the exciton diffusion characteristics is investigated using time-resolved photoluminescence spectroscopy. The photophysical processes are studied in poly(*p*-phenylenevinylene) (PPV)-derivative systems with varying degrees of energetic disorder (Chapter 3 and 4).

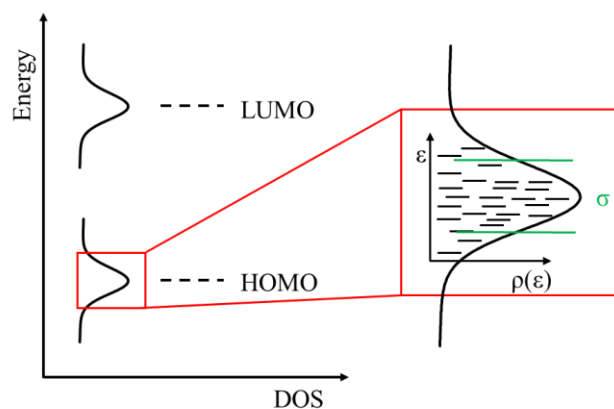


Figure 1.3. Energy distribution of localized states (conformational subunits) in conjugated polymers. The density of states (DOS) is typically described by a Gaussian distribution.

1.2. Photophysics in isolated conjugated molecules

As a first step, the probable photophysical processes in an isolated organic molecule will be introduced here, which are summarized in the Jablonski diagram (Figure 1.4).²⁵ In the ground state an organic molecule is in the lowest vibrational state (thick horizontal line) of its lowest electronic state (S_0) and has net spin zero. By photon absorption (blue arrows) an electron is excited from the ground state to an electronically excited singlet state S_n , where $n \geq 1$ depends on the absorbed photon energy. This promotion occurs in the time scale of 10^{-15} s.²⁶ The excited molecule has several ways to return to the ground state. By vibrational relaxation (VR, orange dotted arrows) the molecule cools down from higher vibrational levels (thin vertical lines) to the lowest vibrational level of the electronic energy level by dissipating the energy to the environment in a time range of 10^{-12} – 10^{-10} s.²⁶ This process is a nonradiative decay process. Higher excited states ($n \geq 2$) can be deactivated to the lowest excited state (S_1) by internal conversion (IC, green dashed arrow) in a time range of 10^{-13} – 10^{-9} s, keeping the same multiplicity.²⁶ Transitions, where the multiplicity is changed are so-called intersystem crossing

transitions (ISC, purple dashed arrows), which occur within the time scale of 10^{-10} – 10^{-7} s.²⁶ The ISC transition is a slow transition (10^{-10} – 10^{-7} s) compared to IC (10^{-13} – 10^{-9} s) due to spin-conversion. However, it is favored by the coupling between singlet and triplet states or/and spin-orbit coupling, which is promoted by heavy atoms like halogens or metals. Eventually, in accordance with Kasha's rule,²⁷ the excited molecule returns from the lowest vibrational state of the lowest electronic state (S_1 or T_1) to the ground state (S_0) by emitting the remained excess energy as a photon. Depending on the initial electronic state the spontaneous emission is called fluorescence (10^{-10} – 10^{-7} s) or phosphorescence (10^{-6} – 1 s).²⁶ The singlet (S_1) and triplet (T_1) state can also be deactivated by a non-radiative channel via IC and ISC, and successive vibrational relaxation.

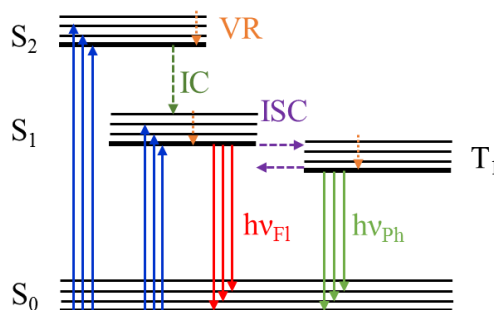


Figure 1.4. Overview of photophysical processes in an isolated organic molecule summarized in Jablonski diagram. The vibrational levels for a given electronic energy level lie above each other, shown as thin vertical lines. The ground vibrational state is highlighted in bold. VR: vibrational relaxation; IC: internal conversion; ISC: intersystem crossing.

The probability for an electronic transition is described by the Franck-Condon principle (Figure 1.5) and depends on the overlap integral between the wave function of the initial and final

vibrational energy level, also called Franck-Condon factors, and the dipole operator.²⁸⁻³⁰ The fundamental assumption for this principle is the Born-Oppenheimer approximation, which separates the motion of the electron and the atomic nuclear as a consequence of their different mass and velocity.³¹

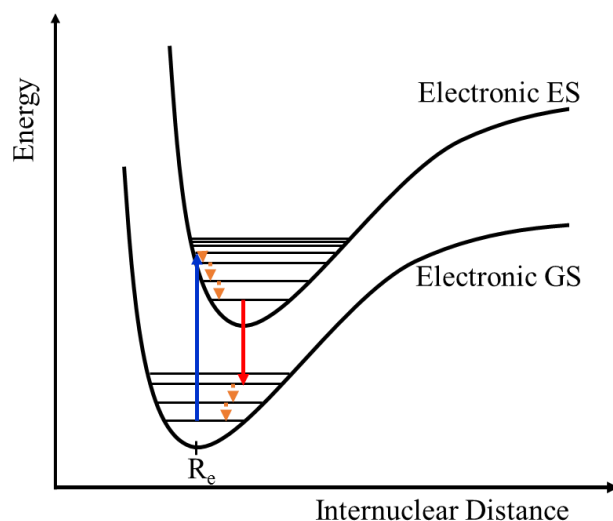


Figure 1.5. Franck-Condon principle describes the transition probability between two electronic states, represented in an anharmonic oscillator. ES: excited state; GS: ground state; R_e : equilibrium separation.

In other words, the absorption of the molecule occurs from the lowest vibrational state of the lowest electronic state, while the nuclei are located at its most probable location, which is the so-called equilibrium separation (R_e). During the excitation (10^{-15} s), the nuclei framework remains constant due to the much faster velocity of the electron than of the nuclei. Thus, the electronic transition from the ground state (lower curve) to the excited state represented by the upper curve, can be represented as a vertical transition. The transition where the integral between the initial wavefunction and the final wavefunction overlaps the most sufficient, is the

most probable termination for the transition. This transition has the highest intensity in an absorption spectrum. However, transitions to other vibrational states can also occur, but with less intensity, leading to a vibronic structure of the absorption spectrum.³⁰ It takes some time until the nuclei ‘realizes’ the transition and adapts the new configuration. As a result, the nuclei separation increases upon excitation, leading to a change of the molecular geometry. The downward transition occurs similar to the upward transition vertical in accordance to the Franck-Condon principle with a characteristic vibrational structure of the emission spectrum of the lower electronic state. Figure 1.4 and 1.5 reveal that the energy (wavelength) of the emission is typically lower (longer) than that of the absorption, which is a direct result of vibrational relaxation and solvent reorganization. This phenomenon is called Stokes shift.^{32,33}

Another way to describe the promotion of an electron from the ground state to the excited state in a conjugated molecule is to use the HOMO/LUMO energy levels, where the HOMO can be considered as the ground state (S_0) and the LUMO as the excited state (S_n). Therefore, upon photon absorption by the molecule, an electron is promoted from the HOMO to the LUMO, leaving a positive charge (hole) in the HOMO and a negative charge (electron) in the LUMO energy level. In an organic semiconductor, this photoexcitation generates a Coulombically-bound electron-hole pair, also known as Frenkel exciton, which is due to the weak intermolecular coupling and low dielectric constant ($\epsilon = 3$) localized at a single conjugated subunit.³⁴ In contrast, electron-hole pairs created in inorganic semiconductors, referred to as Mott-Wannier excitons, have a low binding energy at room temperature (about $kT \sim 0.025$ eV) and a higher dielectric constant (silicon $\epsilon = 12$) leading to a quick separation of the electron and the hole.³⁴ The singlet exciton binding energy (E_B) in conjugated polymers is usually in the order of 0.3–1 eV,³⁵⁻³⁷ which determines the work needed to separate an exciton into free electron and hole. This binding energy plays an important factor in organic optoelectronics. For

example, in a photovoltaic device, the separation of an exciton to create free charges is a crucial process in determining the device efficiency.²

1.3. Photophysics in organic semiconductors

After the photophysical processes in an isolated conjugated molecule were introduced in the previous section, here, the photophysical processes between the conformational subunits (neighboring molecules) in conjugated polymers will be discussed and their dependence on the energetic disorder.

1.3.1. Excitation energy and charge transfer processes

Excitation energy transfer (EET) is the process by which a molecule in the excited state (*) transfers its energy to a nearby molecule which is (initially) in the ground state. The molecule that transfers its energy is the so-called donor (D) and the molecule that accepts the energy is referred to as the acceptor (A). This is a non-radiative process and is distinguished between two mechanisms, as depicted in Figure 1.6. Förster energy transfer is mediated by dipole-dipole interaction and requires that the emission spectrum of the donor sufficiently overlaps with the absorption spectrum of the acceptor. The efficiency (transfer rate constant) of the Förster energy transfer decreases with the distance r between donor and acceptor as r^{-6} , and can proceed over distances up to 10 nm.^{26,38} Dexter energy transfer, also referred to as ‘electron-exchange’, is a short-range process ($< 1\text{nm}$), which requires the overlap of the involved intermolecular orbitals (wavefunctions) of the donor and acceptor molecule. The efficiency of Dexter EET decreases exponentially with the distance between D-A. Usually only singlet excitons can undergo Förster

EET, whereas triplet EET usually proceeds via the Dexter mechanism.^{26,39} However, Förster ET of triplet excitons can be observed when the exciton is located at a phosphorescent donor.⁴⁰

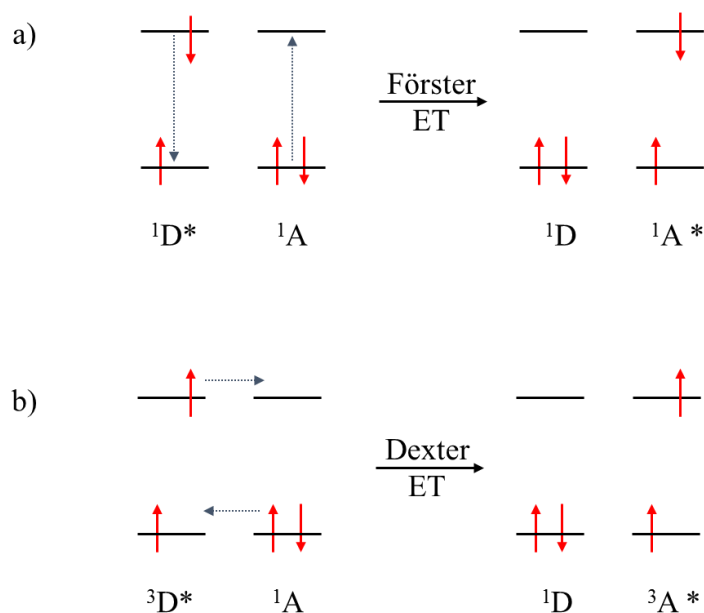


Figure 1.6. Schematic representation of the Förster energy transfer (a) and the Dexter energy transfer mechanism (b) between the donor (D) and the acceptor molecule (A).

This energy transfer is a fundamental process of exciton migration in organic semiconductors, which consist of a sequence of incoherent ET events among and/or between the conformational subunits. Due to the energetic disorder of the conjugated polymer such a migration can be described as a random walk.³⁷ Figure 1.7 depicts the exciton diffusion in an organic semiconductor. Upon the absorption of a high energy photon, singlet excitons are generated at an arbitrary energy-site within the high-energy tail of the Gaussian DOS and simultaneously undergo downhill migration towards lower energy-sites in the inhomogeneously broadened

DOS.^{23,41,42} This spectral diffusion can be detected as a red-shift of the emission spectrum. In the PPV derivatives investigated in this thesis, spectral diffusion usually occurs in the time range of 100 ps.⁴³ Eventually, excitons approach quasi-equilibrium at $-\sigma^2/kT$ below the center of the DOS that is the energy level of the most populated excited states,^{22,44} provided that the time needed to reach equilibrium energy is shorter than the intrinsic exciton lifetime. Thus, the equilibrium level (green line in Figure 1.7) depends on the energetic disorder σ and temperature. Then, temperature activated hopping takes over at room temperature, where balanced downward and thermally activated upward hopping occurs.⁴⁴

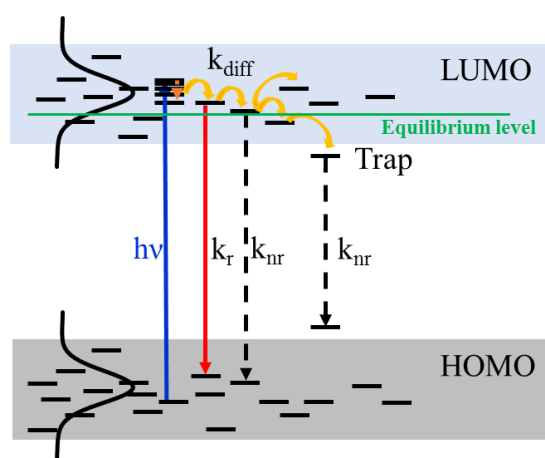


Figure 1.7. Schematic illustration of exciton migration in conjugated polymers.

During the hopping process the exciton can reach a conjugated chain segment containing recombination centers and traps, where it can decay either radiatively or non-radiatively.⁴⁵ When the exciton reaches trap site, the activation energy is not sufficient enough to enable an uphill jump for further exciton migration and the exciton becomes trapped and/or quenched.

In addition to excitation energy transfer, an excited molecule may also undergo charge transfer, or photoinduced electron transfer, with a neighboring ground state molecule. At the end of this redox process, the donor molecule is positively charged, and the acceptor molecule negatively charged. This process is a short-range interaction and requires a significant spatial overlap between the wave function of the donor and acceptor molecules. Charge transfer may occur via electron or hole transfer via the same physical mechanism.¹⁹ In an organic photovoltaic device, for example, electron transfer from the donor (organic semiconductor) to the electron acceptor material (PCBM) is a crucial process, where the exciton is separated at the polymer-acceptor interface into free charges, which then contribute to the photocurrent generation.^{2,46,47}

1.3.2. Intra- and interchain excitations

The degree of exciton propagation depends on the excited state species. When an excited state is located on a single conjugated polymer chain and the exciton diffusion occurs along the polymer backbone direction, the excited state is termed as *intrachain* exciton. When adjacent conformational subunits are in close proximity, either belonging to different polymer chains or brought close to one another as a result of chain folding, mainly *interchain* excitations are formed. There are several ways that closely spaced conjugated polymer chromophores can interact with each other: Two adjacent polymer subunits that share their π -electrons equally in the excited state but not in the ground state are termed ‘excimers’. When the π -electrons of the conjugated polymer are neutrally delocalized over multiple segments in both the ground state and excited state, the interchain excited state is from photophysical point of view referred to as ‘aggregate’. The term ‘polaron pair’ is used for a charge-separated interchain species, where upon the excitation of strongly interacting chromophores charge transfer occurs, leaving a

radical cation (hole polaron) on one segment and a radical anion (electron polaron) on the other. Further, interchain excited states with an unequal sharing of π -electrons between polymer chain segments or a partial degree of charge transfer character (i.e., somewhere between excimers and polaron pairs) are labeled as 'exciplexes'.⁴⁸

In a diluted polymer solution, the polymeric chains are well isolated by the solvent molecules and the exciton diffusion is attributed to pure *intrachain* hopping. Due to the weak dipole coupling of the excitation along the chain direction, this is a slow transfer event (hundreds of ps), which leads to typically longer exciton lifetimes in diluted conjugated polymer solutions compared to the exciton lifetimes in neat polymer films. In the latter one, the larger electronic coupling matrix elements between closely lying polymer chains results to an order of magnitude higher energy transfer rate relative to the solution.^{49,50} Therefore, the *interchain* exciton diffusion occurs in a time range of a few ps and is the most efficient pathway for excitation transfer in solid states (films).

However, the choice of the solvent has a big impact on the *intra*- and *interchain* ratio in diluted polymer solutions, as reported for MEH-PPV, where the photophysical dynamics depends on the solvent. For full name and chemical structures see Chapter 2.1. A reduction of the solvent quality leads to an enhanced interchain species formation due to steric constraints on the polymer backbone motions caused by aggregation of the chains. As a result an almost monoexponential PL decay was obtained in the case of a "good" solvent and more pronounced non-monoexponential PL decays with reduced solvent quality, respectively.⁵¹ In addition, as reported for MEH-PPV and SY-PPV, the exciton lifetime in diluted polymer solution is shorter than in the pristine film.^{52,53} This is attributed to interchain-excitations such as excimers, which expect to have lower oscillator strength and hence longer natural radiative lifetime. Also, due

to the electronic coupling between chains aggregates might be formed, which can lead to a partly forbidden lower-energy state with longer lifetimes than that of an isolated polymer chain.⁵⁴

The nature of the excited state species and/or the ratio between intra- and interchain excitations influences the photoluminescence quantum yield (PLQY), which is the ratio between the radiatively decayed excitons versus overall decay processes. The PLQY in polymer films is nearly an order of magnitude lower than the one in diluted polymer solution or diluted blends.⁵⁵ For instance, the PLQY of MEH-PPV in solution is about 55–70%, while in solid films it is 12–15%.^{53,56,57} Chapter 3 comprehensively discusses how the energetic disorder influences the PLQY and exciton lifetime in thin polymer films, and shows that an increased energetic disorder enhances both the exciton lifetime and PLQY.

As a consequence, the performance of optoelectronic devices depends not only on the energetic disorder of the conjugated polymer, but also on the processing conditions and thus film morphology. In particular, these systems are sensitive to how the polymer chains pack together. The degree of interchain contact (number of interchain species) can be controlled for instance by the choice of solvent,^{51,57} diluted conjugated polymer in a host matrix (blend),⁵⁵ polymer concentration,⁵⁷ thermal annealing,⁵⁷ or even prevented by the encapsulation of the polymer chain in mesoporous silica matrices.^{58,59}

1.3.3. Exciton diffusion-limited quenching

As described above in Figure 1.7, when an exciton reaches a non-radiative quenching-site (exciton trap), it can be quenched via electron transfer. Exciton quenching is a loss process of the radiative decay, and thus results in a reduction in exciton density, PL intensity (number of emitted photons) and PL decay time. The influence of exciton traps on the exciton diffusion

properties was investigated by Athanasopoulos et al., where they applied quantum-chemical calculations to model the energy diffusion on a predetermined chain morphology in a conjugated polymer. They found that the inclusion of a low concentration of trap-sites could remedy the discrepancy between experimentally determined and modelled values and that the exciton migration in conjugated polymers is most likely trap limited rather than transfer rate limited,⁶⁰ provided that the time needed to reach the trap is shorter than the intrinsic exciton lifetime. In Chapter 3 we conclude that the exciton lifetime in thin polymer films is governed by the time an exciton needs to reach a trap, which is consistent with the exciton diffusion-limited quenching model and which is influenced by the energetic disorder of the conjugated polymer.

The origin of these traps is not totally understood but is ascribed to impurities and morphological and chemical defects, respectively. From TRPL measurements Mikhnenko et al. found a typical concentration of exciton quenching defects in the range of 10^{23} – 10^{24} per cubic meter for a large number of organic semiconductors.⁶¹ A nearly identical concentration of electron traps is reported by Nicolai et al. by charge transport measurements. They found a universal electron trap density of 3 – 5×10^{23} per m^{-3} for a whole series of organic semiconductors, which exhibits a Gaussian energy distribution located at 3.6 eV below the vacuum level.⁶² These findings put forth the open question as to whether the electron traps and excitonic traps in pristine polymer films might share the same origin. If the energy level of the electron trap is located below the LUMO of the polymer, than excitons can be quenched at these traps via electron transfer, and vice versa in the case of hole traps. There the hole trap is expected to be located above the HOMO level, and the exciton becomes quenched via hole transfer.

Many possible sources have been purported for the origin of traps in organic semiconductors. Previous work reports that photo-oxidation of the conjugated polymer occurs

in the presence of oxygen, leading to the generation of carbonyl groups and thus to further breaks along the conjugated polymer backbone.⁶³⁻⁶⁶ Also hydrated-oxygen $(\text{H}_2\text{O})_2\text{-O}_2$ complexes could act as electron traps as shown by theoretical calculations.⁶² Further, exciton quenching is reported at metal interfaces.^{67,68} In the case of a PLED exciton quenching at the cathode interface takes place, which reduces the device efficiency. In contrast, in an OPV device, exciton quenching at the polymer/electron acceptor interface is a desired process, which enhances the device efficiency.⁴⁷ When two excitons are in close proximity, they can annihilate each other.^{66,69} This exciton quenching process occurs for instance at high excitation energies and is a method used to investigate exciton propagation in organic semiconductors.⁷⁰⁻⁷⁴ Depending on the polymer synthesis, halogen ions can remain in the polymer chains, leading to exciton quenching at these halogen ions.⁷⁵ Further, exciton quenching is reported at polarons,⁷⁶ and in Chapter 5, the quenching at hole traps formed during device degradation is discussed.

1.4. Investigation of exciton diffusion properties in organic semiconductors

There are many reported techniques to measure the exciton diffusion characteristics – exciton diffusion coefficient and diffusion length – in organic semiconductors. One common method is fluorescence quenching in bilayers, where one of the interfaces of the thin polymer film is brought into contact with an exciton quenching wall, for instance fullerenes or TiO_2 ,^{44,70,77-81} which are known to be effective electron acceptors.^{47,82} Other reports utilize exciton–exciton annihilation,⁷⁰⁻⁷⁴ microwave conductivity,⁸³⁻⁸⁵ electro–optical measurements,⁸⁶⁻⁹⁰ and fluorescence quenching of thin films with randomly distributed exciton quenching molecules.^{61,91-95} This last method was used in the scope of this work and has the crucial advantage of a relatively simple sample preparation and analysis. The results can be interpreted

either by using the Stern-Volmer equation for monoexponential PL decays or an open source Monte-Carlo simulation for multi-exponential decays (see also Chapter 2). This allows a reliable and systematic study of exciton diffusion characteristics in a large number of materials.⁹¹ A comprehensive comparisons of these methods, including their advantages and pitfalls, can be found in a review paper from Mikhnenko et al.¹⁹

Chapter 2. Experimental Section and Materials

This chapter describes the materials studied, the experimental set-ups, as well as the implementations and analysis methods. Furthermore, collaboration partners, who contributed with their work to some results presented in this thesis, will be named in the relevant subchapter.

2.1. Materials

The molecular structures of the materials studied in this thesis are summarized in Figure 2.1. The investigations on the role of energetic disorder on the exciton diffusion properties were mainly performed on poly(*p*-phenylene vinylene) (PPV)-derivatives (compound **1–4** in Figure 2.1), since they exhibit a similar polymer backbone (marked in black) and their energetic disorder can be varied by chemical modification of the side chains (marked in green).⁷ The impacts of the side chains on the polymer energetic disorder is comprehensively discussed in Chapter 3.2.

Poly[2,5-bis(2'-ethyl-hexyl)-1,4-phenylene vinylene] (BEH-PPV) **1**, poly[2-methoxy-5-(2'-ethyl-hexyloxy)-1,4-phenylene vinylene] (MEH-PPV) **2** and poly[4-(3',7'-dimethyloctyloxy)-1,1'-bi-phenylene-2,5-vinylene]-*co*-2-methoxy-5-(3',7'-dimethyloctyloxy)-1,4-phenylene vinylene (NRS-PPV) **3** were synthesized in house. The copolymer Super Yellow (SY-PPV) **4** were purchased from Merck KGaA (PDY-132) as well as the copolymer polyspirobifluorene (PSBF) **5**. Phenyl-C61-butyric acid methyl ester (PCBM) **6** was purchased from Solene BV. SY-PPV, PSBF and PCBM were used without further purifications.

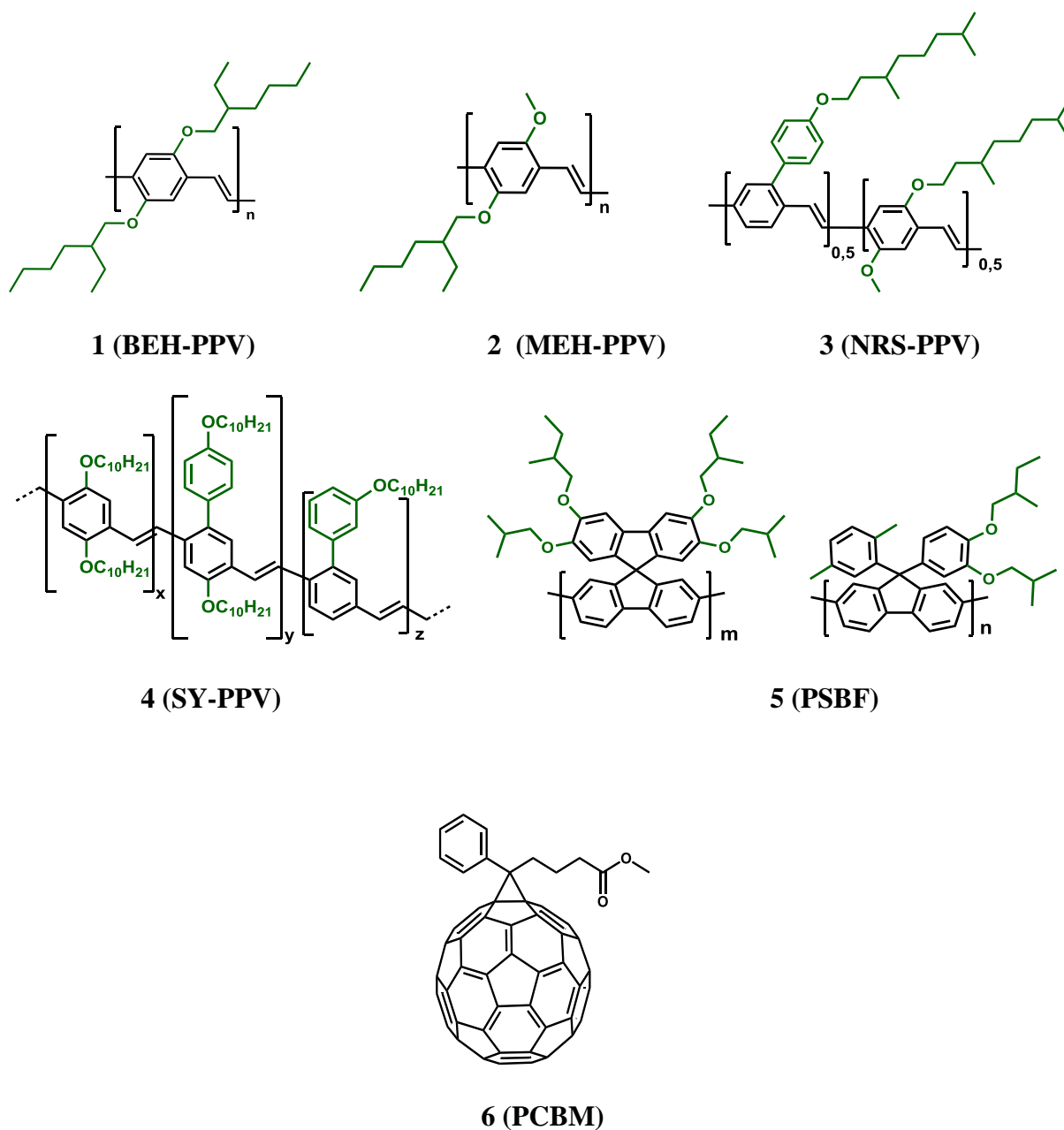


Figure 2.1. Molecular structures of used materials.

2.2. Sample preparation

The polymer solution preparations as well as the spin-coating processes were carried out in an inert nitrogen atmosphere (glovebox, MBraun). All polymer solutions were prepared from

degassed solvents to exclude oxygen in the polymer solution, which can generate carbonyl group defects in the polymer backbone due to photo-oxidation,⁶³⁻⁶⁶ or act as exciton quencher.⁹² For this purpose, usually chlorobenzene (Sigma-Aldrich, anhydrous 99.8%) was taken. The polymer solution was allowed to stir over night at 55 °C. After the polymer was dissolved, the polymer solution was filtered (5 µm, PTFE, ResistTM, Whatman) to prevent large particles in the polymer solution for further applications.

The samples for the optical measurements were measured either as a dilute solution in a quartz cuvette or as a thin film spin-coated on a glass or quartz substrate, which were cleaned before spin-coating. The substrates (Corning[®]EAGLE XGTM AMLCD glass substrates with a size of 30x30 mm or quartz substrates from Präzisions Glas & Optik GmbH with a size of 10x20 mm) were scrubbed for 30–60 s with a soap solution (Extran[®] MA 02, Merck KGaA). The soap was then washed away with deionized water, and the substrates were subsequently cleaned with acetone and then propanol in an ultrasonic bath and dried for 10 minutes at 140 °C.

For the PLED device fabrication, glass substrates with a patterned indium tin oxide (ITO) layer (30x30 mm) were cleaned, in a similar way, and then the dried substrates were treated with ultraviolet (UV)-ozone for 20 minutes. The PLED device fabrication will be described in more detail in Chapter 2.9.1.

In addition to pristine polymer film measurements, semiconductor:PCBM blend films were prepared for fluorescence quenching experiments. The semiconductor:PCBM blend solution preparation proceeds via ongoing-mixing as follows: A polymer solution and very diluted PCBM solution (0.1–1 mg/mL) were prepared, as described above, and then a known amount of the PCBM solution (10–100 µL) was added to the polymer solution by Eppendorf pipette, and allowed to stir for 1 hour at 50 °C. From this blend solution a film was spin-coated, and then again, a certain amount of PCBM solution was added to the polymer blend solution,

and so forth. To describe the amount of PCBM molecules either the concentration in cm^{-3} and m^{-3} is used or the term volume fraction v_{frac} . The latter one describes the occupied volume by the PCBM molecules (V_{PCBM}) divided by the total volume of the blend ($V_{PCBM} + V_{polymer}$). The concentration of the quencher molecules c_{PCBM} correlates with the v_{frac} as follows:

$$c_{PCBM} = \frac{v_{frac}}{V_{PCBM}} \quad (2.1)$$

where

$$V_{PCBM} = \frac{4}{3}\pi r^3 \quad (2.2)$$

The PCBM radius r is set to 0.5×10^7 cm.⁹⁶ The volume can also be calculated with the following relationship using the molar mass m and the density ρ of the compound:

$$V = \frac{m}{\rho} \quad (2.3)$$

For PCBM a density between $1.3\text{--}1.5$ g/cm³ is reported.⁹⁷⁻⁹⁹ Therefore, in our calculations the PCBM density was set to 1.5 g/cm³ and the polymer density to 1.3 g/cm³.⁹¹

The films for the TRPL experiments were spin-coated using the following spin-speeds: 60 s at 1000 rpm followed by 30 s at 4000 rpm. The film thicknesses were usually between 100–120 nm, determined by using a surface profilometer (Bruker, DektakXT). Other thicknesses than these, will be noted in the relevant Chapters. In order to limit polymer degradation due to oxygen exposure, all experiments on thin film samples were performed under

a dynamic vacuum of 10^{-4} – 10^{-5} mbar within a few hours upon preparation. For the temperature-dependent measurements (Chapter 4), the thin polymer films were spin-coated on a quartz substrate and loaded into a constant flow nitrogen cooled cryostat (Optistat CF-V2, Oxford) equipped with temperature controller (Mercury iTC, Oxford).

2.3. Time-resolved photoluminescence spectroscopy

Time-resolved photoluminescence (TRPL) spectroscopy was measured with a Hamamatsu Streak Camera system (Hamamatsu C5680). This experimental setup enables a simultaneous spectral and temporal characterization of the photon emission, and is a widely used technique to study photophysical processes in organic semiconductors.¹⁰⁰ The experimental set-up is shown schematically in Figure 2.2. The frequency-doubled output from a Ti:Sapphire laser (**A**) (Coherent, Libra HE 3.5 mJ, Vitesse 750 mW) supplies a short laser pulse (100 fs) for excitation at 400 nm. The laser repetition rate is either 1 kHz (10 ns time window, 0.12 ns instrument response) or 80 MHz (2 ns time window, 14 ps instrument response). The excitation light is focused onto the sample and the laser fluence at the sample position (**B**) was $<1 \mu\text{J}/\text{cm}^2$ in order to prevent sample damage and secondary effects, such as exciton-exciton annihilation (see also Chapter 1.3.3). The fluorescence emission was detected in a front-facing geometry.

Upon the excitation by the short laser pulse, the emitted photons of the conjugated polymer are collected and guided by two convex lenses (**C**) into the narrow slit of a spectrograph (Chromex250is) (**D**), which separates the incident light into its different wavelengths by means of a grating. The photons, then, reach the photocathode (**E**) of the streak camera system (**F**), where they are converted into a number of electrons proportional to their intensity. The photogenerated electrons pass through a pair of sweep electrodes (**H**), across which a time-

dependent electric field is applied, and interact with this field perpendicular to the propagation direction and perpendicular to the spectrograph dispersion, resulting in a time-dependent spatial deviation of the electrons in the direction of the electric field.¹⁰⁰ These accelerated electrons enter then the micro channel plate (MCP) (**I**) at slightly different times and slightly different angles, where the electrons are multiplied several thousands of times and then are bombarded against a phosphor screen (**J**).

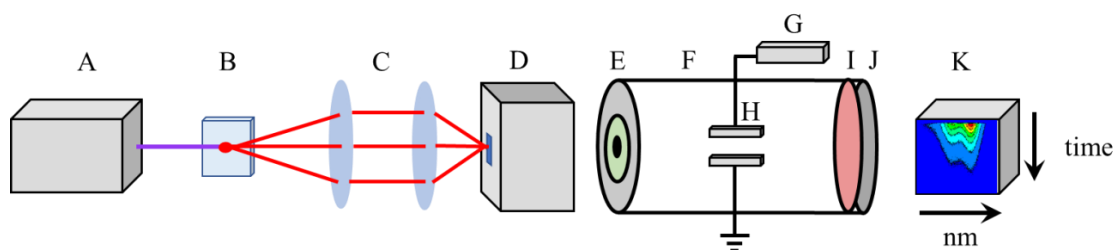


Figure 2.2. Schematic representation of TRPL experimental set-up using streak camera system. A: Ti:Sapphire laser, B: Sample, C: Optics, D: Spectrograph, E: Photocathode, F: Streak Camera System, G: Delay unit, H: Accelerating electrodes, I: MCP, J: Phosphor screen, K: CCD.

There, the electrons are converted again into light. In this way, the streak camera converts the changes in the temporal and spatial light intensity of the incident photons, emitted by the sample, into an image showing the brightness distribution on the phosphor screen, where the vertical direction on the phosphor screen serves as the time axis and the horizontal direction as the wavelength axis of the incident light. An example of the obtained contour plot is shown in Figure 2.3a. To readout the images from the streak camera a charge-coupled device (CCD) (**K**) was used along with the HPD-TA 8.30 software.

Another crucial component in order to measure high-speed phenomena using a streak camera is a trigger section, which applies a high voltage on the electric field at a timing synchronized to incident light. Therefore, the electric field is triggered by a streak sweep initiated when the emitted photons being measured arrive at the streak camera (photocathode) and the corresponding electrons experience accelerations in the electric field. For this purpose, a delay unit (**G**) is used, which controls for how long the trigger signal, which initiates the streak sweep, is delayed.¹⁰⁰

2.4. Analysis of TRPL experimental data

The determined TRPL data is exported as a contour plot, as shown in Figure 2.3a for a pristine BEH-PPV thin film measured at room temperature. Thus, the data set enables a 3D analysis of the photophysical processes present in the conjugated polymer. The horizontal axis contains the emission wavelength data, the vertical axis represents the time-dependent emission, and the PL intensity is defined by the color scale. With these, we can collect for each horizontal line a specific time-dependent PL spectrum, while each vertical line gives us the PL decay at specific wavelength. In the scope of this thesis, the PL spectra were collected at decay time zero (black line in Figure 2.3a), indicated by the PL decay maximum, and the PL decay times were collected at the polymer luminescence maximum (red line in Figure 2.3a). In BEH-PPV this is between 580–600 nm. The determined PL decay trace and spectrum is shown in Figure 2.3b.

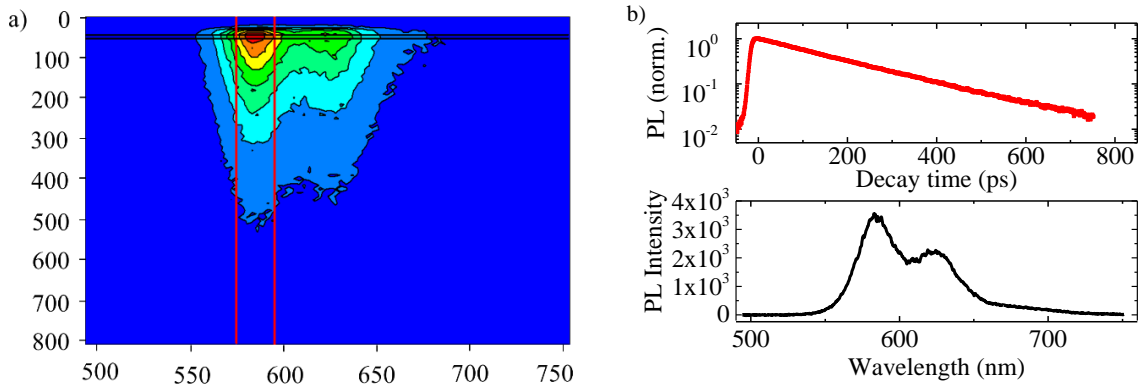


Figure 2.3. (a) Contour plot of neat BEH-PPV thin film determined from TRPL spectroscopy with (b) associated PL decay trace at luminescence maximum and PL spectrum at time zero.

To determine the exciton lifetime, the polymer luminescence decay curve $I(t)$ is fit to an exponential decay function (Origin Pro 9.1) and the weighted average exciton lifetime τ_{av} was calculated using the following equation:

$$\tau_{av} = \langle t \rangle = \frac{\int_0^{\infty} tI(t)dt}{\int_0^{\infty} I(t)dt} = \frac{\sum_i a_i \tau_i^2}{\sum_i a_i \tau_i} \quad (2.4)$$

where a_i is the preexponential factor and τ_i is the time constant of multi-exponential decays.

The above described method is one way to analyze the TRPL data and to determine the exciton lifetimes in conjugated polymers. Another way to look at the data is the global analysis scheme. The first method is sufficient in cases where the decay traces are similar at all wavelengths. However, in some cases, the decay traces differ due to processes such as energy transfer. In order to consider these effects, the latter method is used. Therefore, the global analysis scheme takes into account the decay dynamics across the entire spectral range with respect to the exponential fitting, where the PL decay traces were collected only at the polymer

luminescence maximum ($\Delta\lambda = 20$ nm). Thus, with the global analysis a more comprehensive analysis of the TRPL data is enabled, which was required for the analysis of the temperature-dependent TRPL data (Chapter 4), since at low temperatures additional energy transfer processes are present in the investigated PPV-derivatives. As discussed in more detail in Chapter 4, in BEH-PPV energy-transfer processes from shorter to longer conformational subunits take place with decreasing temperatures, which lead to additional non-radiative decay. Therefore, the exciton lifetime determined from global analysis is shorter (~ 400 ps) at 77 K than the one determined from a single exponential fit (~ 500 ps). In the case of SY-PPV, energy transfer to conformational subunits exhibiting longer decay rates takes place at lower temperatures, leading to different temperature-dependent PL lifetimes in SY-PPV depending on the emission wavelength. Thus, global analysis results in a more reliable value of the exciton lifetime measured at lower temperatures, since it takes into account the decay dynamics of the whole emission wavelengths as well as additional energy-transfer processes that contribute more with decreasing temperature.

Using global analysis, the exciton lifetimes in the conjugated polymers is determined with a two-kinetic component fitting, which gave the lifetimes and relative amplitudes extracted from a fast and slow exponential contribution. The measured exciton lifetime (τ_{av}) is then determined from a weighted average (Eq.2.4). The results of the two-component fitting are discussed comprehensively in Chapter 4.2 and are summarized in Table 4.1 and 4.2.

Global analysis of the temperature-dependent TRPL data (Chapter 4) was done using the R-package TIMP software with the graphical interface Glotaran 1.5.1.^{101,102} The Glotaran software is an open-source software and can be downloaded from the internet.¹⁰³

2.5. Fluorescence quenching measurements

Fluorescent quenching experiments of thin polymer films with randomly distributed exciton quencher molecules (PCBM) were implemented to determine the exciton diffusion coefficient D and exciton diffusion length L_D in the conjugated polymer.^{61,91-94} This method has the crucial advantage of a relative simple sample preparation and analysis, which can be done either by using the Stern-Volmer equation for monoexponential PL decays (Chapter 2.6) or by Monte-Carlo simulation for biexponential decays (Chapter 2.7). With the extracted value of D the exciton diffusion length L_D can be calculated, which is the average distance excitons can diffuse during their lifetime τ_f .

$$L_D = \sqrt{\tau_f D} \quad (2.5)$$

As an example, the PL quenching results of BEH-PPV will be presented here before the analysis of the quenching experiments will be described in the next chapters. The polymer and polymer:PCBM blend solutions and films were prepared as described in Chapter 2.2, and then TRPL was carried out with this samples. Figure 2.4a demonstrates the PL decay time of BEH-PPV in a diluted chlorobenzene solution (1 mg/mL, black circles), in a pristine thin film (red squares) and in a thin film mixed with various content of PCBM molecules (blue triangles = 0.05% v_{frac} PCBM; pink stars = 0.1% v_{frac} PCBM; green diamonds = 0.2% v_{frac} PCBM). The PL decay times were collected at the polymer luminescence maximum (580–600 nm), as described in Chapter 2.4. Figure 2.4b shows the normalized PL spectra of the diluted BEH-PPV chlorobenzene solution and the pristine thin film collected at decay time zero.

In BEH-PPV the exciton lifetime in diluted solution is significantly longer than the one in the pristine thin film. This observation is found in many other organic semiconductors due to different polymer chain packing, as discussed in Chapter 1.3.2. Furthermore, it is seen in Figure 2.4a that the higher the density of PCBM molecules the shorter are the PL decay times, since the excitons reach a quenching site faster and thus non-radiative decay is more probable. This is consistent with the exciton diffusion-limited quenching model. The PL spectra (Figure 2.4b) of the thin film shows a bathochromic shift with respect to the diluted solution, which is assigned to the formation of *interchain* species.¹⁰⁴

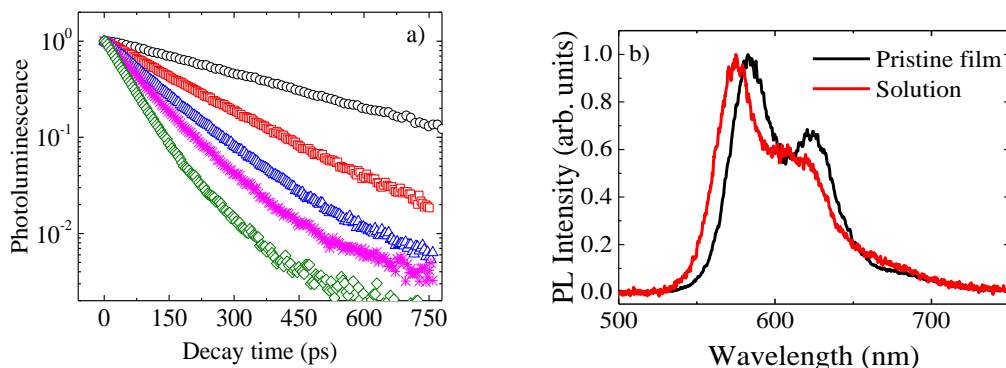


Figure 2.4. (a) PL quenching measurements of BEH-PPV in a diluted solution (black circles), in a pristine thin film (red squares), in a blend with 0.05% v_{frac} PCBM (blue triangles), in a blend with 0.1% v_{frac} PCBM (pink stars) and in a blend with 0.2% v_{frac} PCBM (green diamonds), respectively. (b) associated PL spectra of the diluted solution and pristine thin film collected at decay time zero.

2.6. Stern-Volmer equation

In the case of a single exponential PL decay, the exciton diffusion coefficient D can be extracted from the PL quenching experimental data using the Stern-Volmer equation:^{61,75}

$$\frac{1}{\tau} = \frac{1}{\tau_f} + 4\pi r D c \quad (2.6)$$

where τ is the measured PL decay time of the polymer film mixed with a certain concentration of PCBM c and τ_f the measured exciton lifetime of the pristine polymer film, respectively, and $r = r_e + r_q$ is the sum of the exciton (r_e) and PCBM (r_q) radii that is set to be around 1 nm.^{61,91} The Stern-Volmer equation describes a simple relation between the measured exciton lifetime τ and the quencher concentration (PCBM). Figure 2.5 shows the reciprocal exciton lifetime τ^{-1} versus the PCBM concentration in BEH-PPV:PCBM blends (symbols).

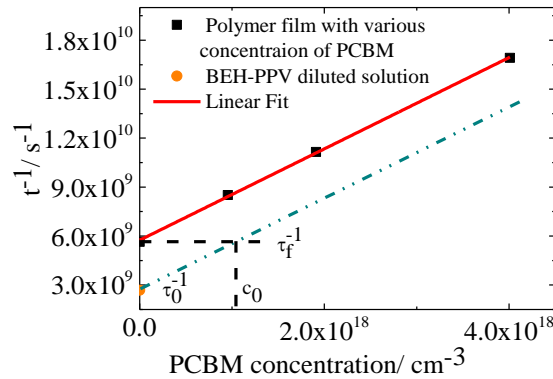


Figure 2.5. Stern-Volmer plot of BEH-PPV:PCBM blends. The experimental data points (symbols) are fitted (red solid line) with Eq. 2.6. The concentration of exciton quenching sites c_0 in pristine polymer films can be accounted for by shifting the Stern-Volmer plot along the abscissa (green dash-dotted line). The cross-points with the ordinate correspond to the measured exciton lifetime τ_f^{-1} and intrinsic exciton lifetime τ_0^{-1} in the pristine film and diluted solution, respectively.

By fitting the experimental data with the Stern-Volmer equation (red solid line) the exciton diffusion coefficient can be determined from the slope. In BEH-PPV an exciton diffusion coefficient D of $2.2 (\pm 0.1) \times 10^{-3} \text{ cm}^2/\text{s}$ is obtained.

The Stern Volmer equation can also be used to estimate the concentration of background quenching sites c_0 that are already present in conjugated polymers. The total concentration of exciton quenchers q is set to:

$$q = c + c_0 \quad (2.7)$$

Assuming that the exciton quenching efficiency is equal for PCBM and the background exciton quenching defects, substitution of (2.7) into (2.6) yields:

$$\frac{1}{\tau} = \frac{1}{\tau_f} - 4\pi r D c_0 + 4\pi r D q \quad (2.8)$$

If there were no exciton quenching defects present in the pristine film, then the PL decay time in such a film would correspond to the intrinsic exciton lifetime τ_0 . By setting $q = 0$ in (2.8), we get the following expression:

$$\frac{1}{\tau_0} = \frac{1}{\tau_f} - 4\pi r D c_0 \quad (2.9)$$

With the intrinsic exciton lifetime τ_0 , which can be approximated by the PL decay time in a diluted solution, the concentration of the background exciton quenchers can be calculated using

Eq. 2.10. We note that this assumption does not generally apply to all conjugated polymer systems (See also Chapter 3.2).

$$c_0 = \frac{I}{4\pi r D} \left(\frac{1}{\tau_f} - \frac{1}{\tau_0} \right) \quad (2.10)$$

Using the PL decay of the diluted solution for BEH-PPV a value of $c_0 = 1 \times 10^{18} \text{ cm}^{-3}$ is then obtained for the exciton quenching defect concentration. It is important to note that the Stern-Volmer equation is only valid for polymers that exhibit monoexponential PL decays

2.7. Monte Carlo Simulations

In the case of organic semiconductors that exhibit non-monoexponential PL decays a simulation based on Monte Carlo (MC) was applied to extract the exciton diffusion parameters. The simulation was developed by Mikhnenko et al. and can be downloaded from the internet.^{91,105,106}

In order to model the PL decay in semiconductor-quencher mixtures, the simulation considers a cubic box of 50x50x50 nm. Quencher molecules (PCBM) are distributed within this box according to the desired concentration (volume fraction) and morphology. The PCBM molecules are approximated as balls of 1 nm in diameter,⁹¹ and are assumed to have a homogeneous random distribution without overlapping of the quencher molecules. The periodic boundary conditions are imposed to the simulation box to mimic an infinitely large medium. Then the excitons, which are described as a sphere with a diameter of 1 nm,⁹¹ are placed at a random position in the simulation box, provided to be non-interacting with each other. The exciton lifetime is defined by the (multi)exponential distribution in accordance with the measured PL decay time of the pristine film (Eq. 2.4).

The use of this simulation to model the exciton diffusion is justified at room temperature, when exciton hopping in conjugated polymers can be described by normal diffusion, and in accordance with Einstein's theory of random walks normal diffusion can be modeled as a random walk with a constant exciton hopping distance (hopsizel).^{91,107-110} Therefore, for each iteration time δt every exciton is moved in a random 3D direction for a fixed distance δs , which correlates with the exciton diffusion coefficient as follows: $D = \delta s^2/6\delta t$. For each generation the motion of 1×10^4 excitons were modeled. If the excitons touch a quencher molecule at the new position, then they are considered to be quenched. This process is iterated until all excitons are quenched or undergo radiative decay. A Boolean 3D grid of 0.05 nm pitch size is superimposed with the simulation box, where each 3D cell of the grid is given the value *true* or *false* if the exciton overlaps or not with a PCBM molecule. A Mersenne twister algorithm was used as a pseudo-random number generator in the Monte Carlo simulation.^{111,112}

As a result, the simulation provides the number of radiatively decayed excitons versus time, ultimately modeling a PL decay trace. Further, the relative quenching efficiency is calculated using the ratio between the number of radiatively decayed excitons and the total number of excitons that were put into the simulation box. The modeled relative quenching efficiency is compared with the measured one that was defined at the beginning of the simulation as follow:

$$Q = 1 - \frac{\int dt PL_{blend}}{\int dt PL_{pristine}} = 1 - \frac{\tau_{blend}}{\tau_{pristine}} \quad (2.11)$$

The simulation is repeated with adjusted exciton hopping distance δs until the modeled PL decay coincides with the experimentally measured one for the specific concentration of PCBM.⁹¹ With

the final δs the exciton diffusion coefficient D can be calculated. Therefore, in principle, only two thin films are needed to determine D , which is the pristine semiconductor and the same semiconductor with homogeneously distributed exciton quenchers of known concentration. To obtain a more significant value for D , in the scope of this thesis, usually three semiconductor:PCBM blends were measured and D was determined from the average of these three blends as well as the associated standard deviation.

The reliability of the Monte Carlo simulation method was verified on BEH-PPV to reproduce the exciton diffusion coefficient that was determined by the Stern-Volmer equation (Chapter 2.6). From the MC simulations a nearly identical exciton diffusion coefficient of $2.0 (\pm 0.1) \times 10^{-3} \text{ cm}^2/\text{s}$ was found. The MC simulated PL decays for BEH-PPV and SY-PPV are shown in Figure 2.6 (red lines), which are in excellent agreement with the experimental ones (black squares) until about 80–90% of the excited states have decayed. On a linear plot (inset in SY-PPV PL decay, right image) this deviation is not visible. At this time the PL decay becomes multi-exponential, and this effect is more pronounced the higher the amount of PCBM molecules. A possible explanation is some small concentration of interchain coulombically bound electron-hole polaron pairs are also formed upon photoexcitation.¹¹³⁻¹¹⁵ The larger the generation number, the smoother is the modeled PL decay, while the simulation time increases significantly with increasing generation number. Therefore, an appropriate generation number of 1000 and 4000 were chosen for BEH-PPV and SY-PPV, respectively, and then the simulated decay times were smoothed using Savitzky-Golay method, points of window 20.

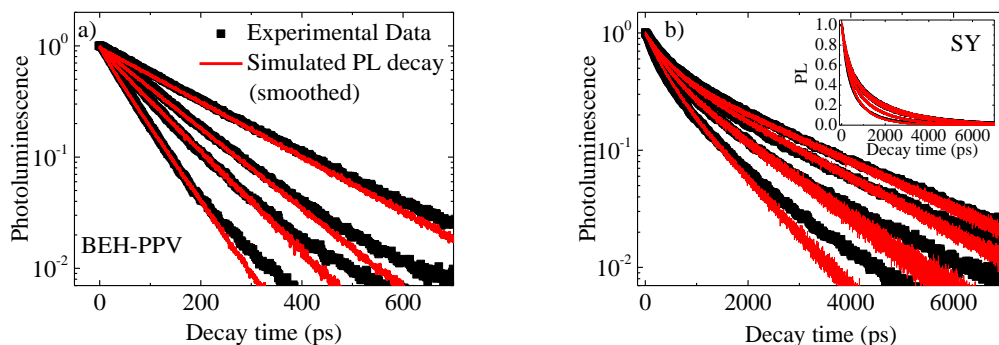


Figure 2.6. Measured (black squares) and simulated (red solid lines) PL decays for narrow σ polymer BEH-PPV (a) and broader σ Polymer SY-PPV (b). The y-axis is plotted in log10 scale. In the inset of SY-PPV plot the linear simulated PL decay based on Monte Carlo is seen.

The MC simulation provides a time-averaged value of D , which in the case of a biexponential decay does not describe the ‘real’ D properly. A more significant value would be a time-dependent D consisting of two diffusion coefficients,¹¹⁶ the hot exciton diffusion right after the excitation (D_h) and the exciton diffusion coefficient of thermalized excitons (D_0). To determine a time-averaged value of D , Mikhnenko adjusted the Monte Carlo simulation.⁶¹ However, since this approach is more time intensive and the time-averaged D results are in a good approximation of the real value, in the scope of this work the time-average method is utilized. The deviation between the time-averaged and time-dependent value of D is shown for MEH-PPV, where the time-dependent D is in the range of $1.48\text{--}1.97 \times 10^{-3} \text{ cm}^2/\text{s}$ for different intrinsic exciton lifetimes,⁶¹ while the time-averaged D is $1.1 \times 10^{-3} \text{ cm}^2/\text{s}$, as determined in Chapter 3.

In addition, the Monte Carlo simulation can be applied to determine the concentration of exciton quenching-sites (background quencher), as described elsewhere,⁶¹ as well as in Chapter 5, where the concentration of hole traps was determined.

2.8. PLQY

For the PL quantum yield measurements (Chapter 3), a 15 cm diameter integrating sphere (Labsphere), coated with Spectralect, was used. To measure the flux of the PL at the exit port a calibrated silicon photodiode (Labsphere SDA-U) was used, the photocurrent was measured with a Keithley electrometer. The PLQY measurements on the PPV derivatives reported in Chapter 3 were done in the previous laboratory of Prof. ██████.

2.9. Polymer light-emitting diodes

2.9.1. PLED device fabrication

Upon the glass substrate with patterned ITO layer was cleaned and treated with UV-ozone, as described in Chapter 2.2, PEDOT:PSS (Heraeus CleviousTM Al 4083) was spin-coated (60 s 1200 rpm; 20 s 4000 rpm) on top of the substrate (55 nm). On top, a layer of the active material was spin-coated in nitrogen atmosphere, while the experimental conditions are summarized below. Then a thin layer of the cathode (Ba 5 nm) was thermally evaporated on top of the polymer layer (chamber pressure 10^{-7} mbar), followed by a 100 nm thick aluminum layer, which prevents oxidation of the barium. The final PLED device structure is glass/ITO/PEDOT:PSS/PPV/Ba/Al.

The SY-PPV-based PLED (Chapter 4), was fabricated by ██████ from a 5.5 mg/mL toluene solution (20 s 1000 rpm; 60 s 250 rpm) and the PPV film thickness was

100 nm. The BEH-PPV PLED (Chapter 4) was prepared by [REDACTED] from a 5.2 mg/mL chlorobenzene solution and spin-speeds of 1000 rpm for 60 s followed by 4000 rpm for 30 s, yielding to a layer thickness of the BEH-PPV of 165 nm. The BEH-PPV PLED in Chapter 5 was prepared by [REDACTED] using a 4.9 mg/mL chlorobenzene solution and spin-speeds of 1000 rpm for 60 s followed by 4000 rpm for 30 s, which results into a 200 nm thick BEH-PPV layer.

2.9.2. PLED current efficiency and EL spectra

The current efficiencies were measured with a Keithley 2400 source meter in nitrogen atmosphere by [REDACTED] (SY-PPV PLED, Chapter 4), [REDACTED] and [REDACTED] (Chapter 4, BEH-PPV PLED). The electroluminescence spectra of the BEH-PPV based PLED (Chapter 4) were measured with an Ocean optics (USB4000-UV-Vis-ES) spectrometer by [REDACTED] and [REDACTED].

2.9.3. PLED device stressing

The BEH-PPV PLED device was measured by [REDACTED] (Chapter 5) with a Keithley 2400 source meter in nitrogen atmosphere and stressed for 211 hours under a constant current density of 35 mA/cm². After stressing, the degraded PLED devices were transferred into a home-made air-tight sample holder, which maintains the inert nitrogen atmosphere during the optical measurements. The PLED was photo-excited through the glass/ITO/PEDOT:PSS side of the device.

2.10. BEH-PPV Synthesis

BEH-PPV was synthesized via Gilch synthesis by [REDACTED] as follows: 8.76 g (16.8 mmol) 1,4-bis(bromomethyl)-2,5-bis(2-ethyl-hexyloxy)benzene (premonomer) was dissolved in 500 mL dry, degassed tetrahydrofuran (THF) in a 1-L three necked flask and cooled down to -95 °C under Ar. In a second flask a base solution of 9.28 g (82.7 mmol) potassium *tert*-butoxide was dissolved in 55 mL dry, degassed THF and also cooled down to -95 °C under Ar. Under vigorous stirring, the base solution was added to the premonomer solution via syringe in order to maintain the Ar atmosphere. The reaction mixture was left to warm up to room temperature over 5 hours. After 24 hours of total stirring time, the flask was equipped with a reflux condenser and the reaction mixture heated to reflux for 24 hours. Subsequently the polymer was precipitated in 3 L methanol, filtered off and dried. The resultant solid was dissolved in 700 mL degassed chloroform to give a concentration of 7 mg/mL. The polymer solution was again heated to reflux for 48 hours, precipitated in methanol, filtered off, and dried. 4.66 g of a red compact solid is obtained with 77% yield. GPC-MALLS (THF, 30 °C): $M_w = 640370$ g/mol, $M_n = 293120$ g/mol, $D = 2.18$.

Chapter 3. Influence of energetic disorder on the exciton lifetime and photoluminescence quantum yield in conjugated polymers

Using time-resolved photoluminescence (TRPL) spectroscopy the exciton lifetime in a range of conjugated polymers is investigated. For poly(*p*-phenylenevinylene) (PPV)-based derivatives and a polyspirobifluorene copolymer (PSBF) we find that the exciton lifetime is correlated with the energetic disorder. Better ordered polymers exhibit a single exponential PL decay with exciton lifetimes of a few hundred picoseconds, whereas polymers with a larger degree of disorder show multi-exponential PL decays with exciton lifetimes in the nanosecond regime. These observations are consistent with diffusion-limited exciton quenching at non-radiative recombination centers. The measured PL decay time reflects the time that excitons need to diffuse towards these quenching sites. Conjugated polymers with large energetic disorder and thus longer exciton lifetime also exhibit a higher photoluminescence quantum yield due to the slower exciton diffusion towards non-radiative quenching sites.*

*I. Rörich, O. V. Mikhnenko, D. Gehrig, P. W. M. Blom, N. I. Crăciun, *J.Phys.Chem.B* **2017**, *121*, 1405–1412.

3.1 Introduction

One of the main processes in organic photovoltaics (OPVs) is the diffusion of excitons towards the donor/acceptor interface. Here the excitons form a spatially separated electron-hole pair, which subsequently dissociates into free charge carriers that generate the photocurrent.^{2,47} A long exciton diffusion length is preferred since it will strongly facilitate the demands on the blend morphology and processing conditions. A long exciton diffusion length is typically accompanied by a long exciton lifetime, such that the exciton can reach the electron donor/acceptor interface before decaying to the ground state. The exciton lifetime of organic semiconductors is therefore an important parameter to be optimized.

As described in Chapter 1.3, singlet excitons are the dominant species created upon the absorption of a photon in conjugated polymers, which undergo migration among conjugated segments via energy transfer in the Gaussian density of states (DOS). The generated excitons are initially delocalized over several conformational subunits on a sub-100 femtoseconds (fs) time scale until they become localized by dynamic coupling between the nuclear and electronic degrees of freedom.^{21,117} The subsequent energy transfer then proceeds on much longer time scales. Interchain transfer between conformational subunits that are physically located within the Förster radius occur in a time range of a few picoseconds (ps) and exciton diffusion along the polymer backbone is found to occur in tens to hundreds of picoseconds.^{21,59,118}

To estimate the natural singlet exciton lifetime τ_n the inverse Einstein coefficient A_{21} for spontaneous emission can be used:

$$\tau_n = 1/k_r = 1/A_{21} \quad (3.1)$$

Theoretical estimations of the natural exciton lifetime have been done for the small molecule tetracene, leading to a singlet exciton lifetime of about 60 nanoseconds (ns).¹¹⁹ However,

experimentally determined values of the exciton lifetime of organic semiconductors range from hundreds of picoseconds to a few nanoseconds.^{63,70,120-122} Next to the radiative decay with rate k_r singlet excited states can also decay via non-radiative decay routes with a rate k_{nr} due to molecular vibrations, which are competing loss processes. As a result, the intrinsic exciton lifetime τ_0 of the excited states is given by

$$\tau_0 = 1/(k_r + k_{nr}) \quad (3.2)$$

Since the exciton migration in conjugated polymers is most likely trap limited rather than transfer rate limited,⁶⁰ as discussed in Chapter 1.3.3, consequently, during the hopping process an exciton can reach a conjugated chain segment containing recombination centers and traps, where it can decay either radiatively or non-radiatively.⁴⁵ When defects play a role, then also the diffusion towards these quenching sites should play a role. In that case the measured exciton lifetime τ_f in thin polymer films can be expressed as follows,

$$\tau_f = 1/ (k_r+k_{nr}+k_{diff}) \quad (3.3)$$

taking into account the non-radiative decay rate related to exciton quenching at defect sites due to exciton diffusion with a rate k_{diff} . Analytical models and Monte Carlo (MC) simulations have been reported in literature regarding the influence of energetic disorder on the exciton diffusion length,^{60,106,123} but there are few experimental investigations on the exciton lifetime. We have investigated the exciton dynamics in four PPV-based derivatives with varying energetic disorder by using time-resolved photoluminescence spectroscopy (TRPL) on spin-coated thin films. We demonstrate that the exciton lifetime increases by one order of magnitude with

increasing energetic disorder. Furthermore, the broader the Gaussian DOS the more pronounced is the non-monoexponential PL decay. The highly disordered organic semiconductors exhibit a high photoluminescence quantum yield (PLQY) that is attributed to the slow exciton transport towards non-radiative quenching centers. In contrast, polymers with less energetic disorder have shorter exciton lifetimes due to faster exciton diffusion to defects, combined with lower PLQYs.

3.2. Results and Discussion

3.2.1. Exciton lifetime in PPV derivatives

The half-width of the excitonic (optical) Gaussian density of states σ in conjugated polymers is usually approximately 2–3 times smaller than the half-width of the charge carrier (electrical) DOS extracted from charge transport measurements.⁴⁴ However, in comparison to the J - V measurements a direct determination of the excitonic DOS is long-winded, since the photophysical processes in conjugated polymer films are governed by the creation of intra- and interchain excitations. For that reason we take as a measure for the energetic disorder in the PPV derivatives the width of the charge carrier Gaussian DOS σ that was determined to be 0.092–0.140 eV by charge transport measurements going from BEH-PPV, to MEH-PPV, NRS-PPV and SY-PPV, respectively.⁷ From the depicted chemical structures in Figure 3.1 (and Chapter 2.7), it is seen that BEH-PPV has two symmetrical alkoxy side chains and thus the configurational freedom of the individual chains is limited compared to MEH-PPV that exhibits unsymmetrical side chains, resulting in a decreased energetic spread between electronic levels of individual chain segments.

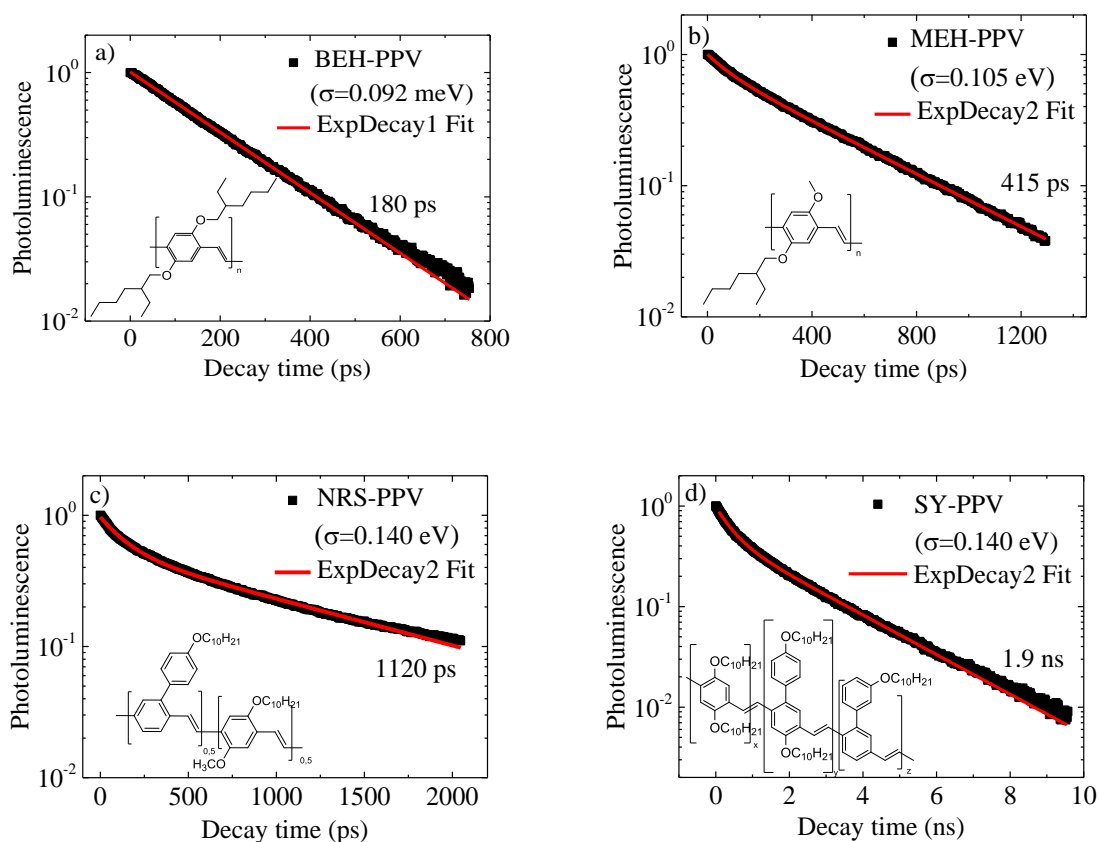


Figure 3.1. Normalized PL decay curves and chemical structures for a series of PPV derivatives. The experimental data (black squares) are fitted either single or biexponential (red lines) with regard to the PL decay curve. The exciton lifetimes have been determined by equation (2.3).

Therefore, the better ordered polymer BEH-PPV has a reduced width of the Gaussian charge carrier DOS (0.092 eV). In contrast, the random copolymers NRS-PPV and SY-PPV exhibit more structural disorder due to more configurational freedom of individual conformational subunits, leading to a larger σ as compared to the other two polymers.

In Figure 3.1 the normalized PL decays of the four pristine PPV derivatives in a thin film at room temperature are shown. The less energetically distributed polymer BEH-PPV

($\sigma=0.092$ eV) shows a single exponential PL decay with a very short exciton lifetime of about 180 ps. In contrast, polymers with a relatively larger degree of disorder such as NRS-PPV ($\sigma=0.125$ eV) or SY-PPV ($\sigma=0.140$ eV) exhibit non-monoexponential PL decay dynamics. Remarkably, a significant enhancement of the exciton lifetime of one order of magnitude is observed with increasing disorder going from BEH-PPV to SY-PPV (180 ps versus 1.9 ns). Since the backbone of the PPV derivatives is chemically identical and the exciton transfer takes place between the conformational subunits generated from conjugation breaks along the backbone,^{20,63} one may ask where this significant change in exciton lifetime and decay originates from.

As described in Chapter 1.3, upon the absorption of a high energy photon, singlet excitons are generated at an arbitrary energy-site within the high-energy tail of the Gaussian DOS and simultaneously undergo downhill migration towards lower energy-sites,^{23,41,42} until they, eventually, approach quasi-equilibrium at $\sim -\sigma^2/kT$ below the center of DOS,^{22,44} provided that the time needed to reach equilibrium energy is shorter than the intrinsic exciton lifetime. At room temperature the spectral diffusion is followed by temperature activated hopping. In a less disordered conjugated polymer as BEH-PPV the higher energy states of the DOS to which the exciton is typically excited are close to the center of the distribution, where the probability to find a nearby energy-site is very high. Furthermore, due to the narrow σ also the equilibrium level at $-\sigma^2/kT$ with the most populated states is close to the center of the DOS. As a result, after only a few downward jumps the exciton already reaches this quasi-equilibrium state, where thermally activated hopping interplays with downward jumps at room temperature. Since finding a near neighbor is highly probable, fast energy transfer between the conformation subunits proceeds, resulting in fast exciton diffusion. As a consequence, in the less energetically

disordered BEH-PPV the exciton diffusion can be described by quasi equilibrium transport following the $\sigma < 3kT$ criterion.^{124,125}

In a more disordered polymer ($\sigma > 3kT$) as SY-PPV, however, the process of downhill migration is slower and cannot be neglected. There, excitons predominantly undergo downward jumps toward energy-sites that are further away from the center of the DOS. This process can be described by non-equilibrium hopping transport, which has been reported for low temperatures.^{126,127} Eventually, excitons reach thermal equilibrium state or decay due to its finite lifetime to the ground state. Since the thermal equilibrium state $-\sigma^2/kT$ shifts for increasing disorder strength σ deeper into the tail states of the Gaussian DOS, the probability to find a nearby energy-site to which a jump is probable decreases noticeably. Therefore, the measured excitation lifetime depends on the coupling strength between the energy sites and on the starting singlet excitation energy within the DOS.¹²⁵ As a result, in less ordered polymers the diffusion of hot excitons is initially fast, followed by slower transport of thermalized excitons via thermally activated hopping.

The observed simultaneous occurrence of a short monoexponential PL decay for more ordered polymers as BEH-PVV and a longer PL decay with a non-monoexponential decay for disordered polymers is consistent with diffusion-limited exciton quenching. In a better-ordered polymer with narrower width of the Gaussian DOS, excitons have a high probability to jump to a nearby energy-site leading to fast exciton diffusion towards quenching defects. Since the transport occurs under quasi equilibrium conditions, a single exponential PL decay is obtained. In contrast, polymers that are more disordered exhibit a biexponential PL decay that is ascribed to an initial fast exciton diffusion followed by a slower migration via thermally activated hopping towards quenching defects, resulting in a much longer PL decay time. As a result, the measured PL decay times do not represent the intrinsic exciton lifetime of these polymers, but

rather the time an exciton needs to find a quenching center. The origin of these non-radiative quenching centers is, as discussed in Chapter 1.3.3, not totally understood but ascribed to impurities and morphological and chemical defects.

3.2.2. Exciton diffusion

In order to obtain more quantitative information about the spatial and temporal evolution of the singlet exciton population we determine the exciton diffusion coefficient for the series of PPV derivatives by investigating fluorescence quenching of thin polymer films with randomly distributed exciton quencher molecules, such as PCBM.^{61,91,93,94} Therefore, either the Stern-Volmer equation for monoexponential PL decays (see Chapter 2.3.1) or the Monte-Carlo simulation for biexponential decays (see Chapter 2.3.2) was used to model the experimental data. As demonstrated in Figure 2.2a, the PL decay time of BEH-PPV in a diluted chlorobenzene solution (370 ps) is significantly longer than the one in the pristine thin film (180 ps). This observation is found in many other organic semiconductors due to different polymer chain packing (see also Chapter 1.3.2). A one order of magnitude higher energy transfer rate is reported in thin polymer films with respect to the intrachain transfer in diluted polymer solutions originating mainly from larger electronic coupling matrix elements between closely lying polymer chains.^{49,50} In a diluted solution the polymeric chains are well isolated by the solvent molecules and the exciton diffusion is attributed to pure intrachain hopping leading to longer exciton lifetimes. When we assume that the exciton transport is diffusion-limited quenching rather than transfer rate limited, the decreased exciton lifetime in thin polymer films can be ascribed to the higher probability of the excitons to encounter quenching sites faster with regard to the one in solution. Furthermore, it is seen in Figure 2.2a that the higher the density of PCBM

molecules the shorter are the PL decay times, since the excitons reach a quenching site faster and non-radiative decay is more probable.

The modelling of the well-ordered polymer BEH-PPV using the Stern-Volmer equation (Eq. 2.6) is demonstrated in Chapter 2.3.1, leading to an exciton diffusion coefficient D of $2.2 \times 10^{-3} \text{ cm}^2/\text{s}$. For the organic semiconductors that exhibit non-monoexponential PL decays the Monte Carlo simulation is applied (see Chapter 2.3.2) to extract the exciton diffusion parameters. The MC simulated PL decays for BEH-PPV and SY-PPV are shown in Figure 2.4.

With the extracted D for the various polymers the exciton diffusion length L_D was calculated using Eq. 2.2. The determined exciton diffusion parameters are summarized in Table 3.1. The exciton lifetime increases by one order of magnitude accompanied by an increase of the energetic disorder in the conjugated polymer and is correlated to a decrease of the exciton diffusion coefficient, respectively.

Nevertheless, an energetic disorder independent exciton diffusion length of 6–7 nm is observed. These results are consistent with an exciton lifetime that is limited by the diffusion towards quenchers. The short PL decay time in better ordered polymers is ascribed to fast exciton diffusion towards non-radiative quenching sites represented by a high exciton diffusion coefficient. In contrast, polymers that are more-disordered exhibit slower exciton diffusion towards traps and thus much longer exciton lifetimes, provided that a wide range of conjugated polymers have a nearly equal amount of defect sites (10^{23} – 10^{24} per m^{-3}), as reported by Nicolai et al.⁶²

Table 3.1. Determined exciton diffusion parameters using Monte Carlo Simulation for a series of PPV derivatives and a PSBF copolymer in dependence of their energetic disorder. For multi-exponential decays τ_{av} was determined by equation (2.3).

Polymer	DOS width σ (eV)	Exciton lifetime τ_{av} (ns)	Exciton diffusion coefficient D (cm^2/s)	1D exciton diffusion length L_D (nm)
BEH-PPV	0.092	0.18	2.0×10^{-3}	6.0
MEH-PPV	0.105	0.42	1.1×10^{-3}	6.8
NRS-PPV	0.125	1.12	3.0×10^{-4}	5.8
SY-PPV	0.140	1.92	2.2×10^{-4}	6.4
PSBF	0.150	2.5	1.6×10^{-4}	6.3

Another interesting model compound to study exciton lifetimes is the blue-emitting copolymer polyspirobifluorene (PSBF). The chemical structure of the PSBF copolymer is shown as inset in Figure 3.2 (and in Chapter 2.7), where polyspirobifluorene (m) is randomly copolymerized with a polyfluorene unit (n). The polymer backbone consists of a polyfluorene backbone and exhibits at the 9-position either a spiro-linkage to a substituted fluorene unit with four alkoxy side chains (m) or two substituted phenyl groups (n). Through the spiro-linkage the substituted fluorene group is rigidly perpendicular to the polymer backbone, whereby in the case of the "broken" spiro-linkage the carbon in the 9-position is tetrahedron and thus not perpendicular to the backbone anymore. The PSBF copolymer exhibits a high structural disorder due to more configurational freedom of individual conformational subunits leading to a consequently larger

σ . From charge transport studies it was found that PSBF based polymers exhibit a very large energetic disorder σ in the range of 0.150–0.160 eV.¹²⁸

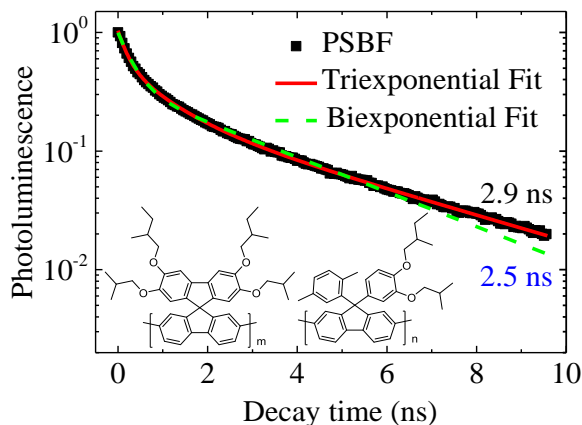


Figure 3.2. Normalized PL decay curve of polyspirobifluorene (PSBF) in a thin film with chemical structure. The experimental data (black squares) are fitted by a bi- and triexponential fit, respectively (blue dashed line, solid red line).

Thus, the energetic disorder of PSBF exceeds the one of SY-PPV ($\sigma=0.140$ eV), where an exciton lifetime of 1.9 ns was found (Figure 3.1). As a result, for diffusion-limited quenching an even longer exciton lifetime for PSBF is expected. Figure 3.2 shows the PL decay time of the PSBF copolymer. A non-monoexponential PL decay with a long exciton lifetime exceeding 2 ns is observed. Using a tri-exponential fit and equation (2.3) an exciton lifetime of 2.9 ns is obtained.

In order to see whether this long exciton lifetime is correlated to the strong energetic disorder by means of slow exciton diffusion also the exciton diffusion coefficient was determined. As before with the PPV derivatives, randomly distributed PCBM exciton quenchers are used.

Figure 3.3 shows the measured PL decays as a function of PCBM quencher concentration, together with the MC simulations.

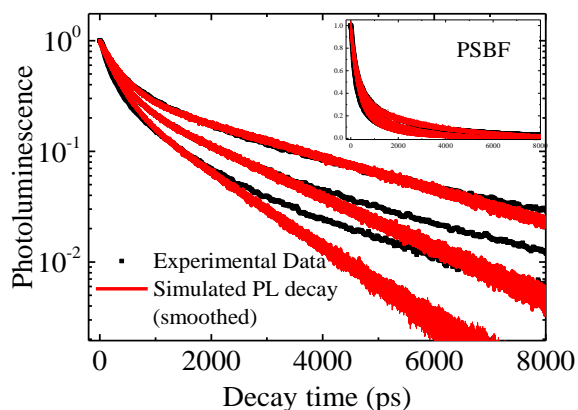


Figure 3.3. Measured (black squares) and simulated (red solid lines) PL decay times for PSBF copolymer mixed with 0%, 0.02% and 0.05% volume fraction of PCBM. The y-axis is plotted in log10 scale. The inset represents the linear simulated PL decay based on Monte Carlo.

The obtained exciton diffusion coefficient amounts to $1.6 \times 10^{-4} \text{ cm}^2/\text{s}$, which is indeed slower than the coefficient of SY-PPV ($2.2 \times 10^{-4} \text{ cm}^2/\text{s}$). As a result, the increased exciton lifetime of the PSBF copolymer as compared to the PPV derivatives can be directly correlated to the slower exciton diffusion due to larger energetic disorder. It should be noted that a complex excited-state behavior of PSBF in thin films has been reported that is related to the formation of charge transfer (CT) states by means of the spiroconjugation between the backbone and the spiro groups. These CT states energetically lie slightly below the singlet-excited states and have been calculated to be approximately 0.014 eV, concluding that the observed long-lived fluorescence resulted from the back and forth energy exchange between these energetically close lying states

at room temperature.^{129,130} Our results indicate that the long exciton lifetime is mainly due to the slow exciton diffusion, but might be further enhanced when the exciton reaches an energy-site near to the CT state where it can transfer back and forward. In spite of the long exciton lifetime an exciton diffusion length of only 6 nm is observed for the PSBF copolymer, similar to the PPV derivatives. Considering that there is a universal amount of non-radiative recombination centers in a wide range of organic semiconductors and that the measured exciton lifetime is governed by the time excited states need to diffuse towards these traps, provide a possible explanation why different materials have a similar exciton diffusion length of ~6 nm in spite of a large variation in exciton lifetime.¹⁹

3.2.3. Photoluminescence Quantum Yield

When the exciton decay time is related to the presence of non-radiative recombination centers, preventing excitons to reach these quenching sites by slowing down their diffusion towards the traps would not only result in long exciton lifetime but also in an increased PL quantum yield (ϕ_f).¹³¹ Therefore, it is expected that highly disordered polymers that exhibit slow exciton diffusion towards traps, represented by a low exciton diffusion coefficient, have higher PL quantum yields relative to better ordered polymers, where excitons reach quenching sites more easily due to faster diffusion. This correlation is pointed out in Figure 3.4, where the PL quantum yield is plotted versus the measured exciton diffusion coefficient for a series of conjugated polymers.

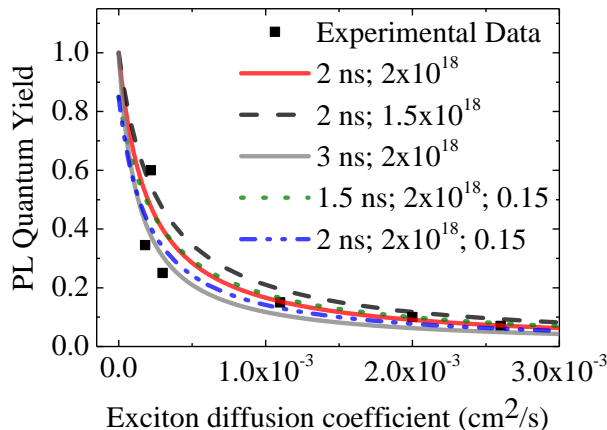


Figure 3.4. PL quantum yield versus exciton diffusion coefficient for whole series of conjugated polymers. Black squares represent experimental data, plots have been determined using equation (3.7). Red solid line was obtained with the following parameters: $\tau_0 = 2\text{ ns}$, $c_0 = 2 \times 10^{18} \text{ cm}^{-3}$, $\tau_0 k_{\text{nonrad}} = 0$, assuming an intrinsic exciton lifetime of about 2 ns without non-radiative decay rates and a PL quantum yield of one. Further calculated lines consider lower number of non-radiative quenching centers $c_0 = 1.5 \times 10^{18} \text{ cm}^{-3}$ (black dash-dotted line) or shorter exciton lifetimes and non-radiative decay rates, respectively (green dotted line and blue dashed line).

It is clearly seen that well-ordered polymers such as poly[2,6-(4,4-bis-(2-ethylhexyl)-4H-cyclo-penta[2,1-b;3,4-b']-dithiophene)-alt-4,7-(2,1,3-benzothiadi-azole)] (PCPDTBT)⁹¹ and BEH-PPV, which exhibit short PL decay times, have low PL quantum yields due to fast diffusion towards traps. In contrast, materials with higher energetic disorder, such as SY-PPV and PSBF, exhibit higher PLQYs since the exciton diffusion is slowed down.

To fit the experimental data, we used the following equations and assumptions. The PL quantum yield in a thin film can be expressed by the measured exciton lifetime in thin polymer films τ_f and the natural exciton lifetime τ_n determined by equations (3.1) and (3.3):

$$\phi_f = \frac{\tau_f}{\tau_n} \quad (3.4)$$

In addition, since the exciton diffusion towards traps plays a significant role, the concentration of background exciton quenching sites c_0 needs to be considered. As comprehensively derived in Chapter 2.6, the concentration of background exciton quenching sites c_0 can be calculated using the following equation:

$$c_0 = \frac{1}{4\pi r D} \left(\frac{1}{\tau_f} - \frac{1}{\tau_0} \right) \quad (3.5)$$

The intrinsic exciton lifetime τ_0 can be approximated by the PL decay time in a diluted solution. However, this assumption does not generally apply to all conjugated polymer systems. First, due to the electronic coupling between chains H aggregates might be formed, which can lead to a partly forbidden lower-energy state with longer lifetimes than that of an isolated polymer chain.⁵⁴ Furthermore, the dielectric surroundings in a film are different than in solution, which affects the transition matrix element.^{49,50} As an example, it has been reported that MEH-PPV in a diluted solution shows different photophysics depending on the solvent. A reduction of the solvent quality leads to an enhanced interchain species formation due to steric constraints on the polymer backbone motions caused by aggregation of the chains. As a result an almost monoexponential PL decay was obtained in the case of a "good" solvent and more pronounced

non-monoexponential PL decays with reduced solvent quality, respectively.⁵¹ In the case of BEH-PPV a value of $c_0 = 1 \times 10^{18} \text{ cm}^{-3}$ is obtained for the exciton quenching defect concentration (Chapter 2.6).

By using equation (3.2) and (3.3), and the rewritten Stern-Volmer equation (3.5) we get the following expression for the pristine polymer:

$$k_{\text{diff}} = \frac{1}{\tau_f} - \frac{1}{\tau_0} = 4\pi r D c_0 \quad (3.6)$$

The combination of equation (3.4) and (3.6) give us a correlation between the photoluminescence quantum yield ϕ_f and the exciton diffusion coefficient:

$$\phi_f = \frac{k_{\text{rad}}}{k_{\text{rad}} + k_{\text{nonrad}} + k_{\text{diff}}} = \frac{k_{\text{rad}}}{\frac{1}{\tau_0} + 4\pi r D c_0} = \frac{1 - \tau_0 k_{\text{nonrad}}}{1 + 4\pi r D c_0 \tau_0} \quad (3.7)$$

It is reasonable to set $r = 1 \text{ nm}$, the rest of the parameters can be measured, except k_{nonrad} . The lines in Figure 3.4 are plotted using equation (3.7). A reasonable fit (red solid line) is already obtained with the following parameters: $\tau_0 = 2 \text{ ns}$, $c_0 = 2 \times 10^{18} \text{ cm}^{-3}$, $\tau_0 k_{\text{nonrad}} = 0$. It should be noted that we used a substantial simplification to determine equation (3.12), since the used Stern-Volmer equation is only valid for monoexponential PL decays. Further we assumed an intrinsic exciton lifetime of about 2 ns without non-radiative decay rates, providing a PL quantum yield of one. Since most of the polymers decay non-monoexponential and some polymers might show much shorter exciton lifetimes, Figure 3.4 shows further calculated lines: with lower number of non-radiative quenching centers as $c_0 = 1.5 \times 10^{18} \text{ cm}^{-3}$ (black dash-dotted line) or considering shorter exciton lifetimes and non-radiative decay rates, respectively (green

dotted line and blue dashed line). However, it is seen that small changes in these parameters do not change the correlation between the PLQY and the exciton diffusion coefficient significantly. The PL quantum yields were determined using an integrating sphere and are comparable with literature.^{52,130,131} The dependence between the exciton diffusion coefficient and PL quantum yield is clearly reflected. As a result, for a range of conjugated polymers we have shown that the exciton lifetime and photoluminescence quantum yield are directly correlated to the diffusion of excitons towards quenching centers. Increased energetic disorder slows down the exciton diffusion and strongly enhances the exciton lifetime (180 ps to 2.9 ns) and PLQY (7% to 45%).

3.3 Conclusions

We have investigated the role of energetic disorder on the PL decay and PL quantum yield in four PPV derivatives and a PSBF copolymer. We demonstrate that the exciton lifetime increases by more than an order of magnitude (0.18–2.9 ns) with increasing energetic disorder. The increase of the exciton lifetime is correlated with a decrease of the exciton diffusion coefficient by one order of magnitude (2.0×10^{-3} – 1.6×10^{-4} cm²/s), respectively, going from BEH-PPV to PSBF. Our findings suggest that the PL decay time in the polymer film is not limited by the intrinsic exciton lifetime, but governed by the time excitons need to diffuse towards non-radiative recombination centers. Highly disordered polymers with slow exciton diffusion, such as PSBF and SY-PPV, not only show a long exciton lifetime but also exhibit a higher PLQY relative to the more ordered polymers.

Chapter 4. Temperature dependence of photo- and electro-luminescence of poly(*p*-phenylene vinylene) based polymers

We characterize the temperature dependence of the exciton transport and decay processes in two poly(*p*-phenylene vinylene) (PPV) based semiconducting polymers with varying degree of energetic disorder. The exciton diffusion coefficient and diffusion length exhibit distinct temperature dependence based on the disorder. To disentangle the contributions from radiative and non-radiative decay processes, with the latter including non-radiative decay processes due to exciton diffusion toward excitonic traps, we use temperature-dependent time-resolved photoluminescence (PL) spectroscopy and Monte Carlo exciton diffusion simulations. We show that for the less disordered polymer the exciton lifetime and quantum yield increase with decreasing temperature, due to both freezing out vibrations and less exciton quenching by slowing down the diffusion toward traps. For highly disordered polymers the exciton lifetime and quantum yield are nearly temperature independent. The temperature dependence of the electroluminescence of polymer light-emitting diodes is directly correlated to photoluminescence.*

* I. Rörich, A.-K. Schönbein, C. Kasparek, D. K. Mangalore, C. Bauer, N. I. Crăciun, P. W. M. Blom, C. Ramanan, J. Mater. Chem. C, accepted.

4.1 Introduction

The device operation of a PLED is determined by three processes: charge carrier (electron and hole) injection from the electrodes, charge transport through the polymer active layer and charge recombination generating an exciton, which can then decay radiatively.¹³² Charge carrier and exciton transport in organic semiconductors can be regarded as a hopping process between localized states on conjugated chain segments that are inhomogeneously distributed in size and energy within a Gaussian density of states (DOS).^{22,23,44,45} The three processes that drive PLED operation depend on the DOS width σ (polymer energetic disorder): charge injection is mediated by the relative energy-level matching to the electrodes, and charge transport and subsequent exciton diffusion, prior to radiative decay, depends on the energy level distribution. Thus, the energetic disorder resulting from molecular conformation, structural defects, and the variety of *inter-* and *intrachain* interactions due to the irregular morphologies, will govern the exciton diffusion and decay characteristics in PPV films for PLEDs.

An exciton, formed either by photo-excitation or Langevin recombination in a PLED, will decay back to the ground state within a lifetime τ_f . The PL quantum yield (ϕ_f) represents the ratio between radiative and non-radiative processes (Eq. 3.4). As discussed in Chapter 1.3. and 3.2, in a thin film with significant chromophore-chromophore interaction, energy-transfer will occur via hopping along *inter-* and *intrachain* segments until the exciton decays either radiatively or non-radiatively. Thus, the PL lifetime τ_f (Eq. 3.3) and quantum yield ϕ_f are governed by the intrinsic radiative (k_r) and non-radiative (k_{nr}) decay rates, as well as the non-radiative decay rate related to the exciton quenching at defect sites due to exciton diffusion with a rate k_{diff} (see also Chapter 1.2.1, Figure 1.7). Further reported in Chapter 3 is that τ_f and ϕ_f

directly correlate with the energetic disorder of conjugated polymers, where increased disorder slows down the diffusion of the exciton toward non-radiative quenching sites and strongly enhances both τ_f and ϕ_f (Figure 3.4). This is consistent with diffusion-limited exciton quenching at defects in organic semiconductors (as discussed in Chapter 1.3.3). It should be noted that while the electronic DOS relevant for charge transport and exciton DOS are not the same, both represent the energy level distribution in the polymer. In accordance with this and the previous results, Markov et al. observed a three orders of magnitude enhanced charge carrier mobility in PPV derivatives with decreasing energetic disorder.⁷

Although charge transfer and exciton diffusion processes are well studied in disordered conjugated polymers, a significant open question remains as to how the PL characteristics of a polymer influence the PLED conversion efficiency. For example, the PLED efficiency is charge carrier mobility independent, and is therefore expected to be temperature independent with regards to the active layer material.^{133,134} However, the PL behavior of a polymer thin film may vary with temperature as the chromophore-chromophore interactions will affect the balance of k_r , k_{nr} , and k_{diff} . Since the PLED efficiency is governed by the formation of excitons, it follows that the respective temperature dependencies of the PLED and PL characteristics should have a direct correlation.

Here, this relationship is investigated by measuring the temperature-dependence of the PL and PLED efficiencies in the two derivatives BEH-PPV and SY-PPV. The width of the charge carrier Gaussian DOS σ was determined from charge transport measurements to be 0.092 and 0.140 eV for BEH-PPV and SY-PPV, respectively.⁷ The exciton lifetime is strongly enhanced with increasing disorder, ranging from 200 ps for BEH-PPV to 1.9 ns for SY-PPV, which is consistent with the results in Chapter 3. Time-resolved photoluminescence spectroscopy (TRPL) at varying temperature shows a correlation between the conformational energetic

disorder and the balance between radiative (k_r) and non-radiative decay processes, the latter of which includes exciton diffusion towards traps (k_{nr} and k_{diff}). The thin film of the highly disordered polymer SY-PPV exhibits an increase in the formation of non-radiative quenching sites with decreasing temperature (increase of k_{nr}), while the more ordered BEH-PPV demonstrates a decrease in non-radiative quenching with decreasing temperature (decrease of k_{nr} and k_{diff}). In addition to the experimental results, simulations based on Monte Carlo were carried out to model the exciton diffusion in the semiconductors depending on energetic disorder and concentration of non-radiative quenching-sites. We found that PLEDs based on the disordered SY-PPV show temperature independent current efficiencies, whereas the better ordered BEH-PPV demonstrates enhanced PLED efficiency with lowering temperature, consistent with the temperature dependence of the photoluminescence quantum yield.

4.2. Results

4.2.1. Temperature-dependent time-resolved photoluminescence

The PL spectrum of SY-PPV (Figure 4.1a) exhibits a broad line shape from 500–700 nm, which fits to a sum of three Gaussian peaks (Table A1), ascribed to the electronic $S_{0,0}$ and vibronic $S_{0,1}$ and $S_{0,2}$ transitions. The peak positions are in good agreement with previous reports,¹³¹ and the PL spectrum red-shifts with lowering temperature. The peak intensity stays relatively constant from 290–130 K, and then slightly decreases at 100 and 77 K. The PL spectrum of BEH-PPV spans 550–750 nm (Figure 4.1c) and is similarly characterized by one primarily electronic transition ($S_{0,0}$) and two vibronic peaks ($S_{0,1}$, $S_{0,2}$). The peak positions from a fit to a sum of three Gaussians are shown in Table A2. With lowering temperature, the PL spectrum of BEH-PPV red-shifts and the peak intensity increases. The relative intensity between the electronic

($S_{0,0}$) and vibronic peaks ($S_{0,x}$) also changes with decreasing temperature. At 298 K, the $S_{0,0}$ and $S_{0,1}$ transitions are of similar intensity, while at 77 K, the $S_{0,0}$ transition is more than twice as intense as the $S_{0,1}$ transition, in agreement with previous work. This indicates a decrease in electron-vibrational coupling with decreasing temperature.¹³⁵ The narrowing of the fluorescence peaks with lowering temperature is more evident in BEH-PPV as opposed to SY-PPV.

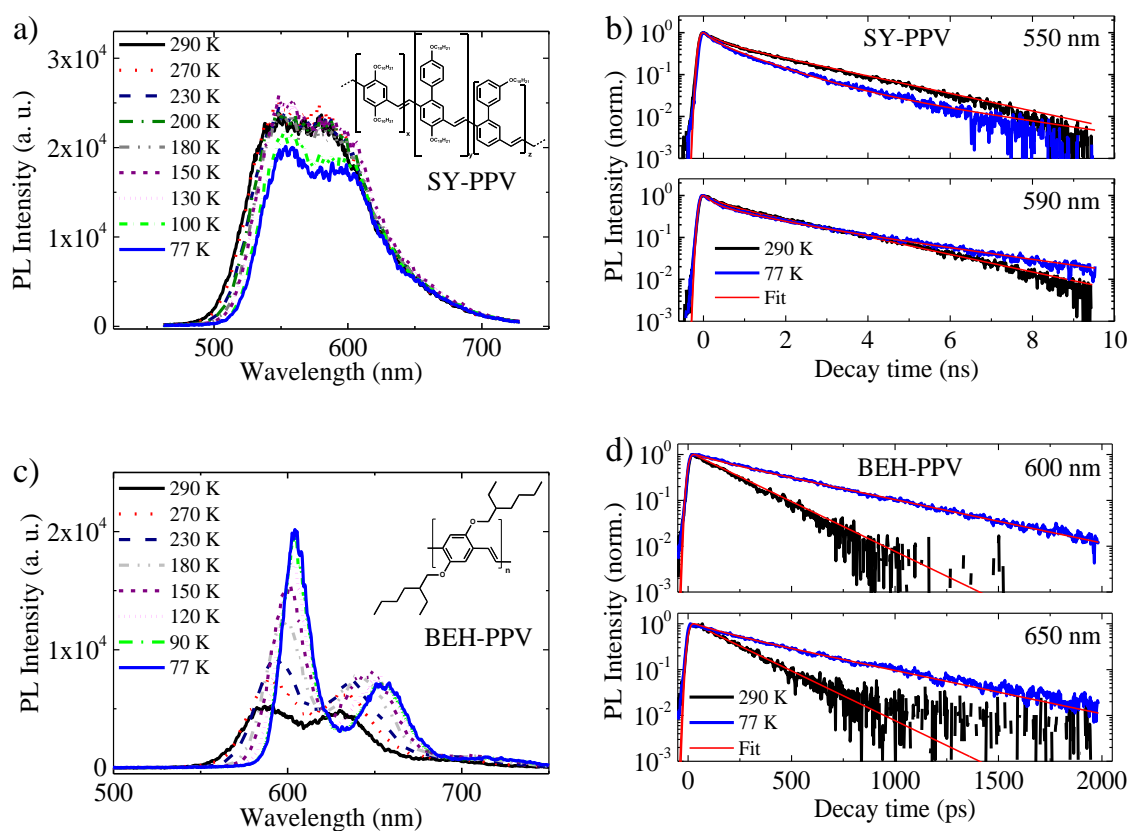


Figure 4.1. (a,c) Temperature dependent photoluminescence spectra and (b,d) associated normalized PL decay traces at specified wavelengths for SY-PPV and BEH-PPV. Spectral traces are taken at the maximum from the time-resolved measurements. Fits to the decay traces are from global analysis as described in the text.

The comparison of the normalized PL decay kinetics measured at the $S_{0,0}$ (550 nm) and $S_{0,1}$ (590 nm) transitions (Figure 4.1b, black and blue traces) demonstrate that the SY-PPV temperature-dependence depends on the emission wavelength. At 550 nm, the 77 K trace decays faster than the 290 K trace, while at 590 nm, the traces are mostly similar, with the 290 K trace decaying faster by a small amount. Figure 4.1b shows only the lowest and highest measured temperatures for the $S_{0,0}$ and $S_{0,1}$ transition, for clarity, but the observed trend is consistent throughout the entire measured temperature range (Figure A1). The normalized BEH-PPV PL decay traces (Figure 4.1d), monitored at 600 and 650 nm, demonstrate that the PL lifetime at 77 K is longer than at 290 K at all wavelengths. This trend is consistent through the measured temperature range (Figure A2).

The TRPL decay dynamics were modeled with a global analysis scheme, which takes into account the decay dynamics across the entire spectral range (see also Chapter 2.4).^{101,102} The fits are represented as red lines in Figure 4.1b,d and the lifetimes and relative amplitudes are summarized in Tables 4.1 and 4.2. For both materials, the data were fit to a sum of a fast and slow exponential contribution. The measured exciton lifetime (τ_f) is then determined from a weighted average of the two kinetic components (Eq.2.4) and the relative PL quantum yields (ϕ_T/ϕ_{290K}) are determined from the integral under the spectrum. In SY-PPV (Table 4.1), both the fast and slow lifetimes become longer with decreasing temperature, which is attributed to a decrease in non-radiative contributions. Simultaneously, the relative amplitude of the fast component increases with decreasing temperature. This is consistent with an increase in non-radiative processes due to energy transfer/hopping to conformational subunits exhibiting longer decay rates.

Table 4.1. Temperature dependence of the average PL lifetime τ_f and calculated relative quantum yield ϕ_T/ϕ_{290K} in SY-PPV.

T (K)	A ₁	τ_1 (ps)	A ₂	τ_2 (ps)	τ_f	ϕ_T/ϕ_{290K}
290	0.39	356	0.61	2076	1905	1.00
270	0.42	372	0.58	2185	1985	1.02
230	0.46	409	0.54	2390	2138	0.99
200	0.47	424	0.53	2478	2203	0.98
180	0.49	442	0.51	2537	2238	0.96
150	0.51	451	0.49	2573	2249	1.01
130	0.51	459	0.49	2599	2262	0.99
100	0.53	476	0.47	2680	2315	0.84
77	0.51	489	0.49	2711	2364	0.78

Table 4.2. Temperature dependence of the average PL lifetime τ_f and calculated relative quantum yield ϕ_T/ϕ_{290K} in BEH-PPV.

T (K)	A ₁	τ_1 (ps)	A ₂	τ_2 (ps)	τ_f	ϕ_T/ϕ_{290K}
290	0.89	161	0.11	368	207	1.00
270	0.91	179	0.09	452	236	1.32
230	0.90	215	0.10	552	292	1.49
180	0.87	265	0.13	671	374	1.70
150	0.83	286	0.17	626	391	1.84
120	0.79	304	0.21	599	405	1.76
90	0.62	190	0.38	485	370	1.71
77	0.56	130	0.44	484	393	1.76

These varying contributions to the non-radiative PL decay result in an overall slight increase in the average PL lifetime, τ_f , from 1.9 ns at 290 K to 2.4 ns at 77 K. The relative quantum yield does not vary significantly with temperature until 130 K. The reduction of ϕ_f at temperatures

< 130 K is attributed to an increased energy transfer to non-luminescent sub-species due to increased interchain interactions at low temperatures.

In BEH-PPV (Table 4.2), the two-component model was required to account for energy transfer from shorter to longer conformational subunits, which contributes more with decreasing temperature. Both the fast and slow components get longer with decreasing temperature until 150 K. In this case, the relative amplitude of the slow component increases with decreasing temperature. As a result, the average lifetime τ_f increases from 207 ps at 290 K to 405 ps at 150 K. At temperatures < 150 K, the faster component shortens, probably due to increased energy transfer and interchain quenching interactions. The relative quantum yield ϕ_T/ϕ_{290K} of BEH-PPV also increases with decreasing temperature. The concomitant increase in lifetime and quantum yield with decreasing temperature indicate that in BEH-PPV the PL is predominantly radiative, where lower temperatures result in a decrease in competitive non-radiative processes, consistent with the observed decrease in electron-vibrational coupling.

4.2.2. Exciton diffusion coefficient and diffusion length

As a next step, the spatial and temporal evolution of the singlet exciton population is investigated as a function of temperature, characterized by the exciton diffusion coefficient D and exciton diffusion length L_D . Therefore, fluorescence quenching experiments of thin polymer films with randomly distributed PCBM molecules were performed, as described in Chapter 2.5. Thin films of SY-PPV and BEH-PPV, each blended with known concentrations of PCBM, were prepared from chlorobenzene solution. The average fluorescence lifetime was determined from TRPL experiments, using the same procedure described in the previous section (Chapter 4.2.1). The results were analyzed by Monte Carlo simulation, which is appropriate for multi-

exponential decays, to return the exciton diffusion coefficient D (see for more details in Chapter 2.7).^{91,105} The exciton diffusion length L_D is then calculated using following equation $L_D = \sqrt{\tau_f D}$ (Eq. 2.5), where τ_f is the average lifetime calculated from the TRPL measurements (Figure 4.1). The results are shown in Figure 4.2.

The better ordered BEH-PPV exhibits overall higher exciton diffusion coefficients and exciton diffusion lengths than the less well-ordered SY-PPV. With lowering temperature, SY-PPV shows a significant reduction of the exciton diffusion parameters between 298–180 K, with D decreasing from 3.1×10^{-4} cm²/s to 8.0×10^{-5} cm²/s and L_D decreasing from 7.7 nm to 4.2 nm. Further cooling from 180 K to 77 K reveals nearly constant exciton diffusion parameters for SY-PPV. In contrast, the exciton diffusion parameters for the better ordered BEH-PPV display less temperature dependence in the higher temperature range (298–120 K), while in the lower temperature range 100–77 K, there is greater dependence on temperature, with D decreasing from 2.5×10^{-3} cm²/s to 6.8×10^{-4} cm²/s and L_D decreasing from 9.6 nm to 5.2 nm. Both polymers exhibit an approximately 75% reduction in D at 77 K vs. 290 K.

For BEH-PPV, we also compared these results with a monoexponential fluorescence decay, which has been reported before for this polymer at room temperature in Chapter 2.6 and 3.2. The temperature-dependent exciton diffusion parameters, in this case determined by the Stern-Volmer equation, and exciton lifetimes determined from monoexponential fits of the PL decays are shown in Figure A4. The results show a similar trend of D and L_D in BEH-PPV compared to the results determined from global analysis and Monte Carlo simulations (Figure 4.2), with slightly higher values for L_D . As D is quite similar for the two fits, the difference in L_D is most likely due to the longer fluorescence lifetime from the monoexponential

fits, which do not account for the increased energy transfer between polymer chains at lower temperatures.

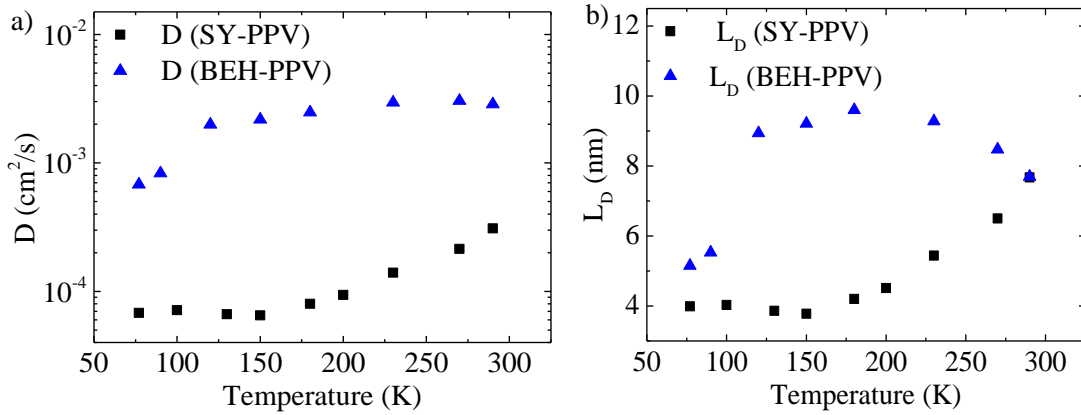


Figure 4.2. Temperature-dependence of (a) exciton diffusion coefficient D and (b) exciton diffusion length L_D for SY-PPV and BEH-PPV, determined from time-resolved fluorescence quenching experiments of thin films.

4.2.3. Temperature-dependent polymer-light emitting diode efficiencies

PLEDs of each SY-PPV and BEH-PPV were fabricated in order to test the temperature dependence of the device efficiency. The device structure ITO/PEDOT:PSS/PPV/Ba/Al was used for both active layer materials. The SY-PPV active layer is 100 nm thick and the BEH-PPV layer is 165 nm thick. Figure 4.3 shows the temperature dependent current efficiencies vs. voltage of the devices. The current efficiency is calculated as the light output divided by the current, and describes the relation between the number of emitted photons and the number of charges that pass through the device for a given time interval. The SY-PPV PLED exhibits no change in current efficiency with decreasing temperature in the range of 295–233 K. The current

efficiency of the BEH-PPV PLED, however, increases by more than a factor of two when the device temperature is decreased between 295–215 K. Additionally, the rise of current efficiency with increasing voltage becomes steeper as the BEH-PPV device temperature is lowered.

Temperature dependent EL spectra of BEH-PPV (Figure 4.4) demonstrate a different spectral line shape than the BEH-PPV PL spectra in the same temperature range. The $S_{0,0}$ and $S_{0,1}$ peak positions remain mostly unchanged (Table S3). However, the relative intensities of these peaks in the EL spectra match more closely with that in the lower temperature PL spectra, with the $S_{0,0}$ peak exhibiting always higher intensity than the $S_{0,1}$. This EL spectral line shape is consistent with an optical microcavity effect in the PLED, wherein the near-field coupling results in a narrowing of the spectral line shape and enhances the spontaneous emission rate.^{37,136}

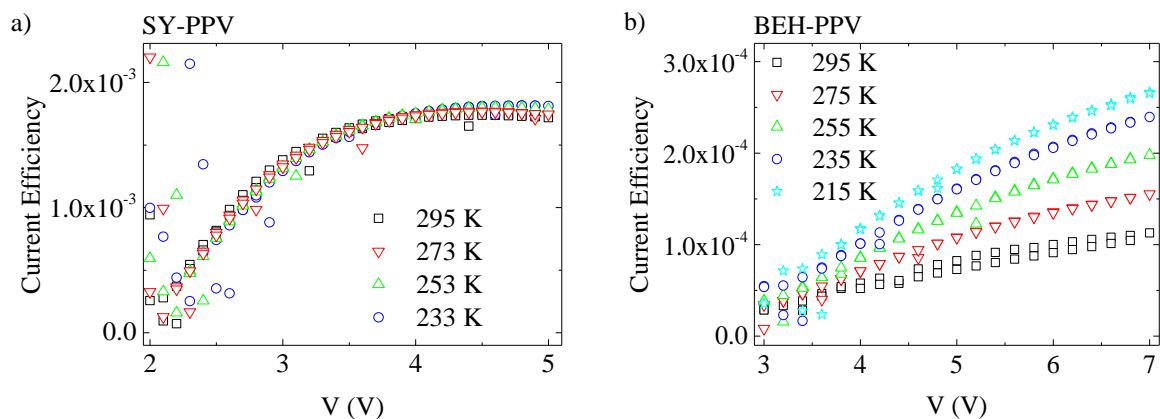


Figure 4.3. Current efficiencies vs. voltage of PLEDs comprised of (a) SY-PPV and (b) BEH-PPV measured at various temperatures.

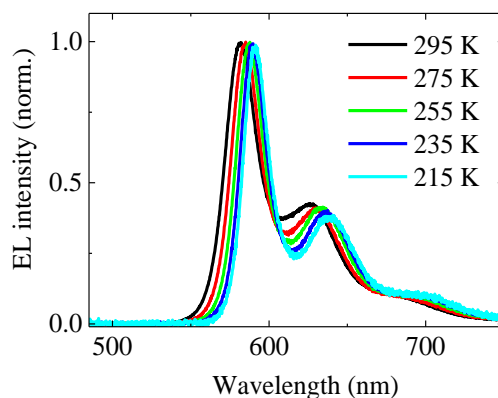


Figure 4.4. Temperature-dependent electroluminescence spectra of the BEH-PPV PLED measured at 7 V, normalized to the spectral maximum.

4.3. Discussion

4.3.1. Temperature-dependent exciton decay characteristics

As discussed already in Chapter 3.2, the configurational freedom of individual conformational subunits determines the difference in the width of the Gaussian DOS in the BEH-PPV and SY-PPV polymers, and thus their energetic disorder. For chemical structures see Figure 2.1. The width of the excitonic DOS (σ) is calculated by assuming that the energy position of the $S_{0,0}$ transition from our PL measurements corresponds to the level of the most populated states, which lies at the equilibrium level $-\sigma^2/kT$ below the center of the DOS.^{22,44} The slope of the relationship between the $S_{0,0}$ peak position vs. $1/T$ allows us to extract $\sigma_{optical}$. From this we find that energetic disorder of BEH-PPV ($\sigma_{optical}=0.033$ eV) is indeed less than that of SY-PPV ($\sigma_{optical}=0.048$ eV) (Figure A5). The half-width of the excitonic (optical) Gaussian DOS is about 3 times smaller than the half-width of the charge carrier (electrical) DOS extracted from charge transport measurements, for BEH-PPV $\sigma_{electrical}=0.092$ eV and SY-PPV $\sigma_{electrical}=0.140$ eV,

respectively.⁷ Previous work showed that $\sigma_{electrical}$ is larger than $\sigma_{optical}$ due to the different nature of interactions between charge carriers and excitons within the DOS.²² Nonetheless, BEH-PPV reproducibly exhibits a narrower DOS than SY-PPV. Further discussed comprehensively in Chapter 3.2 is that the exciton diffusion characteristics (and quantum yield) of a conjugated polymer thin film depend strongly on the disorder parameter σ and the temperature T ,¹²⁶ as well as on the starting singlet excitation energy within the DOS and the coupling strength between the energy sites.¹²⁵

Here, the differences in energetic disorder between BEH-PPV and SY-PPV manifest in the temperature dependent PL and exciton diffusion characteristics as measured in thin films. The exciton decay processes in these systems are governed by radiative decay, non-radiative decay, and exciton diffusion to non-radiative traps (Figure 1.7 in Chapter 1).¹³⁷ The TRPL experiments show that, with decreasing temperature, both the SY-PPV and BEH-PPV films demonstrate longer fluorescence lifetimes. However, while the relative quantum yield for SY-PPV is fairly constant until very low temperatures, the one of BEH-PPV increases along with the lifetime.

To obtain more information about the exciton lifetimes, the excited state transfer rates for the two-different disordered PPV derivatives were calculated using equation (3.3) and (3.4). The resultant transfer rates are summarized in Tables 4.3 and 4.4 for SY-PPV and BEH-PPV, respectively. The lifetime τ_i correlates with the transfer rate k_i with the following relation: $\tau_i = 1/k_i$. The radiative decay rate k_r is calculated by Equation 4.1:

$$k_r = \phi_f / \tau_f = (\phi_T / \phi_{290K} \cdot \phi_{abs}) / \tau_f \quad (4.1)$$

where ϕ_f corresponds to the product of the relative PLQY (ϕ_T/ϕ_{290K}) and the absolute PLQY (ϕ_{abs}) of a pristine film at 290K. We used the literature reported $\phi_{abs} = 60\%$ for an SY-PPV film,⁵² which returns a natural exciton lifetime $\tau_r = 1/k_r \sim 3$ ns. The absolute PLQY of our BEH-PPV thin film is approximately ten times smaller ($\phi_{abs} \sim 6\%$) than the one of SY-PPV, also leading to a natural exciton lifetime τ_r of ~ 3 ns. Considering the two materials have the same polymer backbone, a similar natural exciton lifetime for both PPV derivatives is expected. We note that in literature ϕ_{abs} has been reported as high as 12% for a BEH-PPV film,¹³⁸ which would give rise to a natural exciton lifetime of $\tau_r \sim 1.7$ ns. However, a value of $\phi_{abs} = 12\%$ does not change the trend of the transfer rates in BEH-PPV.

In order to disentangle k_{nr} from k_{diff} , which represents the non-radiative transfer rates due to exciton diffusion toward non-radiative quenching-sites, we used the exciton diffusion model to simulate quenching efficiencies Q ($Q = 1 - N_R/N_0$) for a range of diffusion coefficients D . The solid lines in Figure 4.6 show the dependence of Q as determined by the ratio of the number of radiatively decaying exciton (N_R) and the number of excitons that would decay radiatively in the absence of a quencher (N_0). The curves represent Q for a constant intrinsic exciton lifetime $\tau_r = 3$ ns. The model also assumes a constant number of exciton defects (background quenchers). In SY-PPV an electron trap density of $1 \times 10^{17} \text{ cm}^{-3}$ was determined by charge transport measurements,⁸ and in BEH-PPV a trap concentration of $6.5 \times 10^{17} \text{ cm}^{-3}$ was determined by using Stern-Volmer analysis, as described in Chapter 2.6. Figure 4.5 shows, as expected for an exciton diffusion model, that Q increases with enhanced D , since a high exciton diffusion coefficient represents a fast exciton diffusion toward traps, leading to more efficient exciton quenching, and vice versa. The quenching efficiency is then retrieved from the calculated value of D from TRPL, and k_{diff} is determined by $k_f * Q$.

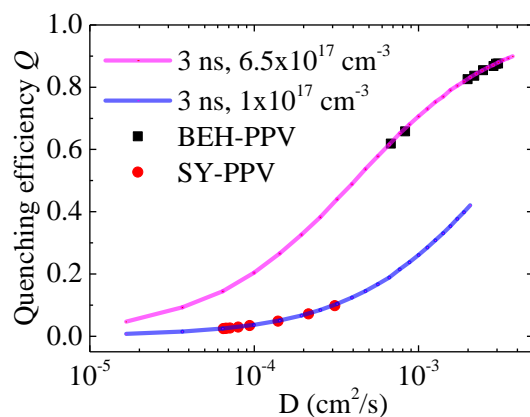


Figure 4.5. Exciton diffusion coefficient D dependent quenching efficiency Q for SY-PPV and BEH-PPV. The amount of background quenchers equals $1 \times 10^{17} \text{ cm}^{-3}$ and $6.5 \times 10^{17} \text{ cm}^{-3}$ for SY-PPV and BEH-PPV, respectively.

Figure 4.5 shows that for BEH-PPV almost 90% of the excitons is quenched at a defect at room temperature, whereas for SY-PPV this is less than 10%. From Table 4.3 and 4.4 it is seen that k_{diff} of BEH-PPV is two orders of magnitude higher than the one of SY-PPV. As a result, the non-radiative losses in BEH-PPV are almost fully dominated by diffusion-limited quenching at the defects present in the polymer. Furthermore, both PPV derivatives demonstrate a decrease in k_{diff} with lowering temperature, in agreement with the diffusion limited exciton quenching model. With now k_{diff} known, the non-radiative transfer rates k_{nr} were determined using equation (3.3) and (3.4).

Table 4.3. Exciton transfer rates in SY-PPV, using an absolute PLQY of 60% for the pristine film at 290 K.⁵²

T (K)	ϕ_f	k_f (s ⁻¹)	k_r (s ⁻¹)	k_{diff} (s ⁻¹)	k_{nr} (s ⁻¹)
290	0.60	5.25×10 ⁸	3.15×10 ⁸	5.15×10 ⁷	1.58×10 ⁸
270	0.61	5.04×10 ⁸	3.10×10 ⁸	3.62×10 ⁷	1.58×10 ⁸
230	0.59	4.68×10 ⁸	2.78×10 ⁸	2.27×10 ⁷	1.67×10 ⁸
200	0.59	4.54×10 ⁸	2.68×10 ⁸	1.54×10 ⁷	1.71×10 ⁸
180	0.57	4.47×10 ⁸	2.56×10 ⁸	1.30×10 ⁷	1.78×10 ⁸
150	0.60	4.45×10 ⁸	2.69×10 ⁸	1.08×10 ⁷	1.65×10 ⁸
130	0.60	4.42×10 ⁸	2.63×10 ⁸	1.10×10 ⁷	1.68×10 ⁸
100	0.51	4.32×10 ⁸	2.18×10 ⁸	1.12×10 ⁷	2.02×10 ⁸
77	0.47	4.23×10 ⁸	1.99×10 ⁸	1.08×10 ⁷	2.14×10 ⁸

Table 4.4. Exciton transfer rates in BEH-PPV, using an absolute PLQY of 6% for the pristine film at 290 K.

T (K)	ϕ_f	k_f (s ⁻¹)	k_r (s ⁻¹)	k_{diff} (s ⁻¹)	k_{nr} (s ⁻¹)
290	0.06	5.00×10 ⁹	3.00×10 ⁸	4.34×10 ⁹	3.60×10 ⁸
270	0.08	4.70×10 ⁹	3.72×10 ⁸	4.12×10 ⁹	2.11×10 ⁸
230	0.09	3.91×10 ⁹	3.50×10 ⁸	3.42×10 ⁹	1.38×10 ⁸
180	0.10	2.89×10 ⁹	2.95×10 ⁸	2.47×10 ⁹	1.27×10 ⁸
150	0.11	2.67×10 ⁹	2.95×10 ⁸	2.24×10 ⁹	1.41×10 ⁸
120	0.11	2.87×10 ⁹	3.04×10 ⁸	2.37×10 ⁹	1.97×10 ⁸
90	0.10	2.73×10 ⁹	2.80×10 ⁸	1.79×10 ⁹	6.52×10 ⁸
77	0.11	2.71×10 ⁹	2.86×10 ⁸	1.68×10 ⁹	7.48×10 ⁸

The calculated values show that k_r in SY-PPV slowly decreases with decreasing temperature, while in BEH-PPV it barely changes. This is consistent with the predominantly radiative PL

observed in BEH-PPV. In contrast to BEH-PPV, where exciton diffusion towards defects is determining the quenching, in SY-PPV k_{nr} is the dominant non-radiative loss process, which remains almost constant until 130 K and then increases with lowering temperature. In BEH-PPV, k_{nr} decreases with decreasing temperature, and then increases again below 150 K. The increase of k_{nr} with a concomitant slight decrease of k_r in SY-PPV is ascribed to increased population of conformational subunits that have higher contribution from non-radiative decay processes, such as may be expected with increased interchain interactions. In contrast, the decrease of k_{nr} in BEH-PPV originates from a reduction in vibronic coupling at lower temperatures, while the increase below 150 K is attributed to increased energy transfer processes from shorter to longer conformational subunits. With decreasing temperature, a decrease in competitive non-radiative processes (k_{nr} and k_{diff}) results in increased exciton lifetime going from 200 ps to 370 ps in BEH-PPV (see Figure 4.1e,f). We found further, that at higher temperatures, the less disordered polymer BEH-PPV exhibits less temperature dependence on exciton diffusion coefficient D and k_{diff} . This is consistent with the low energetic disorder in this system. Since the quasi-equilibrium state is due to the narrow σ close to the center of the DOS, fast energy transfer between the conformational subunits proceeds, represented by a high D at room temperature (2.9×10^{-3} cm²/s). While cooling down to the characteristic temperature (< 120 K), the exciton diffusion coefficient decreases slightly to 2.0×10^{-3} cm²/s, which is consistent with the slight decrease in k_{diff} (from 2.34×10^9 to 1.09×10^8 s⁻¹). Below 120 K, where thermally activated hopping is absent, the exciton diffusion coefficient drops down to 8.3×10^{-4} cm²/s and k_{diff} to 4.96×10^8 s⁻¹, respectively. Due to the narrow energy spread in BEH-PPV, with decreasing temperature there are still enough possible energy-sites for the excitons to jump while the equilibrium-state shifts down into the Gaussian tail. Thus, the exciton diffusion coefficient of BEH-PPV at 120 K is still one order of magnitude higher than

the one of SY-PPV at room temperature ($3.1 \times 10^{-4} \text{ cm}^2/\text{s}$), while k_{diff} is two orders of magnitude higher (see also Table 4.3 and 4.4). The increased excited state lifetime at lower temperatures in BEH-PPV mainly originates from the decrease in exciton quenching due to slower diffusion toward traps (decrease in k_{diff}), since k_{diff} is an order of magnitude larger as compared to k_{nr} . The decrease of k_{nr} (300 K–150 K) results from the decrease in internal vibrational energy redistribution pathways due to the changes in inter- and intrachain packing. This is consistent with the decreased electron-vibrational coupling at lower temperatures, evidenced by the changing peak ratio between $S_{0,0}$ and $S_{0,1}$ (Fig. 4.1d). Reduction of these non-radiative processes at lower temperatures, dominated by a reduced k_{diff} , then give rise an increase in the relative quantum yield ϕ_f as observed in BEH-PPV.

4.3.2. Downhill migration and thermally-activated hopping depends on energetic disorder

In contrast to the exciton diffusion coefficient, the exciton diffusion length of BEH-PPV first increases while cooling to 180 K. This increase from 7.7 nm to 9.6 nm is a consequence of the increased exciton lifetime resulting from less competitive non-radiative decay rates with lowering temperature (see Eq. 4.1). Then, in between 180 K and 120 K the L_D of BEH-PPV slightly decreases. Previous work, including vibrational spectroscopy, has shown that the electronic-vibrational coupling in BEH-PPV is temperature dependent, with even additional vibronic peaks being resolved at temperatures lower than what we have studied here.¹³⁵ Such a change in the electronic-vibrational coupling could affect the disorder parameter σ and thereby also the temperature dependence of L_D . Finally, when a characteristic temperature of 100 K is reached, the exciton diffusion becomes fully determined by downhill migration and the exciton diffusion length drops off from 8.9 nm to 5.2 nm.

Since the thermal equilibrium state $-\sigma^2/kT$ shifts with increasing disorder strength σ deeper into the tail states of the Gaussian DOS, the probability to find a nearby energy-site to which a jump is probable decreases noticeably in the case of a more disordered polymer.¹²⁶ Therefore, in SY-PPV the exciton migration toward quenching defects is much slower at room temperature, leading to an order of magnitude longer exciton lifetime (1.9 ns) compared to BEH-PPV (200 ps).¹³⁷ At room temperature, the slow exciton diffusion in the disordered SY-PPV is represented by a low exciton diffusion coefficient of 3.1×10^{-4} cm²/s and the two orders of magnitude lower transfer rate k_{diff} (Table 4.3 and 4.4) compared to BEH-PPV. The decrease in D and L_D , while cooling to 180 K (Figure 4.2), is a direct consequence of the down-shift of the equilibrium level into the tail of the Gaussian DOS, where the energy difference between occupied and neighboring sites increases, leading to an even lower D (8.0×10^{-5} cm²/s) and k_{diff} . The lower D with a nearly constant exciton lifetime then results in a decrease of L_D from 7.7 nm to 4.2 nm in the temperature range of 290–180 K. Below the characteristic temperature (180 K), where thermally activated hopping is switched off, the exciton diffusion becomes fully determined by downhill migration, represented by temperature-independent exciton diffusion coefficient ($\sim 6.8 \times 10^{-5}$ cm²/s) and diffusion length (~ 3.9 nm). Also, k_{diff} remains temperature-independent ($\sim 3.68 \times 10^6$ s⁻¹). The decrease in the exciton diffusion rate k_{diff} with lower temperature leads to a slight increase in the overall (average) exciton lifetime from 1.9 ns to 2.4 ns going from 290 K to 77 K. The wavelength dependent exciton lifetimes are attributed to different sub-populations of emitting species with varying degrees of radiative and non-radiative emission, where at higher energies the radiative species dominates the fluorescence. At lower energies, there are greater contributions due to spectral diffusion caused by energy transfer from shorter to longer conformational subunits as well as from energy transfer to

interchain excimer like species, which will have a lower oscillator strength and subsequently longer PL lifetime.^{52,131}

The better ordered BEH-PPV exhibits PL characteristics that are temperature sensitive and are dominated by the exciton diffusion-limited quenching model. The increase in L_D of BEH-PPV with lowering temperature is governed by the increase in τ_f , while in the case of SY-PPV temperature-dependence of L_D is dominated by the temperature-dependence of D . These findings demonstrate that the temperature at which thermally activated hopping diminishes scales with the energetic disorder. Better ordered PPV derivatives correlate with lower transition temperatures between thermally activated hopping and downhill migration.

4.3.3. Origin of temperature-dependent PLED efficiency enhancement in BEH-PPV

PLEDs based on these materials demonstrate that BEH-PPV exhibits temperature dependent efficiencies while SY-PPV does not. The current efficiency (CE) in polymer light-emitting diodes (PLEDs) is defined as light output divided by current (exciton/charge carrier), and describes the relation between the number of emitted photons divided by the number of charges that passed the device in the same time interval. Since the charge current and the recombination prefactors of the radiative Langevin and nonradiative Shockley-Read-Hall recombination scale linearly with mobility, dividing these rates for current and light output, the mobility drops out and the efficiency is expected to be mobility independent.^{8,132,139} In a space-charge limited device such as PLEDs, the number of charge carriers is mainly determined by the applied voltage and not by the temperature. Therefore, the current efficiency in PLEDs is reported to be temperature-independent.¹³³ Previous work on the temperature-dependent characteristics of PLEDs have focused on the role of the charge-injection barrier with temperature.^{134,140}

However, the PLED efficiency also depends on the decay dynamics of a formed exciton,^{133,141} which is described by the PL efficiency. The temperature-independence of the CE in the high disordered polymer SY-PPV PLED (Figure 4.3a) can now be explained as follows: after formation of the exciton, it subsequently diffuses along the conjugated chain segments until it reaches a radiative or non-radiative recombination center and decays either radiatively or non-radiatively. The increased population of non-luminescent conformational subunits present in the SY-PPV copolymer compensates for the decrease in exciton diffusion toward non-radiative quenching-sites with lowering temperature. Therefore, the current efficiency, which directly correlates with the PL efficiency ϕ_f , shows no temperature-dependence in the SY-PPV based PLED.

In contrast, the increased current efficiency in the less disordered BEH-PPV PLED in the temperature-range of 295 K–215 K (Figure 4.3b) is a direct consequence of enhanced ϕ_f , resulting from less competitive non-radiative diffusion-dominated decay processes with lowering temperature. Note that the temperature-dependence of the current efficiency in BEH-PPV is stronger with respect to the relative quantum yield ϕ_f . This can be attributed to the difference in the relative intensity of peaks in the EL spectra compared to the PL spectra due to interference in the optical microcavity of the EL device. This will influence the device efficiency and the rate of spontaneous emission.¹³⁶ In the optical microcavity, the BEH-PPV EL spectra demonstrate decreased electron-vibrational coupling with decreasing temperature. This is evidenced by the increasing ratio between the $S_{0,0}$ and $S_{0,1}$ peaks (Figure 4.4), and is consistent with the temperature-dependent PL measurements.

4.4. Conclusion

We have shown that the temperature-dependent excited state lifetime, relative quantum yield, and exciton diffusion characteristics, i.e. exciton diffusion coefficient, exciton diffusion length, depend on the energetic disorder of the conjugated polymer system. The less disordered polymer BEH-PPV shows a decrease in non-radiative decay due to both freezing out vibrations (influences k_{nr}) with decreasing temperature and less exciton quenching due to slowing down the diffusion toward traps (decrease in k_{diff}), leading to increase in exciton lifetime and relative quantum yield. Since the CE of a PLED is directly correlated to the PL efficiency, we found in that the PLED based on the better ordered polymer showed enhanced CE at low temperatures due to reduced quenching at defect centers. Polymers with higher energetic disorder, as SY-PPV, show different temperature-dependence of the exciton diffusion properties. With lowering temperature the exciton lifetime slightly increases, while the relative quantum yield decreases, due to different conformational subunits and increased competitions from radiative and non-radiative sites. As a consequence, PLEDs based on strongly disordered polymers show temperature independent conversion efficiencies and PLQYs, respectively.

Chapter 5. Exciton quenching due to hole trap formation in aged polymer light-emitting diode

The polymer light-emitting diode based on the poly(*p*-phenylene vinylene) derivative BEH-PPV is aged at a constant current density, leading to the formation of hole traps. Time-resolved photoluminescence spectroscopy (TRPL) shows that the degraded polymer light-emitting diode (PLED) also demonstrates a decrease in exciton lifetime. The amount of non-radiative exciton quenching sites in the aged device is quantified by Monte Carlo simulations. We find that the number of hole traps predicted from electrical charge transport measurements is similar the number of non-radiative quenching sites determined from the TRPL experiments. Our results reveal the origin for the apparent different behavior of the electroluminescence and photoluminescence upon PLED degradation. The decrease of the electroluminescence is governed by recombination of free electrons with trapped holes, whereas the photoluminescence is reduced by non-radiative quenching processes between excitons and hole traps.

*I. Rörich, Q. Niu, N. Irina Crăciun, C. Ramanan, P. W. M. Blom, in preparation.

5.1. Introduction

One of the main drawbacks in polymer-based light-emitting diodes (PLEDs) is their relatively low stability and short lifetime. The short device lifetime of the PLEDs has been ascribed to device degradation under current stress,³ although the mechanism of this degradation remains unclear. The degradation of a PLED stressed at a constant current is characterized by a decrease of the electroluminescence and an increase of the driving voltage.¹⁴² Possible causes for PLED degradation are the decrease of charge carrier mobility, the formation of charge traps and reduced charge carrier injection by electrodes due to e.g. chemical impurities.¹⁴²⁻¹⁴⁵ A remarkable observation is that although the electroluminescence of a PLED strongly decreases under aging the photoluminescence efficiency seems to hardly be affected.^{144,146} From this it has been concluded that the majority of the polymer molecules is not affected by the current stress. Apparently, only a small volume of the polymeric semiconductor seems to be affected like the polymer electrode interface. A decrease of the charge injection would lead to a decrease of the electroluminescence due to imbalanced transport as well as to a rise of the driving voltage at constant current.

In a recent study, numerical simulations on pristine and degraded PLEDs have been performed to discriminate between the various proposed degradation mechanisms.⁸ It was found that the formation of hole traps simultaneously explains the increase of driving voltage and the decrease of the electroluminescence in the PLED. The additional non-radiative recombination process of free electrons with trapped holes is then responsible for the loss of light output and device efficiency with aging time. A possible mechanism for the formation of hole traps could be exciton-free hole interactions, whereby the energy of the exciton is transferred to the hole, which subsequently is excited to higher energetic states. While the majority of excited holes decay to the ground state via internal energy conversion, some of

these ‘hot molecules’ can lead to bonds breaking via direct dissociation route to dissociated products,^{147,148} which may act as hole traps themselves or interact with adjacent molecules by forming hole traps. What is not straightforward is why the formation of hole traps in the bulk of the polymer would not strongly affect the photoluminescence efficiency as well.

Photo-excitation measurements allow a direct way to investigate exciton properties in organic semiconductors. The upon photon-absorption generated exciton diffuses along/between the conjugated chain segments in the Gaussian DOS until it reaches a recombination center where it can decay either radiatively or non-radiatively, and/or it can reach a trap-site. At these traps, the excitons can be quenched via electron transfer (see also Chapter 1).

Herein, we investigated the degradation of a BEH-PPV PLED by using time-resolved photoluminescence (TRPL) spectroscopy. We found that the exciton lifetime decreases upon stressing the device at a constant current density with respect to the unstressed one. We combine the TRPL results with Monte Carlo simulations to calculate the number of non-radiative quenching-sites in the device. From charge transport measurements and a numerical drift-diffusion model, the generation of hole traps for a certain current density can also be determined.^{8,149} Our results show that the number of generated hole traps N_t calculated from charge transport measurements is similar to the concentration of nonradiative quenching-sites c_0 retrieved from the TRPL experiments. This indicates that hole traps formed during PLED degradation quench excitons via an additional non-radiative decay process between trapped holes and excitons, leading to a shorter exciton lifetime. The apparent contradiction of strong electroluminescence decrease with a nearly unaffected photoluminescence efficiency is the result of different physical mechanisms. The electroluminescence decay under current stress is governed by the trap-assisted recombination between trapped electrons and free holes (Shockley-Read-Hall

recombination), which leads to an additional non-radiative recombination process in PLEDs that compete with the radiative Langevin recombination. The exciton decay time and photoluminescence efficiency are governed by the diffusion of excitons towards the hole traps, which is a slow process in PPV derivatives.

5.2. Results and Discussion

5.2.1. Hole trap formation

In an earlier study the current-voltage (J - V) and luminescence-voltage (L - V) characteristics of degraded PLED could be modeled by the formation of hole traps.⁸ By modelling the J - V and L - V of degraded PLEDs at different aging times also the time evolution of the hole trap formation can be derived.¹⁴⁹ As an example, in Figure 5.1 the evolution of the hole trap concentration for the BEH-PPV PLED stressed at a constant current density 35 mA/cm^2 is shown. After 211 hours the concentration of hole traps formed amounts to $2.8 \times 10^{17} \text{ cm}^{-3}$ (Table 4.1).

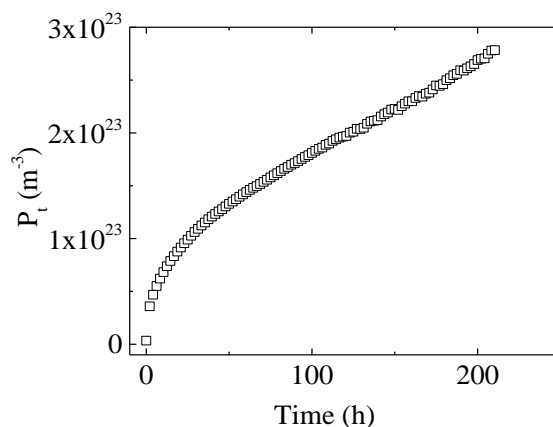


Figure 5.1. Density of hole traps (symbols) formed during degradation of BEH-PPV PLED as a function of aging time at current densities 35 mA/cm^2 . Active layer thickness of the BEH-PPV is 200 nm.

5.2.2. Exciton lifetime

Figure 5.2 shows the PL decay times of BEH-PPV PLEDs unaged and stressed under constant current density of 35 mA/cm^2 for 211 h. The aged device demonstrates faster PL decay relative to the unaged sample, while the exciton lifetime (τ_f , shown in brackets) decreases from 170 ps to 140 ps upon stressing the device. The exciton lifetime of the unaged device (170 ps) is only slightly shorter compared to pristine BEH-PPV thin film (180–200 ps, in Chapter 3 and 4), which is attributed to charge transfer/exciton quenching at the electrode interface.⁷⁰

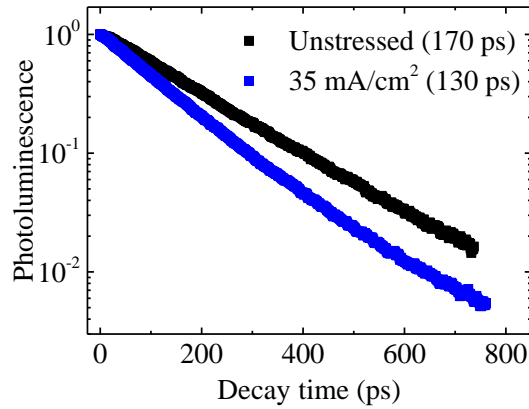


Figure 5.2. Normalized PL decay curves of BEH-PPV PLEDs measured at the PL maximum (580–600 nm). The device was stressed for 211 h under constant current density: unstressed (black) and 35 mA/cm^2 (blue). The exciton lifetime has been determined by using equation 2.3.

As reported in Chapter 3, the exciton lifetime τ_f in thin conjugated polymer films is governed by the diffusion of excitons toward non-radiative quenching-sites and can be expressed by the following equation:

$$\tau_f = 1 / (k_{\text{rad}} + k_{\text{nonrad}} + k_{\text{diff}}) \quad (5.1)$$

where k_{rad} and k_{nonrad} are the radiative and non-radiative decay rates, and k_{diff} is the non-radiative decay rate originating from exciton quenching at defect sites due to exciton diffusion. Therefore, the measured exciton lifetime represents the time an exciton needs to find a quenching-site. Since the decay rates k_{rad} and k_{nonrad} are intrinsic numbers and considered to remain constant during the BEH-PPV PLED device aging process, the only parameter that influences the exciton lifetime is k_{diff} .

The two factors that determine k_{diff} , are the exciton diffusion toward non-radiative quenching-sites and the concentration of these quenching-sites. In the first case, a decrease in exciton lifetime can be correlated to an increase in exciton diffusion rate with a constant concentration of defect sites in the conjugated polymer. Faster exciton diffusion would then result in a higher probability of the excitons reaching a quenching energy-site and, consequently, the exciton lifetime would decrease. On the other hand, the concentration of quenching-sites can change, while the exciton diffusion remains unchanged. In this case, the exciton lifetime decreases with increasing concentration of trapping-sites, since more non-radiative quenching-sites in the conjugated polymer increase the probability of the exciton to be quenched.

We have previously shown that the exciton diffusion correlates with the energetic disorder of the conjugated polymer, as described by the width of the Gaussian DOS. Better ordered polymers have narrower DOS and this results in faster exciton diffusion and shorter exciton lifetime (Chapter 3). Considering this, enhanced exciton diffusion in the BEH-PPV PLED would correlate with a decrease in energetic disorder. This energetic disorder is predominantly determined by molecular structure and is unexpected to change upon device stressing. We thus assume that the exciton diffusion rate in the BEH-PPV PLED should not change with device stress. This leads us to conclude that the decrease in exciton lifetime is due to an increase in non-radiative quenching sites in the BEH-PPV PLED. With increasing

number of quenching-sites, the excitons can find a quenching-site faster, resulting in a shorter exciton lifetime. This is consistent with diffusion-limited exciton quenching at defect sites.

However, the origin of these defect-sites is not straightforward to identify, since many photophysical processes take place at the same time in conjugated polymer films. For example, time-resolved photoluminescence spectroscopy measurements have found a concentration of exciton quenchers in the range of 10^{17} – 10^{18} cm^{-3} in a series of unaged organic semiconductors.⁶¹ Remarkably, the number of “background” exciton quenchers present in organic semiconductors is similar to the universal electron trap density that has been reported for a large range of conjugated polymers, as measured by charge transport measurements.⁶² Furthermore, Mikhnenko et al. proposed that the electron traps and the exciton quenching defects share the same origin and that the excitons can be quenched at these traps via electron transfer.⁶¹ Barbara and co-workers reported exciton quenching by holes (polarons).⁷⁶ Analogous to exciton quenching at electron traps, it is expected that excitons can be quenched at hole traps via hole transfer.¹⁵⁰

Electrical measurements and numerical simulations have ascribed PLED degradation to the formation of hole traps.⁸ The question is now whether such generated hole traps will also quench excitons via an additional non-radiative decay process and are therefore responsible for the decrease in exciton lifetime, followed by how this would affect the photoluminescence efficiency of the degraded device.

5.2.3. Monte Carlo simulation

We subsequently used the Monte Carlo based simulation to determine the amount of non-radiative exciton quenchers (hole traps) in the aged BEH-PPV PLED. The simulation models the PL decays in semiconducting-quencher mixtures and is comprehensively

described in Chapter 2.7. The following parameters are taken as simulation input: the measured PL decay time of the pristine semiconductor film τ_f , the measured PL decay time of the specific semiconductor-quencher blend τ , the volume fraction (concentration) of quencher molecules (e.g. PCBM) and the sample morphology, which is represented by the relative quenching efficiency Q (Eq. 2.11). The simulation uses the random walk model and assumes that the quenching molecules are homogeneously distributed at low concentrations.

The first step is to calculate the exciton diffusion coefficient D , which represents the spatial and temporal exciton population in BEH-PPV. Here, the only fitting parameter is D , and the output includes the simulated PL decay kinetics. The simulation is then repeated with adjusted values of D until the modeled PL decay agrees sufficient with the experimentally determined PL decay. Therefore, the simulation output is the number of radiatively decayed excitons versus time. In Chapter 2.5 and Chapter 3, fluorescence quenching experiments in thin BEH-PPV films with randomly distributed PCBM molecules were used to retrieve an exciton diffusion coefficient of $D = 2.0 \times 10^{-3} \text{ cm}^2/\text{s}$.

As noted above, the exciton diffusion is not expected to change upon aging of the BEH-PPV PLED, but the amount of non-radiative quenchers is expected to increase. So as a next step, the exciton diffusion coefficient was kept constant, and the quencher concentration was adjusted until the simulation modeled PL decays agreed with the measured PL decay of the aged PLED. Figure 5.3 shows the simulated PL decay for a specific concentration of exciton quencher (red line), which shows good agreement with the measured PL decay aged under the constant current density of $35 \text{ mA}/\text{cm}^2$ (black squares). From the simulated PL decay, the concentration of non-radiative quenching sites has been determined to $4.4 (\pm 0.5) \times 10^{17} \text{ cm}^{-3}$. We note that in the PL decay of the pristine PLED already the quenching of excitons by electron traps ($c_0 = 1.0 \times 10^{18} \text{ cm}^{-3}$) has been included.

The reported quenching-site densities here are the *additional* quenching-sites formed after 211 hr of current stress.

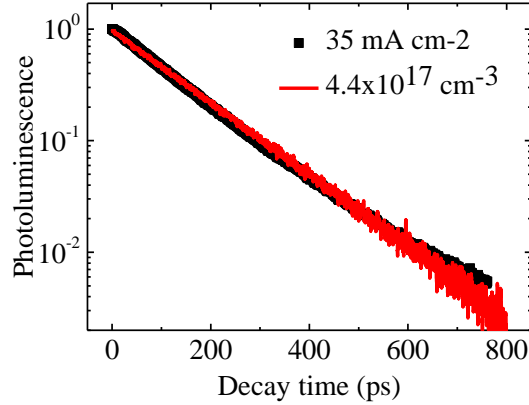


Figure 5.3. Measured (black squares) and simulated (red solid lines) PL decay of BEH-PPV PLED stressed under constant current density of 35 mA/cm².

Table 5.1 compares the density of hole traps P_t after 211 h of aging determined by modelling the J - V and L - V of the degraded PLED,⁸ and the amount of non-radiative quenching-sites c_0 determined via photoluminescence measurements and Monte Carlo simulations. We find that the number of quenching-sites calculated from the optical experiments is close to the concentration of hole traps measured electrically.

Table 5.1. Comparison between concentration of hole traps P_t determined from electrical measurements and number of exciton quenchers c_0 determined via optical measurements.

Aging current density	35 mA cm ⁻²
P_t (cm ⁻³)	2.8×10^{17}
c_0 (cm ⁻³)	4.4×10^{17}

As final step to find out how the measured amount of quenching-sites will affect the photoluminescence quantum yield (PLQY), the relative quenching efficiency Q is calculated $Q = I - \tau_{stressed} / \tau_{unstressed}$, and converted in a relative photoluminescence quantum yield $rPLQY$ using $rPLQY = 1 - Q$. The resulting relative PLQY is determined to 76%.

Therefore, we observe that after 211 h of bias stress at $J = 35 \text{ mA/cm}^2$ the PLQY of the film is still above 75%, whereas the electroluminescence has already dropped to less than 40%. This difference is the result of different mechanisms for quenching; the electroluminescence is reduced by nonradiative recombination of free electrons with trapped holes, which is an efficient process. The PLQY on the other hand is governed by diffusion of excitons towards the newly formed hole traps.

5.3. Conclusion

TRPL measurements on aged BEH-PPV PLED show an enhanced exciton decay relative to the unaged device. This is ascribed to increased non-radiative quenching due to hole traps that form during the aging process. The amount of non-radiative quenching sites that form during degradation are quantified from the TRPL measurements and Monte Carlo simulations and are in good agreement with the concentration of hole traps determined from electrical measurements. This demonstrates that the formed hole traps are responsible for both the decrease of the electroluminescence by non-radiative recombination of free electrons with a trapped hole as well as the reduction of the photoluminescence quantum yield due to quenching of excitons. The different dependence of these mechanism on hole trap concentration explains why electroluminescence and photoluminescence behave differently during current stress of a PLED.

5.4. Outlook

The identification of hole trap formation as a main cause of electrical degradation enabled a quantitative analysis of the aging-time dependence on hole trap formation and its dependence on stress conditions. As a result, the density of hole traps $P_t(t)$ can be approximated by the following equation:¹⁴⁹

$$P_t(t) = \alpha J \sqrt{t} \quad (5.2)$$

where α is the proportionality constant, J is the aging current density and t is the aging time. Therefore, the formation of hole traps is proportional to the current density and the time.¹⁴⁹

In Chapter 5 the BEH-PPV PLED stressed under a constant current density of 35 mA/cm² is presented. By applying equation 5.2 a hole trap density of $3.0 (\pm 0.2) \times 10^{17} \text{ m}^{-3}$ is calculated, which matches the one determined from electrical measurements ($2.8 \times 10^{17} \text{ m}^{-3}$). Since the density of formation of hole traps correlates with increase driven current density and aging time, a comprehensive study of the impact of different current densities and aging times on the exciton properties should be investigated in a subsequent study; does the exciton trap formation show a similar correlation with increase current density and time? Further, it should be considered that α is a proportionality factor and thus material dependent. Therefore, it would be interesting to see how the formation of hole traps in different PPV derivatives would determines the exciton lifetime and PLQY.

Summary

The introduction of optoelectronic devices based on conjugated polymers on the market is prevented by their relatively short lifetime and low efficiency. One reason is that these typically amorphous materials are subject to energetic disorder, which arises from intrinsic and extrinsic properties, such as molecular conformational irregularities, impurities and chemical defects. Nevertheless, despite their low device performance, conjugated polymers offer the added benefits of low-cost manufacturing, light-weight, flexibility and biocompatibility. Thus, with further understanding of the fundamental properties and limits to device performances, these polymers can open a new field for future applications, such as paper electronics, artificial skin and wearable electronics.

In this thesis, the influence of the energetic disorder of the conjugated polymer on the exciton properties and device performance was investigated. In **Chapter 3**, a correlation between the exciton lifetime and polymer disorder is described in a range of conjugated polymers, while the exciton lifetime increased by more than an order of magnitude with increasing disorder. Simultaneously, the exciton diffusion coefficient decreased by 1 order of magnitude. Our findings suggest that the PL decay time in thin polymer films is not limited by the intrinsic exciton lifetime but governed by the time excitons need to diffuse toward non-radiative quenching centers, which is consistent with the diffusion-limited exciton quenching model. Preventing excitons to reach these quenching-sites by slowing down their diffusion toward traps would not only result in long exciton lifetimes but also in an increased PLQY. As a consequence, highly disordered polymers with slow exciton diffusion not only show a long exciton lifetime but also exhibit a higher PLQY relative to the more ordered polymers.

These issues have been further investigated in **Chapter 4**, where at varying temperature the effect of conformational energetic disorder on the photo and electro-

luminescence behavior has been investigated in two PPV derivatives. A correlation between the energetic disorder and the balance between radiative and non-radiative decay processes is derived, the latter of which includes also non-radiative decay processes due to exciton diffusion toward non-radiative quenching-sites. In addition, distinct temperature dependencies of the exciton diffusion properties based on the polymer disorder were obtained, which also determine the polymer-light emitting diode performance. The PLED based on the more disordered polymer show temperature independent current efficiencies, as it is reported in most polymer-based LED devices, while the PLED based on the better ordered polymer shows enhanced current efficiencies at lower temperatures due to reduced exciton quenching at defect centers.

In **Chapter 5** the impact of hole traps generated mainly from electrical degradation on the exciton properties is demonstrated. A decrease in exciton lifetime upon stressing the device at a constant current density with respect to the unaged one is observed, which is ascribed to increased non-radiative quenching due to hole trap formation. The amount of additional quenching sites is quantified by Monte Carlo simulations and in a good agreement with the number of hole traps predicted from electrical charge transport measurements (and numerical simulations). Our results reveal that the apparent contradiction of strong electroluminescence decrease with a nearly unaffected photo-luminescence decay under current stress is the result of different physical mechanisms. While the decrease of the electroluminescence is governed by recombination of free electrons with trapped holes, the photoluminescence is reduced by non-radiative quenching processes between excitons and hole traps.

Zusammenfassung

Die Markteinführung von optoelektronischen Bauteilen basierend auf konjugierten Polymeren ist aufgrund ihrer kurzen Lebensdauer und niedrigen Effizienz erschwert. Ein limitierender Faktor ist, dass diese – im allgemeinen amorphen Materialien – eine energetische Unordnung aufweisen, die auf intrinsische und extrinsische Eigenschaften zurück zu führen ist, wie z.B. Unregelmäßigkeiten in der molekularen Konformation, Verunreinigungen sowie chemischen Defekten. Trotz dieser Nachteile von polykonjugierten Materialien gegenüber sogenannter „*small molecules*“, die durch ausgereifte Prozessiermethoden (Aufdampfen/Sublimation) die in- und extrinsischen Ursachen für die energetischen Unordnung minimieren, haben Polymere das Potential neue Anwendungsfelder zu erschließen. Insbesondere wenn die Herstellung von kostengünstigen, leichten, flexiblen und/oder biokompatiblen Bauteilen einer höheren Gewichtung zukommt.

Im Rahmen dieser Arbeit wurde untersucht inwiefern die energetische Unordnung des konjugierten Polymers die Exciton-Diffusion-Charakteristika beeinflusst sowie mögliche Faktoren, die die Bauteilperformanz limitieren.

In **Kapitel 3** wurde der Zusammenhang zwischen der energetischen Unordnung des Polymers und der Exciton-Lebensdauer sowie Photolumineszenz-Quantenausbeute einer Reihe konjugierter Polymere untersucht. Dabei wurde beobachtet, dass die Exciton-Lebensdauer mit steigender Polymerunordnung um eine Größenordnung zunimmt. Gleichzeitig nimmt der Exciton-Diffusionskoeffizient um eine Größenordnung ab. Die Untersuchungen ergaben außerdem, dass die Photolumineszenz-Abfallszeit (bzw. Exciton-Lebenszeit) in dünnen Polymerfilmen nicht durch die intrinsische Lebensdauer der Excitonen limitiert ist. Stattdessen spielt die Zeit, die die Excitonen benötigen, um zu einem

Auslöschungszentrum (*non-radiative quenching center*) zu diffundieren eine entscheidende Rolle, welche wiederum mit der '*diffusion-limited exciton quenching*'-Theorie im Einklang steht. Dem folgt, wenn das Erreichen der Excitonen-Auslöschungszentren z. B. durch die Verringerung der Exciton-Diffusion zu diesen '*traps*' verhindert werden kann, dann sollte nicht nur die Excitonen-Lebensdauer ansteigen, sondern auch die Quantenausbeute. Polymere mit einer höher energetischen Unordnung weisen eine langsame Exciton-Diffusion auf und somit nicht nur eine lange Exciton-Lebensdauer, sondern auch eine höhere Photolumineszenz-Quantenausbeute als Polymere mit einer geringeren Unordnung.

Dieser Sachverhalt wurde fortführend in **Kapitel 4** untersucht, wobei der Effekt der energetischen Unordnung auf die Photo- und Elektrolumineszenz-Eigenschaften in zwei energetisch unterschiedlichen Poly(*p*-phenylene-vinylene) Derivativen untersucht wurde. Ein Zusammen-hang zwischen der energetischen Unordnung und dem Gleichgewicht zwischen den strahlenden und strahlungslosen Übergängen wurde abgeleitet. Letztere setzen sich aus den intrinsischen und den strahlungslosen Prozessen aufgrund der Exciton-Diffusion zu den Auslöschzentren zusammen. Zusätzlich wurden unterschiedliche Temperaturabhängigkeiten der Exciton-Diffusions-Eigenschaften basierend auf der energetischen Polymerunordnung beobachtet, die zudem die Performanz der Polymer-Leuchtdiode (PLED) bestimmten. Die Stromausbeute der PLED des Polymers mit einer größeren energetischen Unordnung weist keine Temperaturabhängigkeit auf, was für die meisten Polymer-basierenden LED Bauteile beschrieben wird. Im Gegensatz dazu, weist die PLED des Polymers mit geringerer Unordnung eine Erhöhung der Stromausbeute bei niedrigeren Temperaturen auf. Die durch Temperaturerniedrigung bedingte Erhöhung der Stromausbeute (Effizienz) wird einer Verlangsamung der Exciton-Diffusion zugeschrieben, welche auf eine geringere Wahrscheinlichkeit der Excitonen-Auslöschung an den Defektstellen zurückzuführen ist.

Nach dem die Exciton-Charakteristika in Abhängigkeit der energetischen Unordnung des konjugierten Polymers untersucht wurden, lag der Fokus in **Kapitel 5** auf die Untersuchung des Einflusses von Lochfallen auf die Exciton-Eigenschaften sowie der Bauteil-Performanz. Es wurde kürzlich berichtet, dass durch die elektrische Degradation, d.h. durch das Anlegen einer konstanten Spannung, Lochfallen generiert werden. Diese Lochfallen sind potentielle Excitonen-Auslöschzentren, wodurch eine Verringerung der Exciton-Lebensdauer nach dem Anlegen einer konstanten Stromdichte an der PLED resultierte im Vergleich zu dem elektrisch nicht beanspruchten Bauteil. Die Zunahme der strahlungslosen Übergänge (Auslöschzentren) wird der Entstehung von Lochfallen zugeschrieben. Die Anzahl der Auslöschzentren wurde mittels Monte Carlo Simulation quantifiziert und ist in guter Übereinstimmung mit der Anzahl der Lochfallen, die mithilfe von elektrischen Ladungstransport-Messungen und numerischen Simulationen ermittelt wurden. Des Weiteren kann der Unterschiede im signifikanten Abfall der Elektrolumineszenz vergleichen mit dem beinahe unbeeinflussten Photolumineszenz-Abfall bei einer konstanten Stromdichte auf unterschiedliche physikalische Prozesse zurückgeführt werden. Während der Abfall in der Elektrolumineszenz durch die Rekombination von freien Elektronen und gefangenen (*'getrapped'*) Löchern bestimmt wird, ist die Reduzierung der Photolumineszenz auf den strahlungslosen Auslöschungsprozess zwischen Excitonen und Lochfallen zurück zu führen.

References

- [1] C. K. Chiang, C. R. Fincher Jr., Y. W. Park, A. J. Heeger, H. Shirakawa, E. J. Louis, S. C. Gau, A. G. MacDiarmid. *Phys. Rev. Letters* **1977**, *39*, 1098–1101.
- [2] C. J. Brabec, N. S. Sariciftci, J. C. Hummelen. *Adv. Funct. Mater.* **2001**, *11*, 15–26.
- [3] J. H. Burroughes, D. D. C. Bradley, A. R. Brown, R. N. Marks, K. Mackay, R. H. Friend, P. L. Burns, A. B. Holmes. *Nature* **1990**, *347*, 539–541.
- [4] K. Asadi, D. M. de Leeuw, B. de Boer, P. W. M. Blom. *Nat. Mater.* **2008**, *7*, 547.
- [5] H. Klauk. *Chem. Soc. Rev.* **2010**, *39*, 2643–2666.
- [6] B. Adhikari, S. Majumdar. *Prog. Polym. Sci.* **2004**, *29*, 699–766.
- [7] D. E. Markov, C. Tanase, P. W. M. Blom, J. Wildeman. *Phys. Rev. B* **2005**, *72*, 045217.
- [8] Q. Niu, G. J. A. H. Wetzelaer, P. W. M. Blom, N. I. Craciun. *Adv. Electron. Mater.* **2016**, *2*, 1300103.
- [9] M. E. Gershenson, V. Podzorov, A. F. Morpurgo. *Rev. Mod. Phys.* **2006**, *78*, 973.
- [10] Y. Miao, P. Tao, K. Wang, H. Li, B. Zhao, L. Gao, H. Wang, B. Xu, Q. Zhao. *ACS Appl. Mater. Interfaces* **2017**, *9*, 37873–37882.
- [11] H. Fukagawa, T. Shimizu, T. Kamada, S. Yui, M. Hasegawa, K. Morii, T. Yamamoto. *Scientific reports* **2015**, *5*, 9855.
- [12] Heliatek, URL: <http://www.heliatek.com/de/> (Stand: 05.08.2018).
- [13] D. Tobjörk, R. Österbacka. *Adv. Mater.* **2011**, *23*, 1935–1961.
- [14] A. Nathan, B. R. Chalamala. *Proceedings of the IEEE* **2005**, *93*, 1391–1393.
- [15] T. Yokota, P. Zalar, M. Kaltenbrunner, H. Jinno, N. Matsuhisa, H. Kitanosako, Y. Tachibana, W. Yukita, M. Koizumi, T. Someya. *Sci. Adv.* **2016**, *2*, e1501856.
- [16] J. Clayden, N. Greeves, S. Warren, P. Wothers: *Organic Chemistry*; Oxford University Press, 2001.
- [17] G. D. Scholes, G. Rumbles. *Nature Materials* **2006**, *5*, 683–696.
- [18] R. Hoffmann, C. Janiak, C. Kollmar. *Macromolecules* **1991**, *24*, 3725–3746.
- [19] O. V. Mikhnenko, P. W. M. Blom, T.-Q. Nguyen. *Energy Environ. Sci.* **2015**, *8*, 1867–1888.
- [20] S. T. Hoffmann, H. Bässler, A. Köhler. *J. Phys. Chem. B* **2010**, *114*, 17037–17048.
- [21] I. Hwang, G. D. Scholes. *Chem. Mater.* **2011**, *23*, 610–620.
- [22] H. Bässler. *Phys. Stat. Sol. B* **1993**, *175*, 15–56.
- [23] B. Movaghar, M. Grünwald, B. Ries, H. Bässler, D. Würtz. *Phys. Rev. B* **1986**, *33*, 5545–5554.
- [24] H. Bässler. *Phys. Stat. Sol. B* **1981**, *107*, 9–54.
- [25] A. Jablonski. *Nature* **1933**, *131*, 839–840.
- [26] B. Valeur: *Molecular Fluorescence: Principles and Applications*; Wiley-VCH Verlag GmbH, 2002.
- [27] M. Kasha. *Discussions of the Faraday Society* **1950**, *9*, 14–19.
- [28] J. Franck. *Trans. Faraday Soc.* **1926**, *21*, 536–542.
- [29] E. Condon. *Phys. Rev.* **1926**, *28*, 1182–1201.
- [30] P. Atkins, J. de Paula: *Atkins' Physical Chemistry*, Oxford University Press, 2006.
- [31] M. Born, R. Oppenheimer. *Ann. Phys.* **1927**, *389*, 457–484.
- [32] G. G. Stokes. *Philosophical Transactions of the Royal Society of London* **1852**, *142*, 463–562.
- [33] M. Ravi, A. Samanta, t. P. Radhakrishnan. *J. Phys. Chem.* **1994**, *98*, 9133–9136.
- [34] A. Köhler, H. Bässler. *Materials Science & Engineering R-Reports* **2009**, *66*, 71.

- [35] M. Scheidler, U. Lemmer, R. Kersting, S. Karg, W. Riess, B. Cleve, R. F. Mahrt, H. Kurz, H. Bässler, E. O. Göbel, P. Thomas. *Phys. Rev. B* **1996**, *54*, 5536–5544.
- [36] R. N. Marks, J. J. M. Halls, D. D. C. Bradley, R. H. Friend, A. B. Holmes, *J. Phys. Condens. Matter* **1994**, *6*, 1379–1394.
- [37] A. Köhler, H. Bässler.: Electronic and Optical Processes of Organic Semiconductors. In *Electronic Processes in Organic Semiconductors: An Introduction*; Wiley-VCH Verlag GmbH, 2015.
- [38] S. M. Menke, R. J. Holmes. *Energy Environ. Sci.* **2014**, *7*, 499–512.
- [39] D. L. Dexte. *J. Chem. Phys.* **1953**, *21*, 836–850.
- [40] Y. Kawamura, J. Brooks, J. J. Brown, H. Sasabe, C. Adachi. *Phys. Rev. Lett.* **2006**, *96*, 017404.
- [41] B. Mollay, U. Lemmer, R. Kersting, R. F. Mahrt, H. Kurz, H. F. Kauffmann, H. Bässler. *Phys. Rev. B Condens. Matter* **1994**, *50*, 10769–10779.
- [42] R. Kersting, U. Lemmer, R. F. Mahrt, K. Leo, H. Kurz, H. Bässler, E. O. Göbel. *Phys. Rev. Lett.* **1993**, *70*, 3820–3823.
- [43] T. G. Bjorklund, S. H. Lim, C. J. Bardeen. *J. Phys. Chem. B* **2001**, *105*, 11970–11977.
- [44] O. V. Mikhnenko, F. Cordella, A. B. Sieval, J. C. Hummelen, P. W. M. Blom, M. A. Loi. *J. Phys. Chem. B* **2008**, *112*, 11601–11604.
- [45] M. Grünwald, B. Pohlmann, B. Movaghar, D. Würtz. *Philos. Mag. B* **1984**, *49*, 341–356.
- [46] P. W. M. Blom, V. D. Mihailetschi, L. J. A. Koster, D. E. Markov. *Adv. Mater.* **2007**, *19*, 1551–1566.
- [47] N. S. Sariciftci, L. Smilowitz, A. J. Heeger, F. Wudl. *Science* **1992**, *258*, 1474.
- [48] B. J. Schwartz. *Annu. Rev. Phys. Chem.* **2003**, *54*, 141–172.
- [49] D. Beljonne, G. Pourtois, C. Silva, E. Hennebicq, L. M. Herz, R. H. Friend, G. D. Scholes, S. Setayesh, K. Müllen, J.-L. Brédas. *Proc. Natl Acad. Sci. U. S. A.* **2002**, *99*, 10982–10987.
- [50] E. Hennebicq, G. Pourtois, G. D. Scholes, L. M. Herz, D. M. Russell, C. Silva, S. Setayesh, A. C. Grimsdale, K. Müllen, J.-L. Brédas, D. Beljonne. *JACS* **2005**, *127*, 4744–4762.
- [51] C. J. Collison, L. J. Rothberg, V. Treemanekarn, Y. Li. *Macromolecules* **2001**, *34*, 2346–2352.
- [52] S. Gambino, A. K. Bansal, I. D. W. Samuel. *Organic Electronics* **2013**, *14*, 1980.
- [53] I. D. W. Samuel, G. Rumbles, C. J. Collison, R. H. Friend, S. C. Moratti, A. B. Holmes. *Synth. Met.* **1997**, *84*, 497–500.
- [54] J. Clark, C. Silva, R. H. Friend, F. C. Spano. *Phys. Rev. Lett.* **2007**, *98*, 206406.
- [55] M. Yan, L. J. Rothberg, E. W. Kwock, T. M. Miller. *Phys. Rev. Lett.* **1995**, *75*, 1992–1995.
- [56] N. C. Greenham, I. D. W. Samuel, G. R. Hayes, R. T. Phillips, Y. A. R. R. Kessener, S. C. Moratti, A. B. Holmes, R. H. Friend. *Chem. Phys. Lett.* **1995**, *241*, 89–96.
- [57] T.-Q. Nguyen, I. B. Martini, J. Liu, B. J. Schwartz. *J. Phys. Chem. B* **2000**, *104*, 237–255.
- [58] T.-Q. Nguyen, J. Wu, S. H. Tolbert, B. J. Schwartz. *Adv. Mater.* **2001**, *13*, 609.
- [59] B. J. Schwartz, T.-Q. Nguyen, J. Wu, S. H. Tolbert. *Synth. Met.* **2001**, *116*, 35–40.
- [60] S. Athanasopoulos, E. Hennebicq, D. Beljonne, A. B. Walker. *J. Phys. Chem. C* **2008**, *112*, 11532–11538.
- [61] O. V. Mikhnenko, M. Kuik, J. Lin, N. van der Kaap, T.-Q. Nguyen, P. W. M. Blom. *Adv. Mater.* **2014**, *26*, 1912–1917.

- [62] H. T. Nicolai, M. Kuik, G. A. H. Wetzelaer, B. de Boer, C. Campbell, C. Risko, J. L. Brédas, P. W. M. Blom. *Nat. Mater.* **2012**, *11*, 882–887.
- [63] M. Yan, L. J. Rothberg, F. Papadimitrakopoulos, M. E. Galvin, T. M. Miller. *Phys. Rev. Lett.* **1994**, *73*, 744–747.
- [64] L. J. Rothberg, M. Yan, F. Papadimitrakopoulos, M. E. Galvin, E. W. Kwock, T. M. Miller. *Synth. Met.* **1996**, *80*, 41–58.
- [65] L. J. Rothberg, M. Yan, S. Son, M. E. Galvin, E. W. Kwock, T. M. Miller, H. E. Katz, R. C. Haddon, F. Papadimitrakopoulos. *Synth. Met.* **1996**, *78*, 231–236.
- [66] R. G. Kepler, V. S. Valencia, S. J. Jacobs, J. J. McNamara. *Synth. Met.* **1996**, *78*, 227–230.
- [67] D. E. Markov, P. W. M. Blom. *Phys. Rev. B* **2005**, *72*, 161401.
- [68] H. Becker, S. E. Burns, R. H. Friend. *Phys. Rev. B* **1997**, *56*, 1893–1905.
- [69] I. B. Martini, A. D. Smith, B. J. Schwartz. *Phys. Rev. B* **2004**, *69*, 035204.
- [70] P. E. Shaw, A. Ruseckas, I. D. W. Samuel. *Adv. Mater.* **2008**, *20*, 3516–3520.
- [71] A. J. Lewis, A. Ruseckas, O. P. M. Gaudin, G. R. Webster, P. L. Burn, I. D. W. Samuel. *Org. Electron.* **2006**, *7*, 452–456.
- [72] Y. Tamai, Y. Matsuura, H. Ohkita, H. Benten, S. Ito. *J. Phys. Chem. Lett.* **2014**, *5*, 399–403.
- [73] E. Engel, K. Leo, M. Hoffmann. *Chem. Phys. Lett.* **2006**, *325*, 170–177.
- [74] A. Suna. *Phys. Rev. B-Solid State* **1970**, *1*, 1716–1739.
- [75] J. R. Lakowicz: *Principles of Fluorescence Spectroscopy*; Springer, 2006.
- [76] A. J. Gesquiere, S.-J. Park, P. F. Barbara. *JACS* **2005**, *127*, 9556–9560.
- [77] M. Theander, A. Yartsev, D. Zigmantas, V. Sundström, W. Mammo, M. R. Andersson, O. Inganäs. *Phys. Rev. B* **2000**, *61*, 12957–12963.
- [78] D. E. Markov, E. Amsterdam, P. W. M. Blom, A. B. Sieval, J. C. Hummelen. *J. Phys. Chem. A* **2005**, *109*, 5266–5274.
- [79] A. Haugeneder, M. Neges, C. Kallinger, W. Spirkl, U. Lemmer, J. Feldmann, U. Scherf, E. Harth, A. Gügel, K. Müllen. *Phys. Rev. B* **1999**, *59*, 15346–15351.
- [80] O. V. Mikhnenko, F. Cordella, A. B. Sieval, J. C. Hummelen, P. W. M. Blom, M. A. Loi. *J. Phys. Chem. B* **2009**, *113*, 9104–9109.
- [81] D. E. Markov, J. C. Hummelen, P. W. M. Blom, A. B. Sieval. *Phys. Rev. B* **2005**, *72*, 045216.
- [82] N. A. Anderson, E. Hao, X. Ai, G. Hastings, T. Lian. *Chem. Phys. Lett.* **2001**, *347*, 304–310.
- [83] T. J. Savenije, J. E. Kroeze, M. M. Wienk, J. M. Kroon, J. M. Warman. *Phys. Rev. B* **2004**, *69*, 155205.
- [84] J. E. Kroeze, T. J. Savenije, M. J. W. Vermeulen, J. M. Warman. *J. Phys. Chem. B* **2003**, *107*, 7696–7705.
- [85] M. C. Fravventura, J. Hwang, J. W. A. Suijkerbuijk, P. Erk, L. D. A. Siebbeles, T. J. Savenije. *J. Phys. Chem. Lett.* **2012**, *3*, 2367–2373.
- [86] P. Peumans, A. Yakimov, S. R. Forrest. *J. Appl. Phys.* **2003**, *93*, 3693–3723.
- [87] V. Bulović, S. R. Forrest. *Chem. Phys. Lett.* **1995**, *238*, 88–92.
- [88] J. J. M. Halls, K. Pichler, R. H. Friend, S. C. Moratti, A. B. Holmes. *Appl. Phys. Lett.* **1996**, *68*, 3120–3122.
- [89] H. Najafov, B. Lee, Q. Zhou, L. C. Feldman, V. Podzorov. *Nat. Mater.* **2010**, *9*, 938–943.
- [90] M. Guide, J. D. A. Lin, C. M. Proctor, J. Chen, C. Garcia-Cervera, T.-Q. Nguyen. *J. Mater. Chem. A* **2014**, *2*, 7890.
- [91] O. V. Mikhnenko, H. Azimi, M. Scharber, M. Morana, P. W. M. Blom, M. A. Loi. *Energy Environ. Sci.* **2012**, *5*, 6960–6965.

- [92] L. Lüer, H. J. Egelhaaf, D. Oelkrug, G. Cerullo, G. Lanzani, B. H. Huisman, D. de Leeuw. *Org. Electron.* **2004**, *5*, 83–89.
- [93] D. E. Markov, P. W. M. Blom. *Phys. Rev. B* **2006**, *74*, 085206.
- [94] A. Bruno, L. X. Reynolds, C. Dyer-Snaith, J. Nelson, S. A. Haque. *J. Phys. Chem. C* **2013**, *117*, 19832–19838.
- [95] L. C. Groff, X. Wang, J. D. McNeill. *J. Phys. Chem. C* **2013**, *117*, 25748–25755.
- [96] M. T. Rispens, A. Meetsma, R. Rittberger, C. J. Brabec, N. C. Sariciftci, J. C. Hummelen. *Chem. Comm.* **2003**, 2116–2118.
- [97] C. W. T. Bulle-Lieuwma, W. J. H. van Gennip, J. K. J. van Duren, P. Jonkheijm, R. A. J. Janssen, J. W. Niemantsverdriet. *Applied surface science* **2003**, *203*, 547.
- [98] J. W. Kiel, B. J. Kirby, C. F. Majkrzak, B. B. Maranville, M. E. Mackay. *Soft Matter* **2010**, *6*, 641–646.
- [99] W. Geens, T. Martens, J. Poortmans, T. Aernouts, J. Manca, L. Lutsen, P. Heremans, S. Borghs, R. Mertens, D. Vanderzande. *Thin Solid Films* **2004**, *451*, 498–502.
- [100] Hamamatsu: URL (17.09.2018):
https://www.hamamatsu.com/resources/pdf/sys/SHSS0006E_STREAK.pdf.
- [101] J. J. Snellenburg, S. P. Liptonok, R. Seger, K. M. Mullen, I. H. M. van Stokkum, *J. Stat. Soft.* **2012**, *49*, 1–22.
- [102] K. M. Mullen, I. H. M. van Stokkum. *J. Stat. Soft.* **2007**, *18*, 1–16.
- [103] Glotaran software download: URL: <http://www.glotaran.org/> (17.09.2018).
- [104] R. Jakubiak, L. J. Rothberg, W. Wan, B. R. Hsieh. *Synth. Met.* **1999**, *101*, 230–233.
- [105] O. V. Mikhnenko, J. Lin, Y. Shu, J. E. Anthony, P. W. M. Blom, T.-Q. Nguyen, M. A. Loi. *Phys. Chem. Chem. Phys.* **2012**, *14*, 14196–14201.
- [106] O. V. Mikhnenko, *Software for Monte Carlo simulation for download at URL:* <http://mikhnenko.com/eDiffusion/> (05.08.2018).
- [107] Y. C. Zhou, Y. Wu, L. L. Ma, J. Zhou, X. M. Ding, X. Y. Hou. *J. Appl. Phys.* **2006**, *100*, 023712.
- [108] S. B. Lee, I. C. Kim, C. A. Miller, S. Torquato. *Phys. Rev. B* **1989**, *39*, 11833.
- [109] J. A. Anta. *Energy Environ. Sci.* **2009**, *2*, 387–392.
- [110] Riley, M. R.; Buettner, H. M.; Muzzio, F. J.; Reyes, S. C.. *Biophysical journal* **1995**, *68*, 1716–1726.
- [111] M. Matsumoto, T. Nishimura. *ACM TOMACS* **1998**, *8*, 3–30.
- [112] Pseudo random number generators software download: URL:
<https://www.agner.org/random/> (20.09.2018).
- [113] E. L. Frankevich, A. A. Lymarev, I. Sokolik, F. E. Karasz, S. Blumstengel, R. H. Baughman, H. H. Horhold. *Phys. Rev. B* **1992**, *46*, 9320–9324.
- [114] M. Gailberger, H. Bäessler. *Phys. Rev. B* **1991**, *44*, 8643–8651.
- [115] J. W. P. Hsu, M. Yan, T. M. Jedju, L. J. Rothberg, B. R. Hsieh. *Phys. Rev. B* **1994**, *49*, 712–715.
- [116] G. Schönherr, R. Eiermann, H. Bäessler, M. Silver. *Chem. Phys.* **1980**, *52*, 287–298.
- [117] W. J. D. Beenken, T. Pullerits. *J. Phys. Chem. B* **2004**, *108*, 6164–6169.
- [118] T.-Q. Nguyen, J. Wu, V. Doan, B. J. Schwartz, S. H. Tolbert. *Science* **2000**, *288*, 652–656.
- [119] S. R. Yost, E. Hontz, S. Yeganeh, T. Van Voorhis. *J. Phys. Chem. C* **2012**, *116*, 17369–17377.
- [120] J. Seixas de Melo, H. D. Burrows, M. Svensson, M. R. Andersson, A. P. Monkman. *J. Chem. Phys.* **2003**, *118*, 1550–1556.
- [121] M. A. Loi, C. Gadermaier, E. J. W. List, G. Leising, W. Graupner, G. Bongiovanni, A. Mura, J. J. Pireaux, K. Kaeriyama. *Phys. Rev. B* **2000**, *61*, 1859–1865.

- [122] N. T. Harrison, G. R. Hayes, R. T. Phillips, R. H. Friend. *Phys. Rev. Lett.* **1996**, *77*, 1881–1884.
- [123] S. Athanasopoulos, E. V. Emelianova, A. B. Walker, D. Beljonne. *Organic Photonics IV* **2010**, 7722.
- [124] S. T. Hoffmann, S. Athanasopoulos, D. Beljonne, H. Bässler, A. Köhler. *J. Phys. Chem. C* **2012**, *116*, 16371–16383.
- [125] S. T. Hoffmann, H. Bässler, J. M. Koenen, M. Forster, U. Scherf, E. Scheler, P. Strohriegel, A. Köhler, A. *Phys. Rev. B* **2010**, *81*, 115103.
- [126] S. Athanasopoulos, E. V. Emelianova, A. B. Walker, D. Beljonne. *Phys. Rev. B* **2009**, *80*, 195209.
- [127] S. Athanasopoulos, S. T. Hoffmann, H. Bässler, A. Köhler, D. Beljonne. *J. Phys. Chem. Lett.* **2013**, *4*, 1694–1700.
- [128] H. T. Nicolai, A. J. Hof, M. Lu, P. W. M. Blom, R. J. de Vries, R. Coehoorn. *Appl. Phys. Lett.* **2011**, *99*, 203303.
- [129] S. I. Hintschich, C. Rothe, S. M. King, S. J. Clark, A. P. Monkman. *J. Phys. Chem. B* **2008**, *112*, 16300–16306.
- [130] S. M. King, S. I. Hintschich, D. Dai, C. Rothe, A. P. Monkman. *J. Phys. Chem. C* **2007**, *111*, 18759–18764.
- [131] E. W. Snedden, L. A. Cury, K. N. Bourdakos, A. P. Monkman. *Chem. Phys. Lett.* **2010**, *490*, 76–79.
- [132] M. Kuik, G.-J. A. H. Wetzelaer, H. T. Nicolai, N. I. Crăciun, D. M. De Leeuw, P. W. M. Blom. *Adv. Mater.* **2014**, *26*, 512–531.
- [133] P. W. M. Blom, M. J. M. deJong, S. Breedijk. *Appl. Phys. Lett.* **1997**, *71*, 930–932.
- [134] S. J. Martin, J. M. Lupton, I. D. W. Samuel, A. B. Walker. *J. Phys. Condens. Matter* **2002**, *14*, 9925–9933.
- [135] F. A. C. Oliveira, L. A. Cury, A. Righi, R. L. Moreira, P. S. S. Guimarães, F. M. Matinaga, M. A. Pimenta, R. A. Nogueira. *J. Chem. Phys.* **2003**, *119*, 9777–9782.
- [136] M. Furno, R. Meerheim, S. Hofmann, B. Lüsse, K. Leo. *Phys. Rev. B* **2012**, *85*, 115205.
- [137] I. Rörich, O. V. Mikhnenko, D. Gehrig, P. W. M. Blom, N. I. Crăciun. *J. Phys. Chem. B* **2017**, *121*, 1405–1412.
- [138] M. R. Andersson, G. Yu, A. J. Heeger. *Synth. Met.* **1997**, *85*, 1275–1276.
- [139] M. Kuik, L. J. A. Koster, G. A. H. Wetzelaer, P. W. M. Blom. *Phys. Rev. Lett.* **2011**, *107*, 256805.
- [140] J. M. Lupton, I. D. W. Samuel. *Synth. Met.* **2000**, *111*, 381–384.
- [141] P. W. M. Blom, M. J. M. de Jong. *IEEE J. Sel. Top. Quantum Electron.* **1998**, *4*, 105.
- [142] I. D. Parker, Y. Cao, C. Y. Yang. *J. Appl. Phys.* **1999**, *85*, 2441–2447.
- [143] G. C. M. Silvestre, M. T. Johnson, A. Giraldo, J. M. Shannon. *Appl. Phys. Lett.* **2001**, *78*, 1619–1621.
- [144] K. Stegmaier, A. Fleissner, H. Janning, S. Yampolskii, C. Melzer, H. von Seggern. *J. Appl. Phys.* **2011**, *110*, 034507.
- [145] A. Gassmann, S. V. Yampolskii, A. Klein, K. Albe, N. Vilbrandt, O. Pekkola, Y. A. Genenko, M. Rehahn, H. von Seggern. *Materials Science and Engineering B-Advanced Functional Solid-State Materials* **2015**, *192*, 26–51.
- [146] H. Aziz, G. Xu. *J. Phys. Chem. B.* **1997**, *101*, 4009.
- [147] W. Wild, A. Seilmeier, N. H. Gottfried, W. Kaiser. *Chem. Phys. Lett.* **1985**, *119*, 259–263.
- [148] N. Nakashima, K. Yoshihara. *J. Phys. Chem.* **1989**, *93*, 7763–7771.

References

- [149] Q. Niu, R. Rohloff, G.-J. A. H. Wetzelaer, P. W. M. Blom, N. I. Crăciun. *Nature materials* **2018**, *17*, 557.
- [150] W. Graupner, G. Leditzky, G. Leising, U. Scherf. *Phys. Rev. B* **1996**, *54*, 7610.

List of publications

1. *Influence of energetic disorder on the exciton lifetime and photoluminescence quantum yield in conjugated polymers.*

I. Rörich, O. V. M., D. Gehrig, P. W. M. Blom, N. I. Crăciun, *J. Phys. Chem. B* **2017**, *121*, 1405–1412.

2. *Efficiency of solution-processed multilayer polymer light-emitting diodes using charge blocking layers.*

C. Kasparek, **I. Rörich**, P. W. M. Blom, G.-J. J. A. H. Wetzelaer, *J. Appl. Phys.* **2018**, *123*, 024504

3. *Enhanced photoluminescence properties of a carbon dot system through surface interaction with polymeric nanoparticles.*

R. Momper, J. Steinbrecher, M. Dorn, **I. Rörich**, S. Bretschneider, M. Tonigold, C. Ramanan, S. Ritz, V. Mailänder, K. Landfester, M. B. Bannwarth, *J. Colloid Interface Sci.* **2018**, *518*, 11–20.

4. *Asymmetric Covalent Triazine Framework for Enhanced Visible Light Photoredox Catalysis via Multiple Charge Transfer.*

W. Huang, **I. Rörich**, C. Ramanan, P. W. M. Blom, H. Lu, D. Wang, L. C. da Silva, R. Li, K. Landfester, K. A. I. Zhang, *Angew. Chem. Int. Ed.* **2018**, *57*, 8316–8320.

5. *Polymer energetic disorder mediates temperature dependent photo- and electroluminescence behavior.*

I. Rörich, A.-K. Schönbein, C. Kasparek, D. K. Mangalore, C. Bauer, N. I. Crăciun, P. W. M. Blom, C. Ramanan, *J. Mater. Chem. C*, **2018**, accepted (DOI: 10.1039/C8TC01998C).

6. *Electron Donor-free Photoredox Catalysis via Electron Transfer Cascade by Cooperative Organic Photocatalysts*

L. Wang, **I. Rörich**, C. Ramanan, P. W. M. Blom, W. Huang, R. Li, K. A. I. Zhang, *Catal. Sci. Technol.* **2018**, 8, 3539–3547.

7. *Exciton Quenching Due to Hole Trap Formation in Aged Polymer Light-Emitting Diodes.*

I. Rörich, Q. Niu, N. I. Crăciun, C. Ramanan, P. W. M. Blom, in preparation.

Appendix

Table A.1. Photoluminescence spectra peaks of SY-PPV determined by Gaussian fits.

T (K)	S _{0,0} (nm)	S _{0,1} (nm)	S _{0,2} (nm)
290	537	580	615
270	539	581	612
230	541	583	622
200	542	583	624
180	544	586	635
150	547	589	638
130	547	589	635
100	549	593	635
77	550	593	636

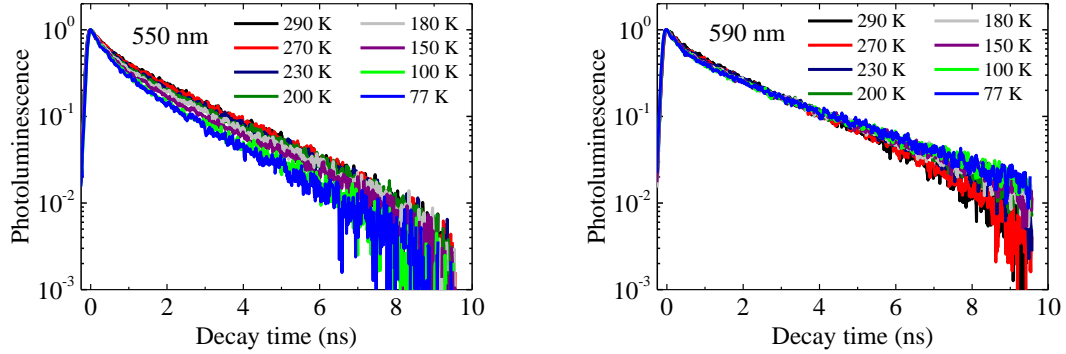


Figure A.1. Normalized PL decays in SY-PPV for a wide temperature-range.

Table A.2. Photoluminescence spectra peaks of BEH-PPV determined by Gaussian fits.

T (K)	$S_{0,0}$ (nm)	$S_{0,1}$ (nm)	$S_{0,2}$ (nm)
290	588	629	677
270	590	632	679
230	594	636	692
180	598	642	699
150	600	645	705
120	603	650	713
90	604	652	717
77	605	653	718

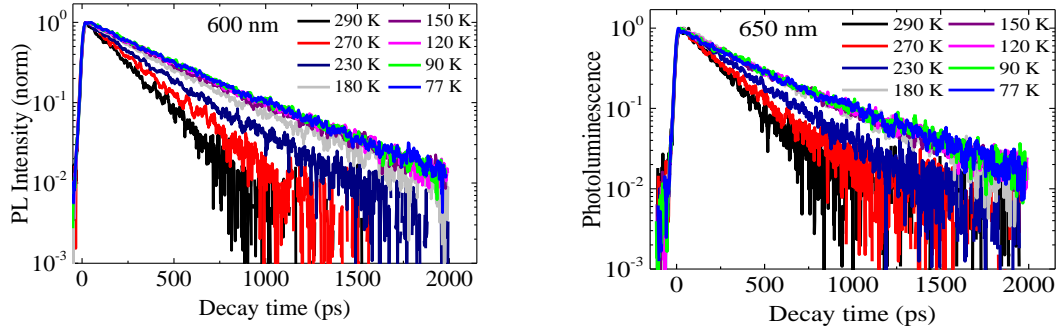
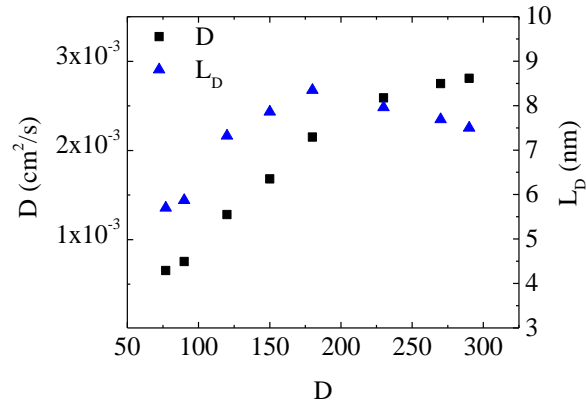

Figure A.2. Normalized PL decays in BEH-PPV for a wide temperature-range.

Figure A.3. Temperature-dependence of exciton diffusion coefficient D (black squares) and diffusion length L_D (blue triangles) for BEH-PPV, determined from monoexponential fits to time-resolved fluorescence quenching experiments and Stern-Volmer equation.

Table A.3. Electroluminescence spectra peaks of BEH-PPV determined by Gaussian fits.

T (K)	S _{0,0} (nm)	S _{0,1} (nm)	S _{0,2} (nm)
295	582	624	687
275	585	630	693
255	588	635	698
235	590	637	701
215	592	638	702

Table A.4. Temperature-dependent exciton diffusion coefficients and diffusion lengths for SY-PPV (left) and BEH-PPV (right).

T (K)	D _{SY-PPV} (cm ² /s)	L _{D,SY-PPV} (nm)	D _{BEH-PPV} (cm ² /s)	L _{D,BEH-PPV} (nm)
290	3.1×10 ⁻⁴	7.7	2.9×10 ⁻³	7.7
270	2.1×10 ⁻⁴	6.5	3.1×10 ⁻³	8.5
230	1.4×10 ⁻⁴	5.4	3.0×10 ⁻³	9.3
200	9.4×10 ⁻⁵	4.5	<i>(not measured)</i>	<i>(not measured)</i>
80	8.0×10 ⁻⁵	4.2	2.5×10 ⁻³	9.6
150	6.5×10 ⁻⁵	3.8	2.2×10 ⁻³	9.2
120	6.6×10 ⁻⁵	3.9	2.0×10 ⁻³	8.9
90	7.1×10 ⁻⁵	4.0	8.3×10 ⁻⁴	5.5
77	6.8×10 ⁻⁵	4.0	6.8×10 ⁻⁴	5.2

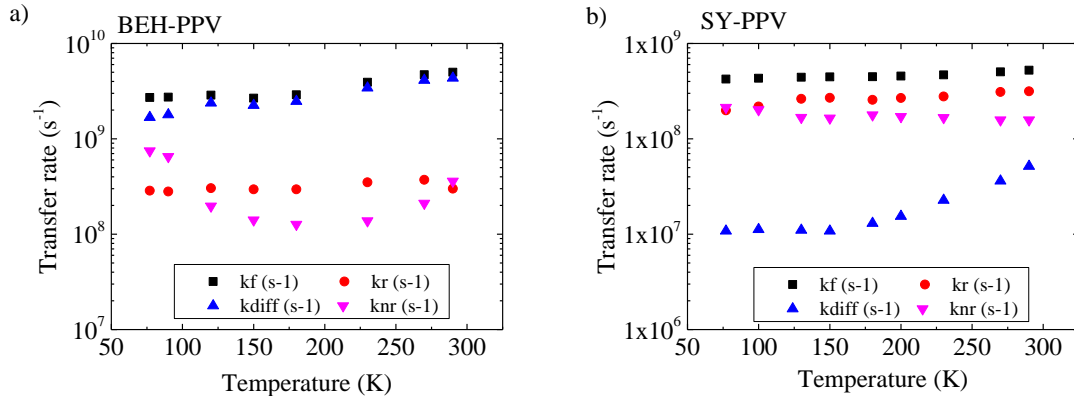


Figure A.4. Exciton transfer rates in (a) BEH-PPV and (b) SY-PPV, respectively. The exact values are summarized in Tables 3 and 4.

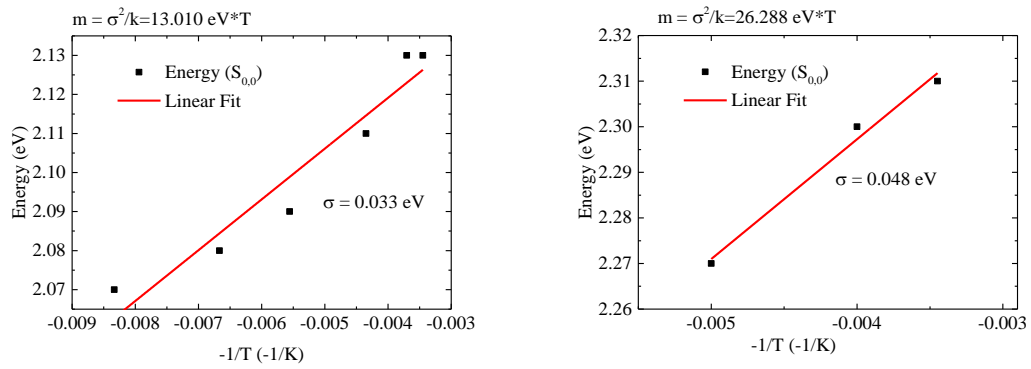


Figure A. 5. Determination of the width of the excitonic Gaussian DOS σ in (a) BEH-PPV and (b) SY-PPV.

Curriculum Vitae

Name Irina Rörich

Date of birth: 14th May, 1987

Place of birth: Solikamsk, Russia

PROFESSIONAL AND ACADEMIC CAREER

since 05/2018 Scientist at CYNORA GmbH in Bruchsal

10/2014 – 04/2018 PhD student at the Max Planck Institute for Polymer Research

Conference contributions:

08/2017: poster contribution at the ECME conference in Dresden (Germany)

09/2016: poster contribution at the IFSOE-2016 in Moscow region (Russia)

06/2016: poster contribution at the ICSM meeting in Guangzhou (China)

09/2015: oral presentation at the CTTN15 Conference in Santiago de Compostela
(Spain)

EDUCATION

04/2008 – 08/2014 Diploma in Chemistry, Johannes Gutenberg University Mainz